

NASA
TP
1914
c.1

NASA Technical Paper 1914



Effects of Vortex Flaps on the Low-Speed Aerodynamic Characteristics of an Arrow Wing

Long P. Yip and Daniel G. Murri

LOAN COPY: RETURN TO
AFWL TECHNICAL LIBRARY
KIRTLAND AFB, N.M.

NOVEMBER 1981

NASA



NASA Technical Paper 1914

Effects of Vortex Flaps
on the Low-Speed Aerodynamic
Characteristics of an Arrow Wing

Long P. Yip and Daniel G. Murri
Langley Research Center
Hampton, Virginia



National Aeronautics
and Space Administration

**Scientific and Technical
Information Branch**

1981

SUMMARY

A low-speed wind-tunnel investigation was made to determine the longitudinal and lateral-directional aerodynamic effects of plain and tabbed vortex flaps on a flat-plate, highly swept, arrow-wing model. Flow-visualization studies were made using a helium-bubble technique. Static forces and moments were measured over an angle-of-attack range from 0° to 50° for sideslip angles of 0° and $\pm 4^\circ$.

Results from flow-visualization studies indicated that the tabbed-vortex-flap arrangement was more effective in trapping a vortex along the wing leading edge than the plain vortex flap. At high angles of attack, the tabbed-vortex-flap configuration did not exhibit an asymmetric vortex breakdown pattern due to sideslip as noted for the plain-vortex-flap and basic-wing configurations. The differences in the vortex flow patterns between the two flap designs resulted in the tabbed-vortex-flap configuration providing a stable rolling-moment variation with sideslip angle, whereas the plain-vortex-flap configuration showed an unstable variation in rolling moment with sideslip angle.

Results from static-force tests indicated that both the plain-vortex-flap and tabbed-vortex-flap configurations exhibited significantly improved lift-drag ratios over that of the basic wing; however, pitch instability was increased by the addition of the vortex flaps. Also, the tabbed-vortex-flap configuration exhibited higher values of lift-drag ratios over a wider range of lift coefficients than measured for the plain-vortex-flap configuration. At high angles of attack, the tabbed-vortex-flap configuration significantly increased the dynamic directional stability which eliminated the directional divergence instability of the basic wing. However, use of trailing-edge flaps for pitch-trim requirements could seriously degrade the lateral stability characteristics and eliminate the beneficial effect of the tabbed vortex flap on dynamic directional stability.

INTRODUCTION

The National Aeronautics and Space Administration is currently conducting a broad research program to provide basic research information on the aerodynamics, stability, and control of advanced aircraft capable of supersonic-cruise flight. Typically, these aircraft employ low-aspect-ratio, highly swept, arrow-wing planforms which have been optimized for supersonic-cruise efficiency. Unfortunately, such configurations usually exhibit significant deficiencies in the areas of low-speed performance, stability, and control (see ref. 1). In addition, the application of arrow-wing designs to advanced fighter aircraft and the desire for increased maneuverability have required careful attention to aerodynamic characteristics in the moderate to high angle-of-attack range. Typically, highly swept wings exhibit strong vortex flows which augment lift at moderate angles of attack; however, this vortex lift is usually accompanied by undesirable pitch-up characteristics and significant increases in drag. At high angles of attack, asymmetric vortex bursting due to sideslip can result in unstable lateral-directional characteristics.

The present investigation was conducted to determine the effects of vortex flaps on the low-speed aerodynamic characteristics of an arrow-wing planform at low and high angles of attack. Previous research on configurations having vortex flaps (see

refs. 2 to 4) have shown considerable gains in lift-drag ratio. The specific intent of this investigation was to provide an assessment of the effects of vortex flaps on lateral-directional characteristics as well as the longitudinal characteristics of an arrow-wing configuration.

Tests were conducted in the Langley 12-Foot Low-Speed Tunnel with a 3.66-m (12-ft) octagonal test section. Static forces and moments were measured over an angle-of-attack range from 0° to 50° for sideslip angles of 0° and ±4°. A flat-plate arrow-wing model with a sharp beveled leading edge of 70° sweep and an outboard panel of 50° sweep was used as the basic-wing configuration. Two types of vortex flaps were studied in the investigation. One flap concept was a "plain" vortex flap similar to that in reference 2 and the second concept was a "tabbed" vortex flap similar to that in reference 4. In addition to static-force tests, flow-visualization studies were made using a helium-bubble flow-visualization technique.

SYMBOLS

The longitudinal aerodynamic coefficients are referred to the wind-axes system while the lateral-directional aerodynamic coefficients are referred to the body-axes system (see fig. 1). The moment reference center was located at 45 percent of the mean aerodynamic chord (see fig. 2). Dimensional quantities are presented in both the International System of Units (SI) and U.S. Customary Units. Measurements and calculations were made in U.S. Customary Units.

A	aspect ratio
b	wing span, m (ft)
C_A	axial-force coefficient, $\frac{\text{Axial force}}{qS}$
C_D	drag coefficient, $\frac{\text{Drag}}{qS}$
C_{D_i}	induced-drag coefficient
C_L	lift coefficient, $\frac{\text{Lift}}{qS}$
C_{L_α}	lift-curve slope, $\frac{\partial C_L}{\partial \alpha}$
C_l	rolling-moment coefficient, $\frac{\text{Rolling moment}}{qSb}$
C_{l_β}	rolling-moment coefficient due to sideslip, per deg
C_m	pitching-moment coefficient, $\frac{\text{Pitching moment}}{qS\bar{c}}$
C_n	yawing-moment coefficient, $\frac{\text{Yawing moment}}{qSb}$
C_{n_β}	yawing-moment coefficient due to sideslip, per deg

$C_{n\beta, \text{dyn}}$ dynamic directional stability parameter,

$$C_{n\beta} = - \frac{I_z}{I_x} C_{l\beta} \sin \alpha$$

C_Y side-force coefficient, $\frac{\text{Side force}}{qS}$

$C_{Y\beta}$ side-force coefficient due to sideslip, per deg

\bar{c} mean aerodynamic chord, m (ft)

I_x, I_z moments of inertia about the X and Z body axes, respectively, kg-m^2 (slug-ft^2)

L/D lift-drag ratio, C_L/C_D

q free-stream dynamic pressure, Pa (lb/ft^2)

S wing reference area, m^2 (ft^2)

V_∞ free-stream velocity, m/sec (ft/sec)

X, Y, Z body axes

α angle of attack, deg

β angle of sideslip, deg

$\delta_{f,le}$ leading-edge flap deflection, deg

$\delta_{f,te}$ trailing-edge flap deflection, deg

Abbreviations:

F.S. fuselage station

L.E. leading edge

V.F. vortex flap

MODEL DESCRIPTION

The model used in this investigation was essentially a flat-plate wing of 70° sweep inboard with a 50° sweep outboard panel (see fig. 2(a)). Figures 2(b) and 2(c) show detailed dimensional characteristics of the vortex flaps tested. The flaps were similar to those of references 2 and 4. In some tests, sheet metal was added to form trailing-edge flaps (see fig. 2(b)). Photographs of the model with these leading- and trailing-edge flap attachments are shown in figure 3. For purposes of nomenclature vortex flaps of reference 2 will be referred to as plain vortex flaps, and vortex flaps of reference 4 will be referred to as tabbed vortex flaps throughout the text of this report. The tabbed vortex flap was attached to the full span of the wing leading edge, while the plain vortex-flap configuration did not include the innermost segment.

TESTS

The tests were conducted in the Langley 12-Foot Low-Speed Tunnel which has a 3.66-m (12-ft) octagonal test section. The free-stream dynamic pressure was 191 Pa (4 psf) which corresponds to a Reynolds number of 620 000 based on the mean aerodynamic chord of 0.50 m (1.65 ft). Data were obtained over an angle-of-attack range from 0° to 50° for sideslip angles of 0° and ±4°. The principal configuration variables were the leading-edge flap elements which were tested at several different deflection angles. Flow-visualization studies using a helium-bubble technique (see ref. 5) were made to provide qualitative assessment of the leading-edge vortex phenomenon.

The model was mounted on a strain-gage balance where forces and moments were measured. The balance was selected with a sensitive axial component such that drag accuracy was within ±0.0010 variance of the drag coefficient. A fairing to house the balance was instrumented with a pressure probe so that base pressure drag could be accounted for. No corrections were made to the data due to jet boundary or blockage; however, the model size was small relative to the tunnel size. The data are corrected for a flow angularity of 1.5° upwash.

PRESENTATION OF RESULTS

	Figure
Flow visualization	4 to 8
Longitudinal aerodynamic characteristics:	
Comparison with theory	9
Plain vortex flap:	
Leading-edge deflection	10
Buildup of leading-edge segments	11
Trailing-edge-flap effectiveness	12 and 13
Tabbed vortex flap	14
Comparison of vortex flaps:	
Trailing-edge flaps off	15
L/D characteristics	16
Axial-force coefficients	17
Lateral-directional characteristics:	
Plain vortex flaps:	
Leading-edge deflection	18
Buildup of leading-edge segments	19
Trailing-edge-flap deflection	20
Tabbed vortex flap	21
Comparison of vortex flaps	22
Effect of vortex flaps on $C_{n\beta, dyn}$	23

RESULTS AND DISCUSSION

Flow Visualization

In order to provide some insight into the vortex-flow characteristics along the wing leading edge, a helium-bubble flow-visualization technique was used. This technique consisted of injecting neutrally buoyant helium soap bubbles into the airstream so that the bubbles could follow the streamlines around the model. On highly swept wing configurations, the separated leading-edge flow forms vortex cores which trail downstream. This vortex system is made visible by illuminating the helium bubbles in the flow with concentrated light and by painting the model black to improve contrast between the bubbles and the model.

The physical concept of the vortex flap is illustrated in figure 4 which shows the flow over the arrow-wing model at $\alpha = 15^\circ$ with the tabbed vortex flap installed on the left leading edge. The tabbed vortex flap tends to trap the vortex core along the leading-edge flap area of the wing. As discussed in past studies, this trapped vortex generates suction on the deflected flap area to produce a thrust component which reduces the drag.

Previous research (see refs. 6 to 8) has shown that vortex cores shed by highly swept wings break down at high angles of attack resulting in loss of lift. Vortex-breakdown phenomena due to angle of attack for the basic-wing, the plain-vortex-flap, and the tabbed-vortex-flap configurations are illustrated in figures 5 to 7. For the basic wing (fig. 5), the vortex-breakdown point occurs at the trailing edge at $\alpha = 25^\circ$ and it rapidly moves forward at higher angles of attack. For the plain vortex flap (fig. 6), two vortex systems can be seen. Since the plain-vortex-flap system did not extend to the apex of the wing, a primary pair of vortices were shed off the leading edge near the apex, and a secondary pair of vortices developed on the vortex flap. Two primary observations from figure 6 are (1) the secondary vortex system does not stay attached along the length of the flap and (2) the secondary vortex merges at a relatively low angle of attack into the primary vortex system. Vortex breakdown on the plain-vortex-flap configuration occurs at a lower angle of attack than on the basic wing.

Flow visualization for the tabbed-vortex-flap configuration is shown in figure 7. A side-view photograph is presented along with the top view to show that the vortex core was trapped within the vortex flap. Vortex bursting occurred on the flap at $\alpha = 20^\circ$ and moved rapidly forward to the apex as α was increased to 30° .

As pointed out in reference 5, highly swept wing configurations exhibit unstable lateral-directional characteristics at high angles of attack due to asymmetric vortex breakdown at small angles of sideslip. The effect of sideslip on the configurations tested at high angles of attack is illustrated in figure 8. These photographs show the vortex-flow pattern on the left and right sides of the model at $\alpha = 35^\circ$ and $\beta = -4^\circ$ and -8° . For the basic wing, the effect of sideslip changed the symmetrical vortex flow at $\beta = 0^\circ$ to an asymmetric flow condition with the windward vortex burst point moving toward the apex of the wing, and the leeward vortex moving toward the wing trailing edge. As noted in reference 5, this type of asymmetric vortex breakdown results in an unstable variation in rolling moment with sideslip due to the lift loss associated with vortex breakdown. Flow visualization of the plain-vortex-flap configuration (fig. 8(b)) also showed an asymmetric vortex-breakdown pattern due to sideslip. However, the vortex breakdown due to sideslip of the tabbed-vortex-flap configuration did not show large asymmetry due to sideslip (see fig. 8(c)). For example, at $\alpha = 35^\circ$ the vortex burst points for the tabbed-vortex-flap configu-

ration were located near the apex of the wing, and there was little variation in the vortex-breakdown location due to sideslip. This result would be expected to improve lateral stability at high α , as will be discussed in a later section.

Longitudinal Characteristics

Comparison with theory.- The vortex-lattice method of reference 9 was used to predict the longitudinal characteristics of the basic-wing planform, and a comparison with the experimental data is shown in figure 9. The theoretical method incorporates the leading-edge suction analogy of reference 10, and is restricted to inviscid flow computations. Theoretical results were in good agreement with the experimental data at low to moderate angles of attack. At high angles of attack the experimental lift data deviated from theoretical values due to the lift losses associated with vortex bursting, which are not accounted for in the theory. Slight differences in pitching moments are due to the planar representation of vortices in the theoretical method. Thus, higher order paneling methods would be needed in order to obtain better agreement between theory and experiment. An increment of drag due to viscous effects was added to the inviscid values to obtain the comparison in figure 9. This comparison of drag indicates that the configuration exhibited a drag polar which was close to that predicted by theory.

Effect of leading-edge deflection.- The effect of the plain vortex flap on the longitudinal aerodynamic characteristics of the model is shown in figure 10. The data of figure 10(a) indicate that the plain vortex flap exhibited more pitch instability and nose-up trim change than the basic wing; however, the pitch instability decreased as the leading-edge flap deflection was increased. The effect of the plain vortex flap on L/D is shown in figure 10(b). Also shown in this figure are curves representing the 0-percent and 100-percent leading-edge suction for the reference wing as computed by the method of reference 11. The condition of minimum induced drag in which $C_{D_i} = C_L^2 / \pi A$ corresponds to 100-percent leading-edge suction, and the condition of completely separated flow in which $C_{D_i} = C_L \tan \left(\frac{C_L}{C_{L\alpha}} \right)$ corresponds to 0-percent leading-edge suction. It should be noted that the data of this report are based on the wing reference area unless otherwise noted. The data of figure 10(b) indicate that the basic wing exhibited L/D values that were close to the 0-percent suction curve, as expected. Adding the plain vortex flap improved L/D , even for a flap deflection of 0° . Although there is no deflected leading-edge flap surface to act on at a 0° deflection angle, an inclined surface results from the beveled leading edge of the wing. The beneficial effects of vortex flaps on suction force are indicated in figure 10(c) for the flap-installed configuration by the negative increase in axial-force coefficient. It can be seen that the axial-force coefficient decreased and became negative by adding the vortex flap with 0° deflection to the basic wing and generally became more negative with increasing leading-edge flap deflection. At low lift coefficients, the data indicate that the configuration with a leading-edge flap deflection of 45° was over deflected for producing thrust.

Leading-edge segments.- A component buildup study was made for the plain-vortex-flap configuration by starting with the inboard segment and adding segments until the complete configuration was formed. The leading-edge flap was divided into five segments, four inboard of the wing leading-edge crank (see fig. 2). A leading-edge deflection of 15° was used in the study. The data shown in figures 11(a) and 11(b) indicate an increase in nose-up pitching moments as the leading-edge segments are added to the basic wing. The data of figure 11(b) indicate that segment one had

little effect on L/D; however, by adding segment two, the configuration showed about as much improvement in L/D as was obtained for the complete leading-edge-flap configuration. The addition of the outboard segment provided an additional improvement in L/D for lift coefficients above about 0.3.

Trailing-edge-flap effectiveness.- The trailing-edge-flap system, shown in figure 2(b), consisted of sheet metal bent to the appropriate deflection angle and attached to the trailing edge of the wing. The flap was nearly full span and represented an extended-flap arrangement. Trailing-edge-flap deflections of 0°, 10°, 20°, and 30° were tested.

Figure 12 presents data which show the trailing-edge-flap effectiveness for various deflections of the plain vortex flap. Data for the basic wing were added to the plot of figure 12(a) to illustrate the effect of adding area. By adding the leading- and trailing-edge flaps with 0° deflection, there is an increase in the lift-curve slope, a decrease in the drag polar, and no change in pitch instability. The data of figure 12 indicate that the trailing-edge-flap system was effective in producing increments of lift and pitching moments for the deflection angles tested. The pitch-up noted for the basic wing became more pronounced for the higher trailing-edge-flap deflections. The leading-edge-flap deflection had little effect on the trailing-edge-flap effectiveness.

Figure 13 presents untrimmed L/D characteristics for various combinations of the leading- and trailing-edge flaps. The data show that trailing-edge-flap deflection was a dominant factor in improving L/D. At the low lift coefficients applicable to take-off and second-segment climb for supersonic-cruise transports, leading-edge-flap deflections of 0° and 15° in combination with a trailing-edge-flap deflection of 10° provided the highest values of L/D. At moderate to high lift coefficients applicable to take-off and second-segment climb for supersonic-cruise transports, leading-edge-flap deflections of 0° and 15° in combination with a trailing-edge-flap deflection of 10° provided the highest values of L/D. At moderate to high lift coefficients applicable to maneuver conditions for fighter aircraft, leading-edge-flap deflection had little effect on improving L/D. It should be noted that trim considerations must be evaluated before optimum flap settings can be selected.

Tabbed vortex flap.- Results of tests for the tabbed-vortex-flap configuration, shown in figure 14, indicate that the stall of the basic wing was extended to a higher angle of attack; however, the pitch instability was significantly increased. A marked increase in instability occurred for this configuration at $\alpha = 20^\circ$, which corresponds to the angle of attack where vortex breakdown started to occur on the vortex flap. With a trailing-edge-flap deflection of 20°, sizeable increments of lift and pitching moments were produced.

The data of figure 14(b) indicate that the tabbed vortex flap significantly improved L/D over the basic wing for lift coefficients above 0.25. With trailing-edge flaps deflected 20°, the configuration had L/D values close to those predicted for 100-percent leading-edge suction for values of C_L greater than 0.7. However, the values of L/D presented are not trimmed, and requirements for trim could alter the results shown.

Comparison of vortex flaps.- A summary plot of the longitudinal aerodynamic characteristics of the basic-wing configuration compared with the vortex-flap configurations is presented in figure 15 to show the effect of vortex flaps. The data of figure 15 indicate that the tabbed-vortex-flap configuration, with undeflected

trailing-edge flap significantly increased the maximum lift coefficient and the angle of attack at which it occurred. However, this increase in lift was accompanied by a significant increase in destabilizing pitching moments.

A comparison of the lift-drag ratios between the vortex-flap configurations and the basic wing is shown in figure 16. Since the flap areas are sized differently, the data are corrected for area and shown in figure 16(b) for the purpose of analysis. The data indicate that the plain-vortex-flap configuration provided significant improvement in L/D at low lift coefficients, but this improvement diminishes with increasing lift coefficient. The tabbed-vortex-flap configuration had a slightly lower value of $(L/D)_{\max}$ than the plain vortex flap, but had higher values of L/D over a wider range of lift coefficients. One explanation for this may be that the tab made this arrangement less sensitive to the leading-edge inflow angle and thus more effective in tripping the flow to set up a trapped vortex along the span of the flap. Another factor which may have influenced the results for the plain vortex flap was that no leading-edge-flap element was used close inboard on the wing (see fig. 2(b)). If the plain vortex flap were allowed to extend inboard to the wing centerline, the data for the plain vortex flap could possibly alter the results obtained in the present investigation (see ref. 4).

Axial-force characteristics are shown in figure 17 for the basic wing, plain vortex flap ($\delta_{f,le} = 30^\circ$), and tabbed vortex flap. Both vortex-flap arrangements resulted in greater leading-edge thrust than that of the basic wing. The tabbed-vortex-flap configuration produced axial forces which approached the 100-percent leading-edge suction curve. At low lift coefficients, the tabbed-vortex-flap geometry was overdeflected, causing an increase in the axial force.

Lateral-Directional Characteristics

A previous investigation (ref. 5) has shown that the current configuration exhibited an unstable dihedral effect at high angles of attack due to asymmetrical vortex breakdown. Thus, it is of interest to determine the effects of vortex flaps on the lateral-directional characteristics of the configuration at high angles of attack.

Plain vortex flaps.— The effects of deflecting the plain vortex flap on the lateral-directional stability characteristics are presented in figure 18. Adding plain vortex flaps to the basic wing markedly decreased the directional stability $C_{n\beta}$ and generally did not affect the variation of $C_{l\beta}$ with angle of attack as noted for the basic wing. The effect of a spanwise component buildup of the plain vortex flap on the lateral-directional characteristics (fig. 19), indicates that the destabilizing trend in $C_{n\beta}$, due to leading-edge-flap segments, generally increased with the buildup of flap segments.

The effect of trailing-edge-flap deflection on the lateral-directional stability characteristics is presented in figure 20 for various deflections of the plain vortex flap. In general, trailing-edge-flap deflections had a large destabilizing effect on $C_{l\beta}$ at the higher angle of attack. This result is in agreement with the results

of reference 5 where a downward elevator deflection produced a destabilizing change in $C_{l\beta}$. This destabilizing effect on $C_{l\beta}$ is caused by large lift losses due to asymmetrical vortex bursting at a sideslip angle.

Tabbed vortex flap.- The lateral-directional stability characteristics of the test configuration with a tabbed vortex flap attached to the leading edge are presented in figure 21. The data of figure 21 show that the tabbed-vortex-flap configuration significantly increased the dihedral effect at high angles of attack and had a destabilizing effect on directional stability. As in the case of the plain-vortex-flap configuration, trailing-edge-flap deflection sharply decreased the dihedral effect and had a destabilizing effect on directional stability near the stall.

A comparison of the effects on lateral-directional stability for the two types of vortex flaps investigated is presented in figure 22. The data of figure 22 indicate that the plain vortex flap exhibited lateral-directional stability characteristics generally similar to those of the basic wing; however, the tabbed-vortex-flap configuration exhibited a substantial improvement in $C_{l\beta}$ compared to that of the basic wing. The significance of this improvement in $C_{l\beta}$ can be seen in figure 23 where $C_{n\beta, dyn}$, a parameter used to indicate directional stability characteristics under dynamic conditions (see ref. 12), is plotted against angle of attack. The parameter $C_{n\beta, dyn}$ is computed from

$$C_{n\beta, dyn} = C_{n\beta} - \frac{I_z}{I_x} C_{l\beta} \sin \alpha$$

and negative values of $C_{n\beta, dyn}$ indicate the possible existence of directional divergence. Using a ratio of $\frac{I_z}{I_x} = 6$, typical of current fighter aircraft, the data of figure 23 indicate a potential divergence for the basic wing at an angle of attack of about 35°. Adding plain vortex flaps to the wing leading edge did not alleviate the instability; however, adding the tabbed vortex flap did result in a significant increase in $C_{n\beta, dyn}$ and thus eliminated the directional divergence. However, use of trailing-edge flaps to trim the configuration would seriously degrade the lateral stability as shown in figure 22, and this could eliminate the beneficial effects of the tabbed vortex flap on $C_{n\beta, dyn}$.

SUMMARY OF RESULTS

The results of low-speed wind-tunnel tests to determine the effects of vortex flaps on the longitudinal and lateral stability characteristics of a flat-plate highly swept arrow-wing planform may be summarized as follows:

1. Flow visualization with a helium-bubble technique illustrated the vortex flow pattern associated with the vortex-flap concept. Results of the flow studies

showed that separated flow off the leading edge of the wing coalesces to form a vortex core that is trapped within the leading-edge flap area. This trapped vortex generated suction on the deflected flap area to produce a thrust component which reduced drag.

2. Results from flow-visualization studies indicated that the tabbed-vortex-flap arrangement was more effective in trapping a vortex along the wing leading edge than the plain vortex flap. At high angles of attack, the tabbed-vortex-flap configuration did not exhibit an asymmetric vortex-breakdown pattern due to sideslip as noted for the plain-vortex-flap and basic-wing configurations.

3. Results from static-force tests indicated that the tabbed-vortex-flap configuration was more effective than the plain-vortex-flap configuration in improving the lift-drag ratio at moderate lift coefficients; however, pitch instability was increased.

4. At high angles of attack, the tabbed vortex flap provided a stable rolling-moment variation with sideslip angle whereas the plain-vortex-flap configuration showed an unstable variation in rolling moment with sideslip angle.

5. The tabbed-vortex-flap configuration significantly increased dynamic directional stability which eliminated the directional divergence instability of the basic wing. However, use of trailing-edge flaps for pitch-trim requirements could seriously degrade the lateral stability characteristics and eliminate the beneficial effect of the tabbed vortex flap on dynamic directional stability.

Langley Research Center
National Aeronautics and Space Administration
Hampton, VA 23665
September 4, 1981

REFERENCES

1. Coe, Paul L., Jr.; Thomas, James L.; Huffman, Jarrett K.; Weston, Robert E.; Schoonover, Ward E., Jr.; and Gentry, Garl L., Jr.: Overview of the Langley Subsonic Research Effort on SCR Configurations. Supersonic Cruise Research '79 - Part 1, NASA CP-2108, 1980, pp. 13-33.
2. Rao, Dhanvada M.: Leading Edge Vortex-Flap Experiments on a 74 Deg. Delta Wing. NASA CR-159161, 1979.
3. Rao, Dhanvada M.: Exploratory Subsonic Investigation of Vortex-Flap Concept on Arrow Wing Configuration. Supersonic Cruise Research '79 - Part 1, NASA CP-2108, 1980, pp. 117-129.
4. Runyan, L. James; Middleton, Wilbur D.; and Paulson, John A.: Wind Tunnel Test Results of a New Leading Edge Flap Design for Highly Swept Wings - A Vortex Flap. Supersonic Cruise Research '79 - Part 1, 1980, pp. 131-147.
5. Johnson, Joseph L., Jr.; Grafton, Sue B.; and Yip, Long P.: Exploratory Investigation of the Effects of Vortex Bursting on the High Angle-of-Attack Lateral-Directional Stability Characteristics of Highly-Swept Wings. A Collection of Technical Papers - AIAA 11th Aerodynamic Testing Conference, Mar. 1980, pp. 282-297. (Available as AIAA-80-0463.)
6. Hummel, D.: Study of the Flow Around Sharp-Edged Slender Delta Wings With Large Angles of Attack. NASA TT F-15,107, 1973.
7. Wentz, W. H., Jr.; and Kohlman, David L.: Wind Tunnel Investigations of Vortex Breakdown on Slender Sharp-Edged Wings. NASA CR-98737, 1968.
8. Erickson, Gary E.: Flow Studies of Slender Wing Vortices. AIAA-80-1423, July 1980.
9. Miranda, Luis R.; Elliott, Robert D.; and Baker, William M.: A Generalized Vortex Lattice Method for Subsonic and Supersonic Flow Applications. NASA CR-2865, 1977.
10. Polhamus, Edward C.: A Concept of the Vortex Lift of Sharp-Edge Delta Wings Based on a Leading-Edge-Suction Analogy. NASA TN D-3767, 1966.
11. Coe, Paul L., Jr.; and Weston, Robert P.: Effects of Wing Leading-Edge Deflection on Low-Speed Aerodynamic Characteristics of a Low-Aspect-Ratio Highly Swept Arrow-Wing Configuration. NASA TP-1434, 1979.
12. Chambers, Joseph R.; and Grafton, Sue B.: Aerodynamic Characteristics of Airplanes at High Angles of Attack. NASA TM-74097, 1977.

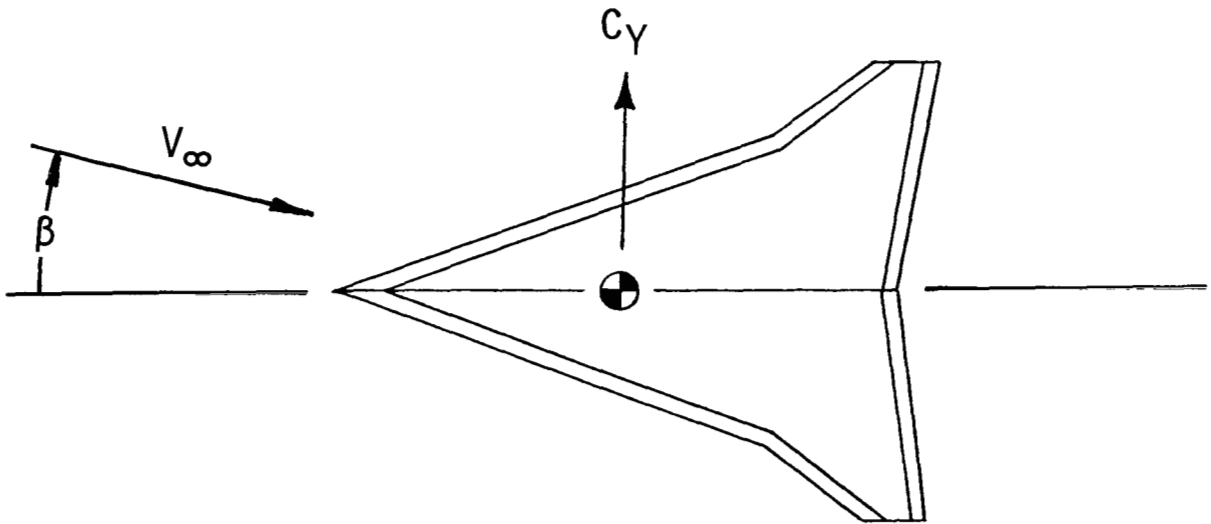
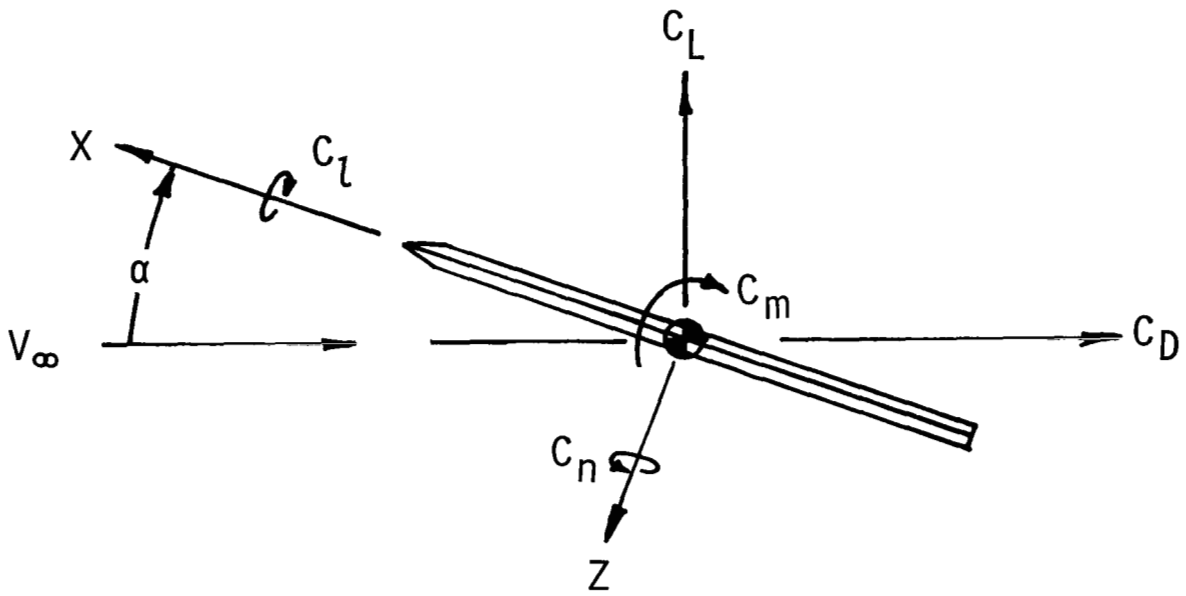
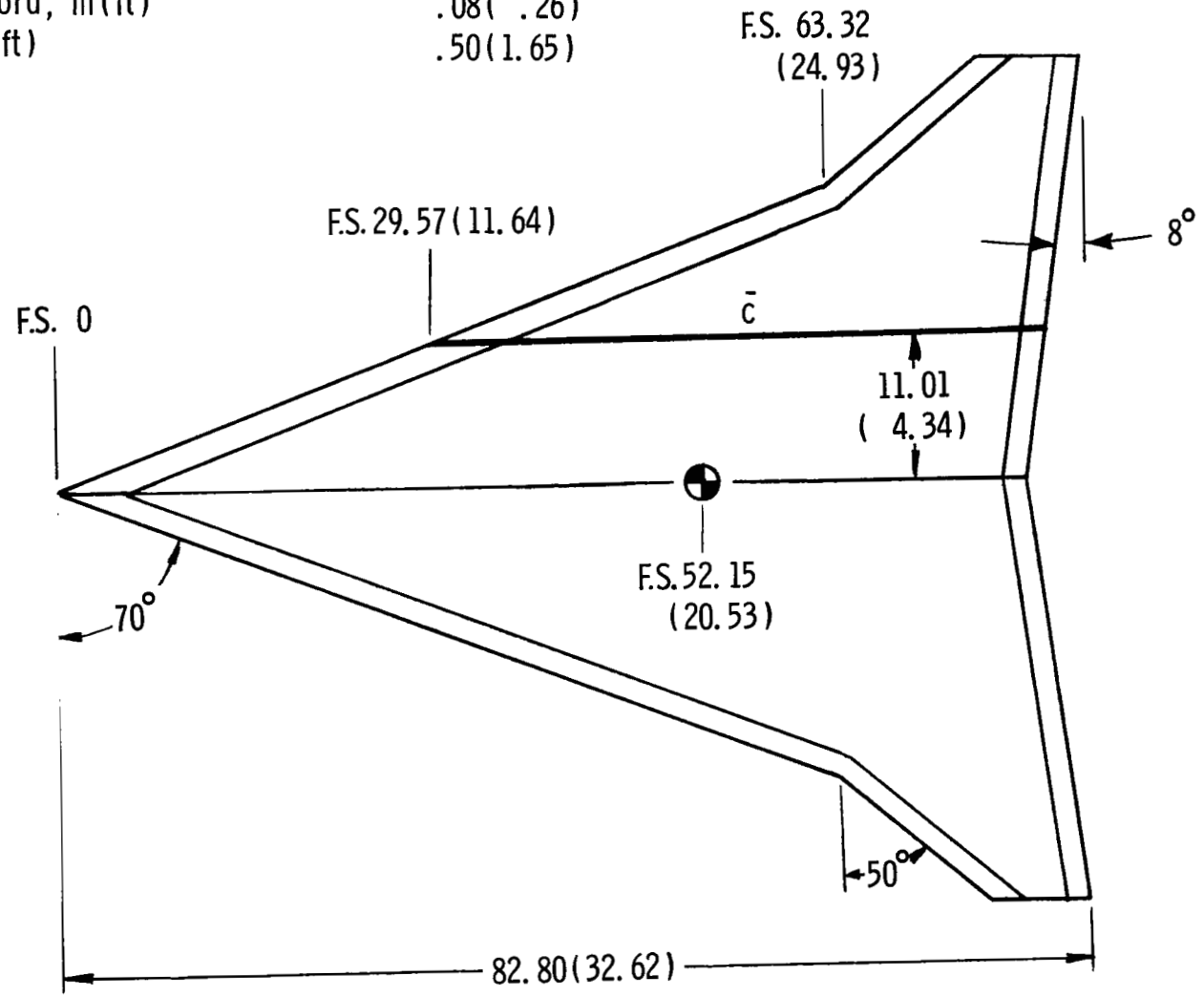


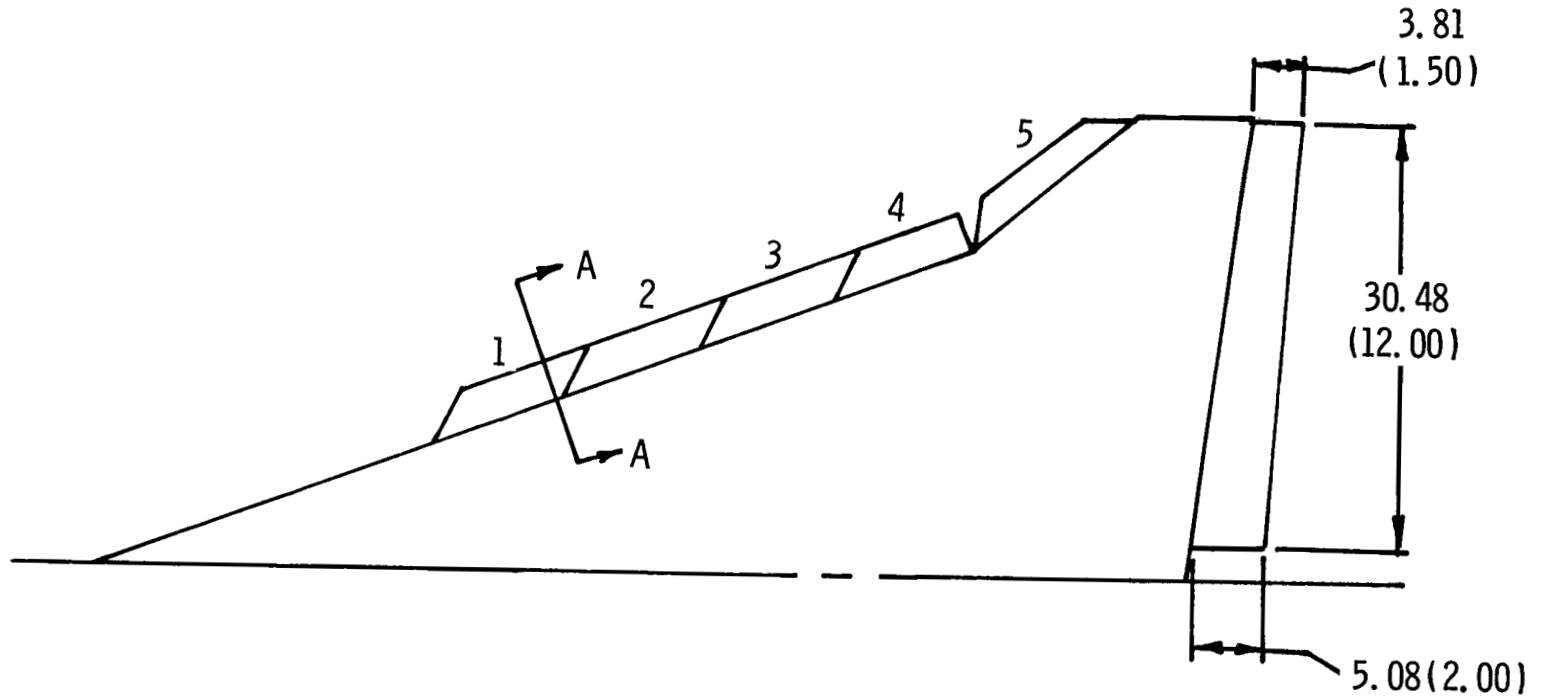
Figure 1.- System of axes.

Wing reference area, $m^2(ft^2)$	0.25 (2.67)
Span, m (ft)	.66 (2.16)
Root chord, m (ft)	.78 (2.57)
Tip chord, m (ft)	.08 (.26)
\bar{c} , m (ft)	.50 (1.65)

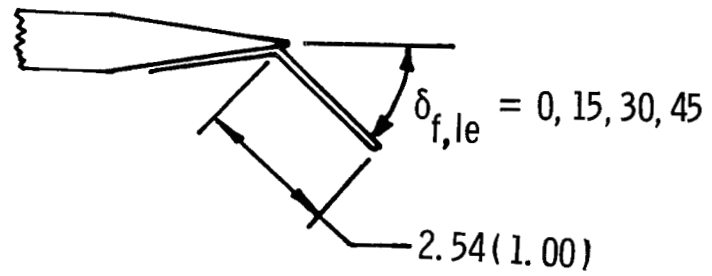


(a) Planform.

Figure 2.- Dimensional characteristics of model. Dimensions given in cm (in.).

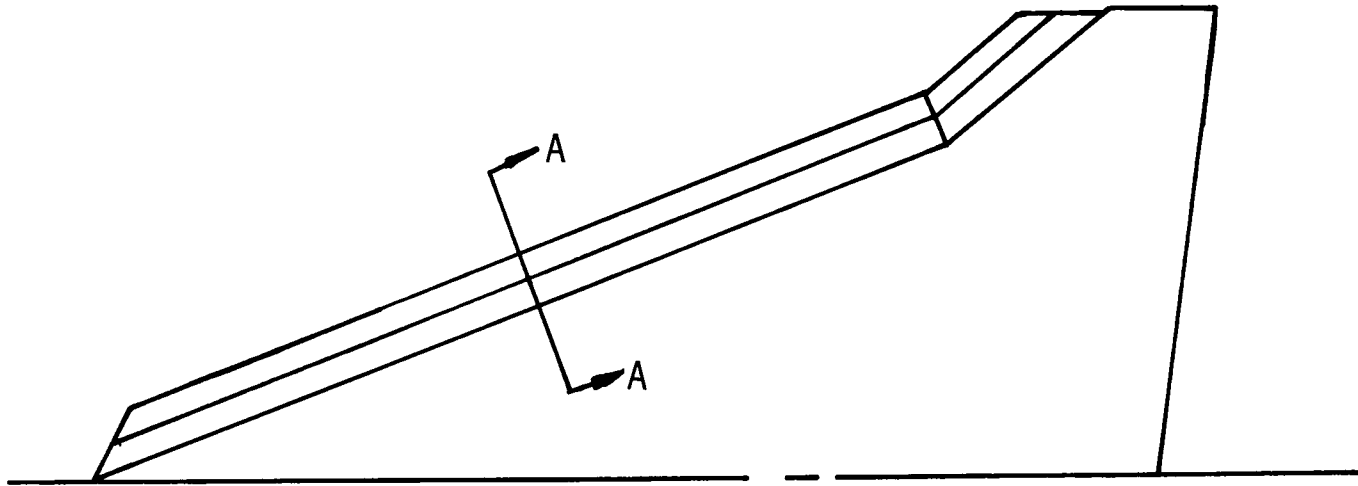


Section A - A

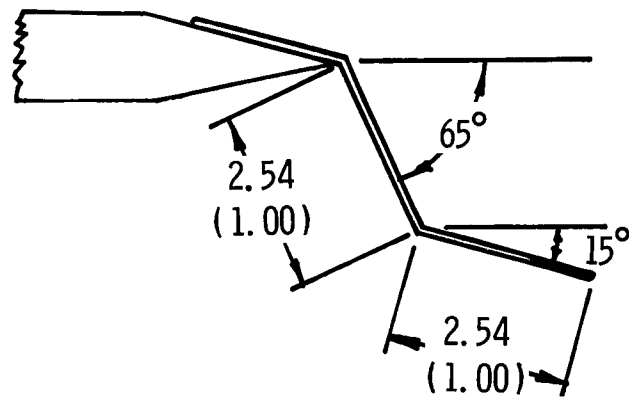


(b) Plain vortex flaps and trailing-edge flaps.

Figure 2.- Continued.

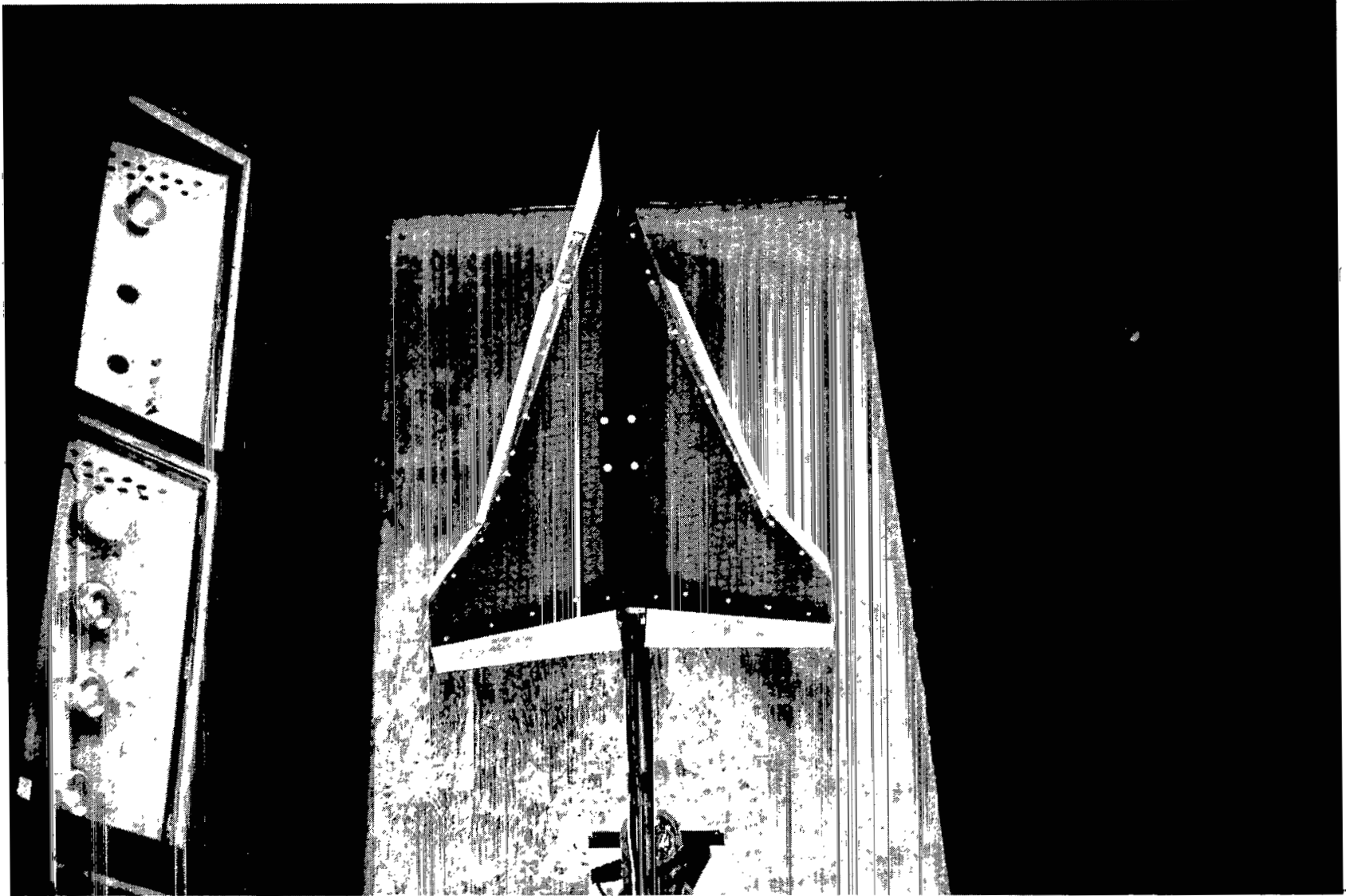


Section A - A



(c) Tabbed vortex flaps.

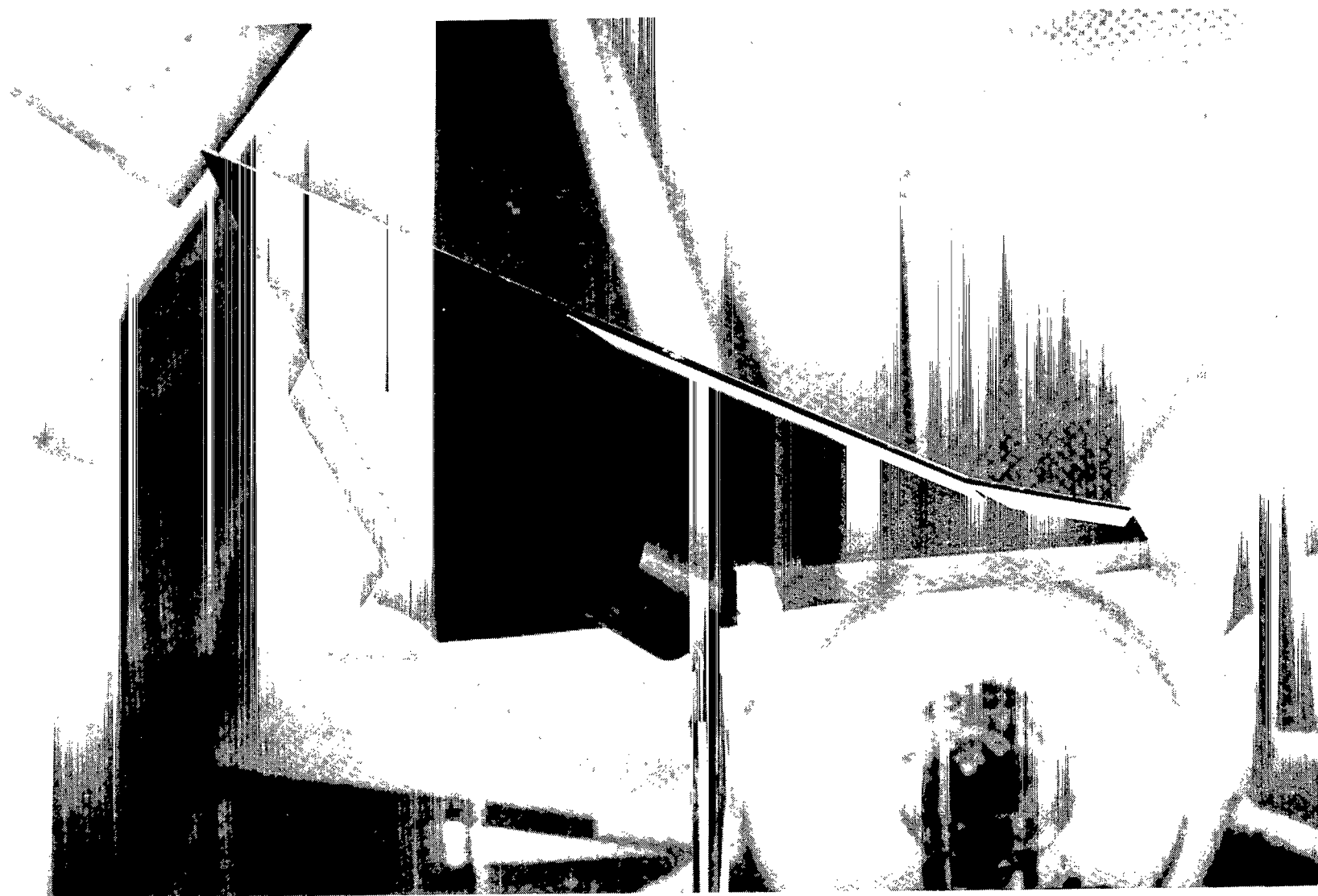
Figure 2.- Concluded.



L-80-5850

(a) Top view with plain vortex flap and trailing-edge flap.

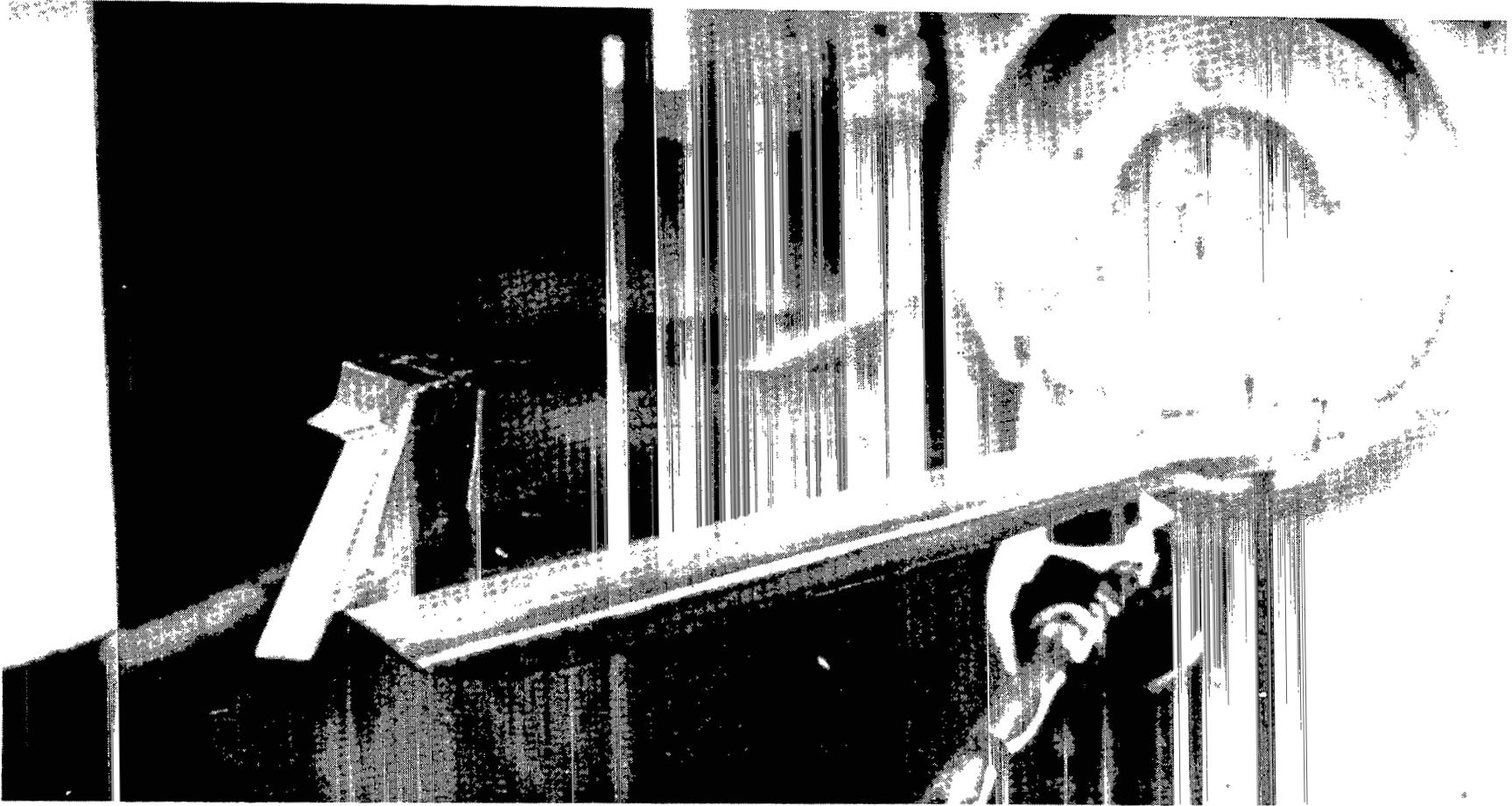
Figure 3.- Photograph of model installed in wind tunnel.



L-80-5851

(b) Three-quarter front view of plain vortex flap.

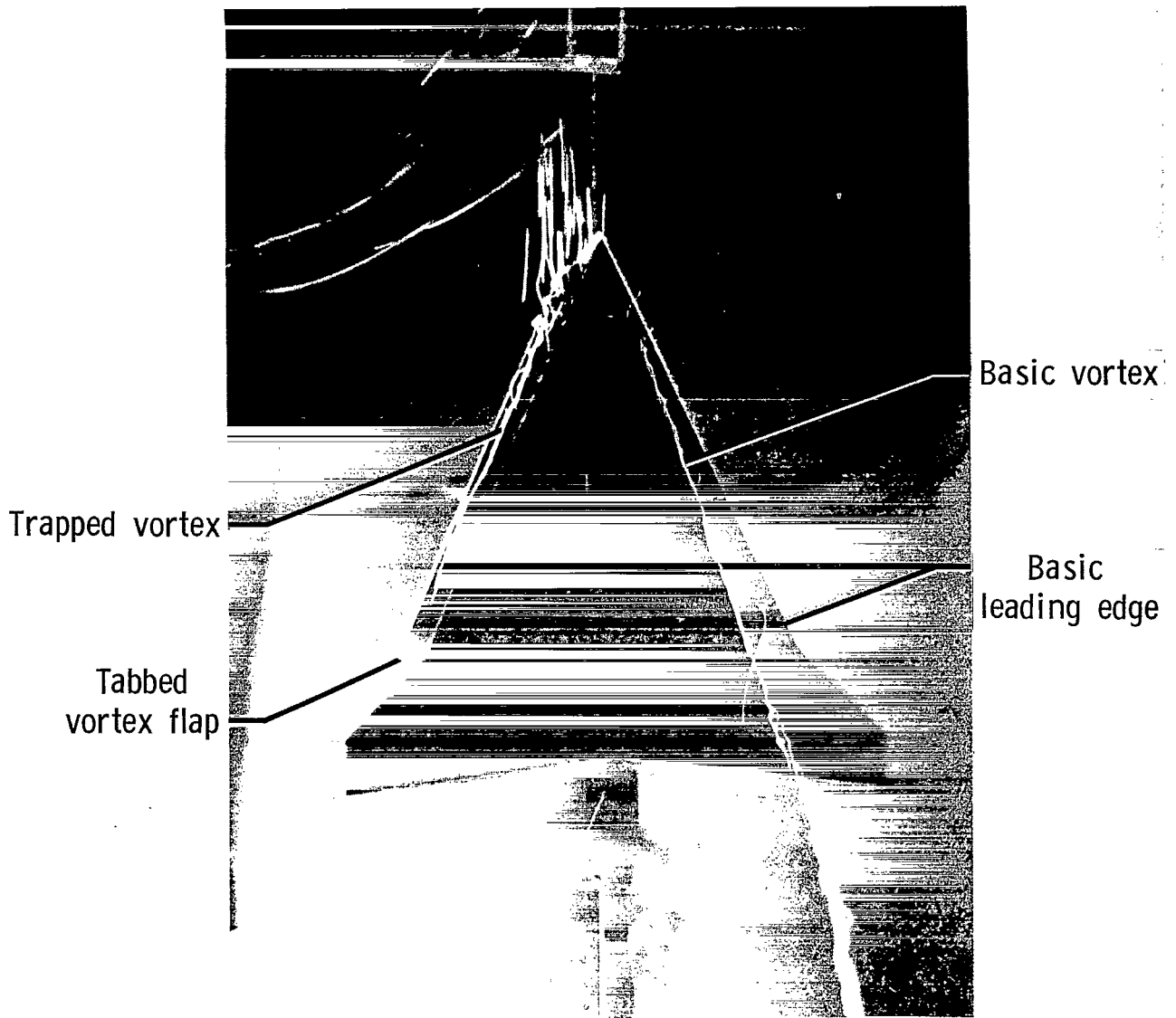
Figure 3.- Continued.



L-81-210

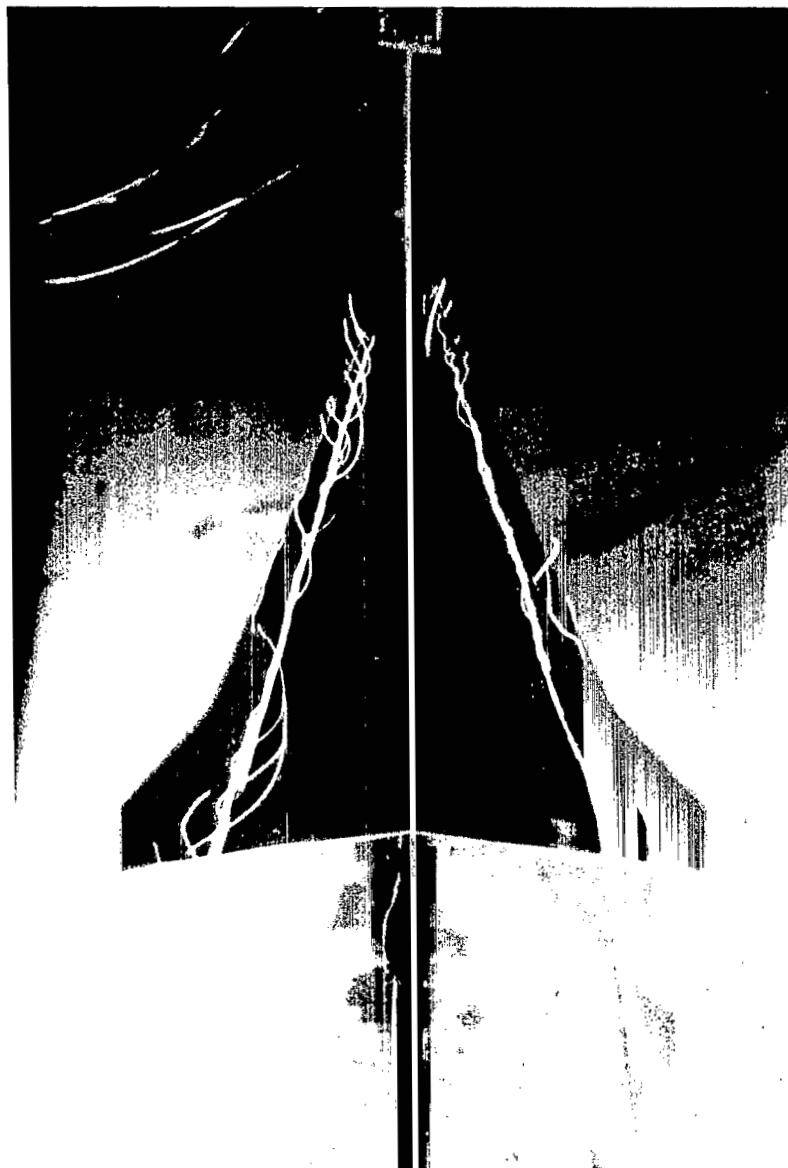
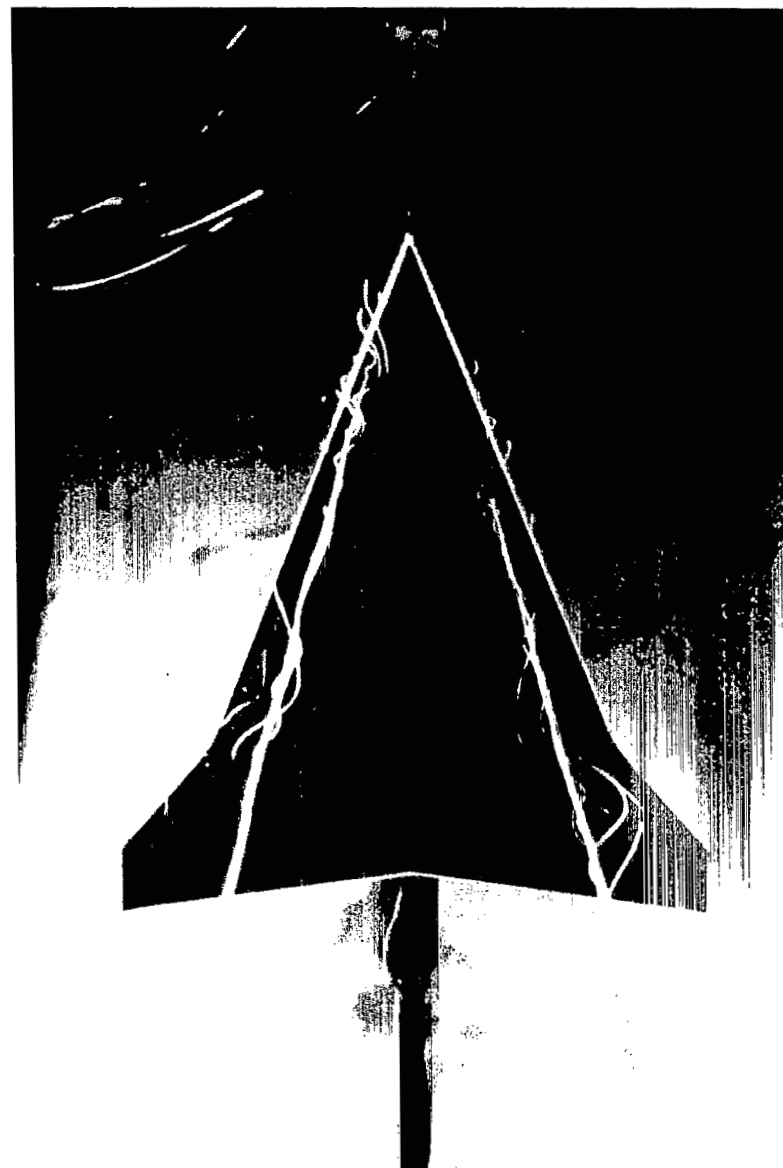
(c) Three-quarter front view of tabbed vortex flap.

Figure 3.- Concluded.



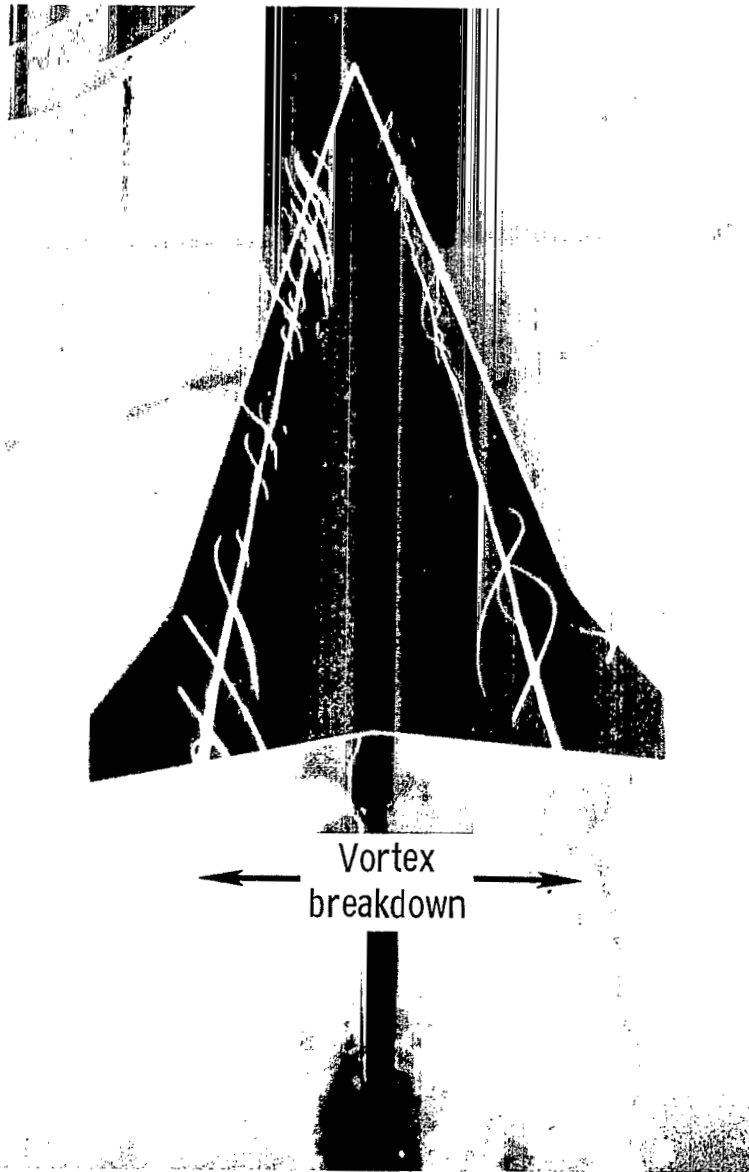
L-81-211

Figure 4.- Helium-bubble flow visualization. $\alpha = 15^\circ$.

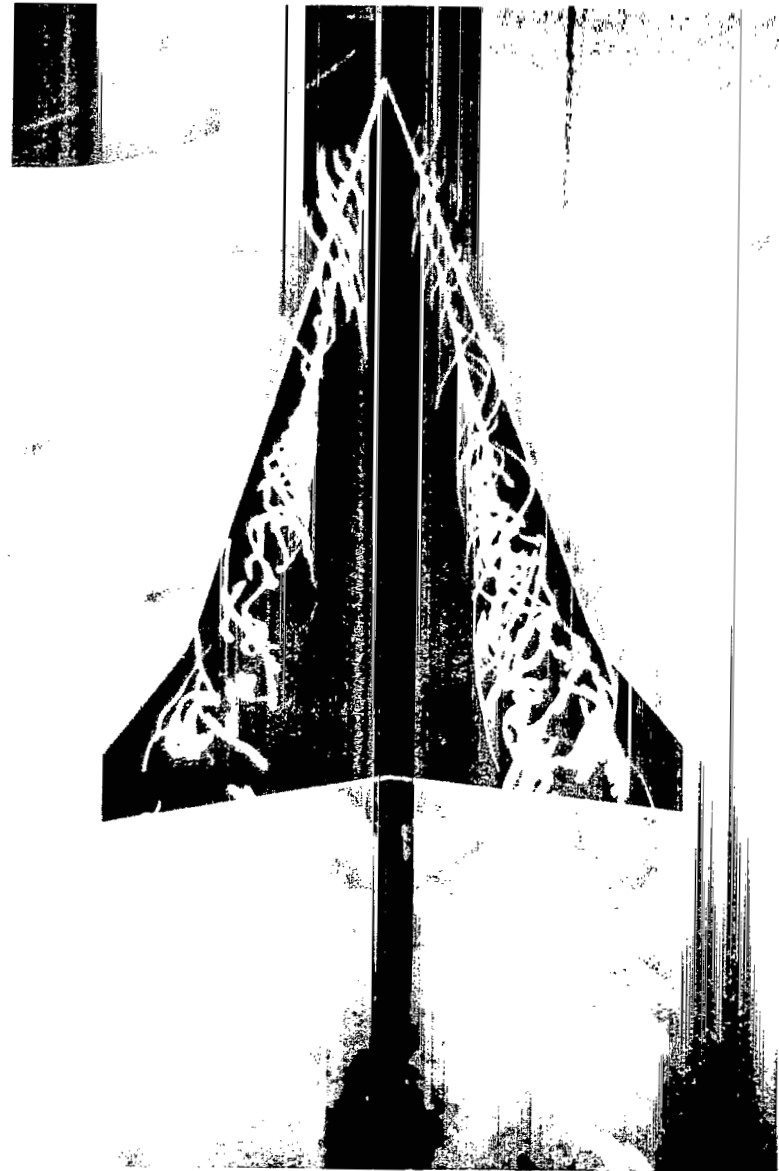
(a) $\alpha = 15^\circ$.(b) $\alpha = 20^\circ$.

L-81-212

Figure 5.- Helium-bubble flow visualization. Effect of angle of attack on basic wing. $\beta = 0^\circ$.



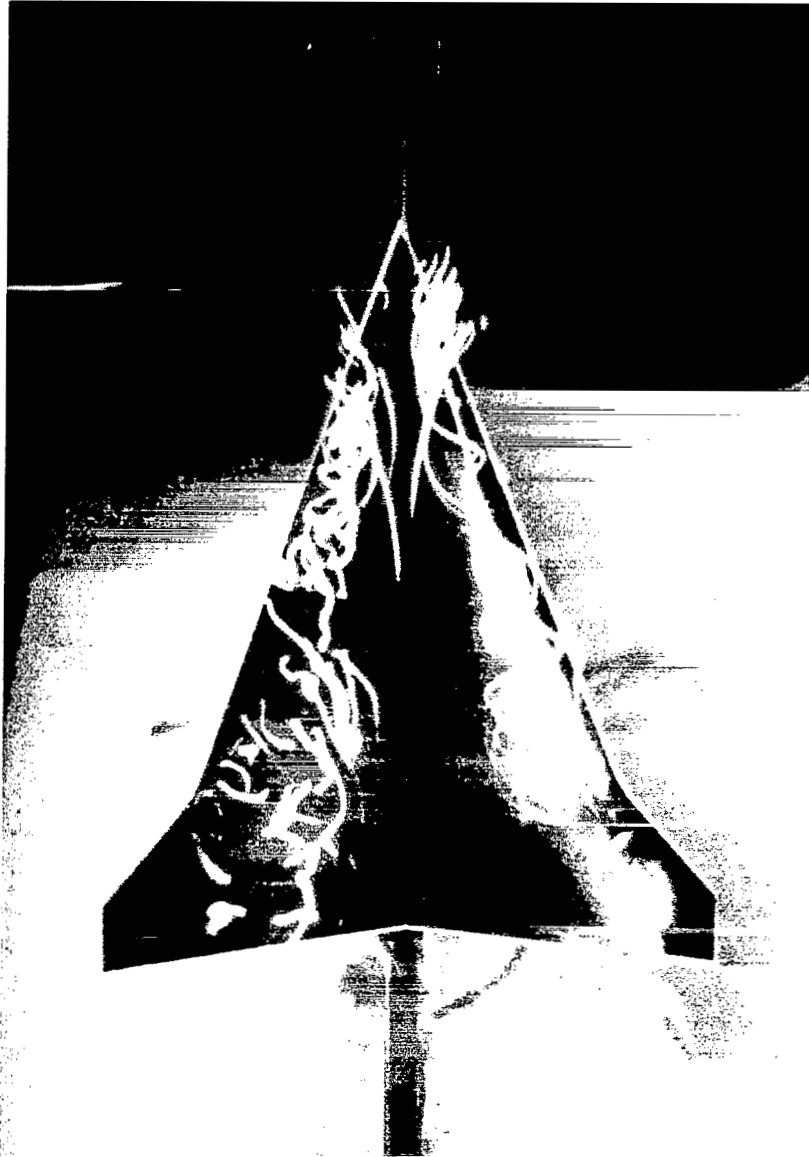
(c) $\alpha = 25^\circ$.



(d) $\alpha = 30^\circ$.

L-81-213

Figure 5.- Continued.



L-81-214

(e) $\alpha = 35^\circ$.

Figure 5.- Concluded.



(a) $\alpha = 20^\circ$.



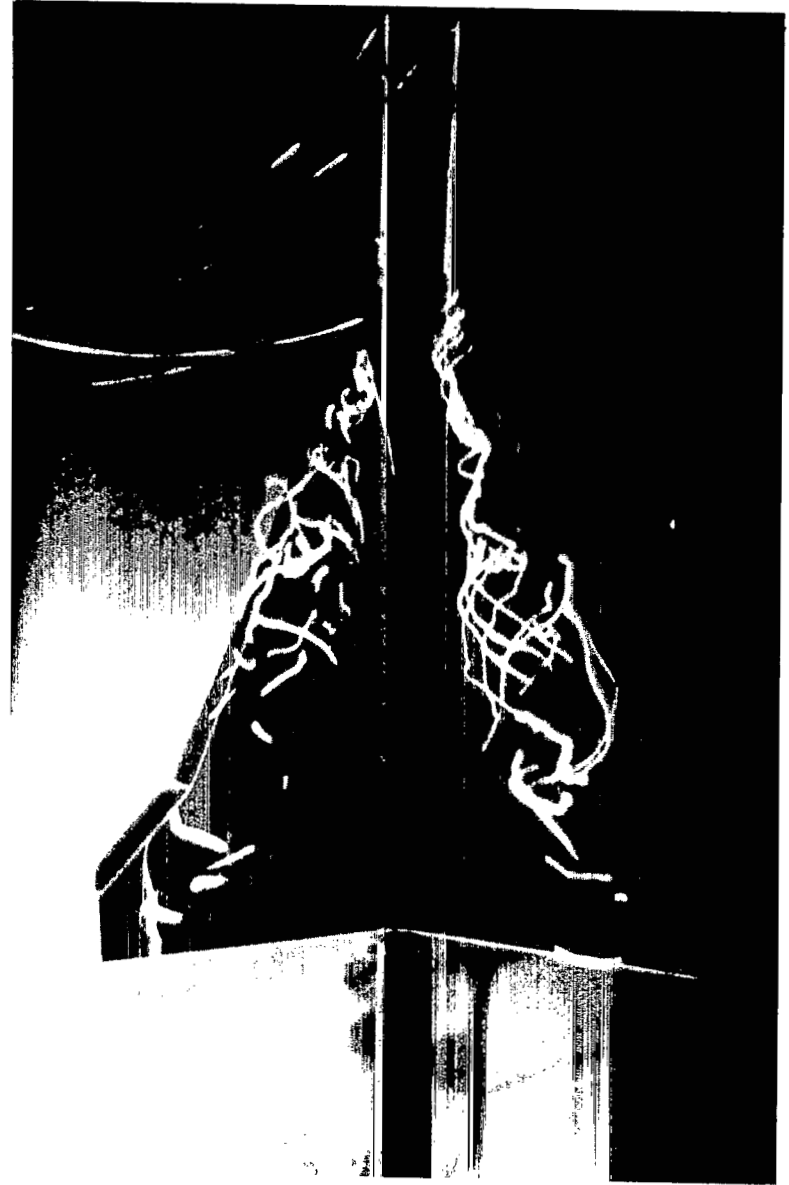
(b) $\alpha = 25^\circ$.

L-81-215

Figure 6.- Helium-bubble flow visualization. Effect of angle of attack on plain-vortex-flap configuration. $\delta_{f,le} = 15^\circ$; $\beta = 0^\circ$.



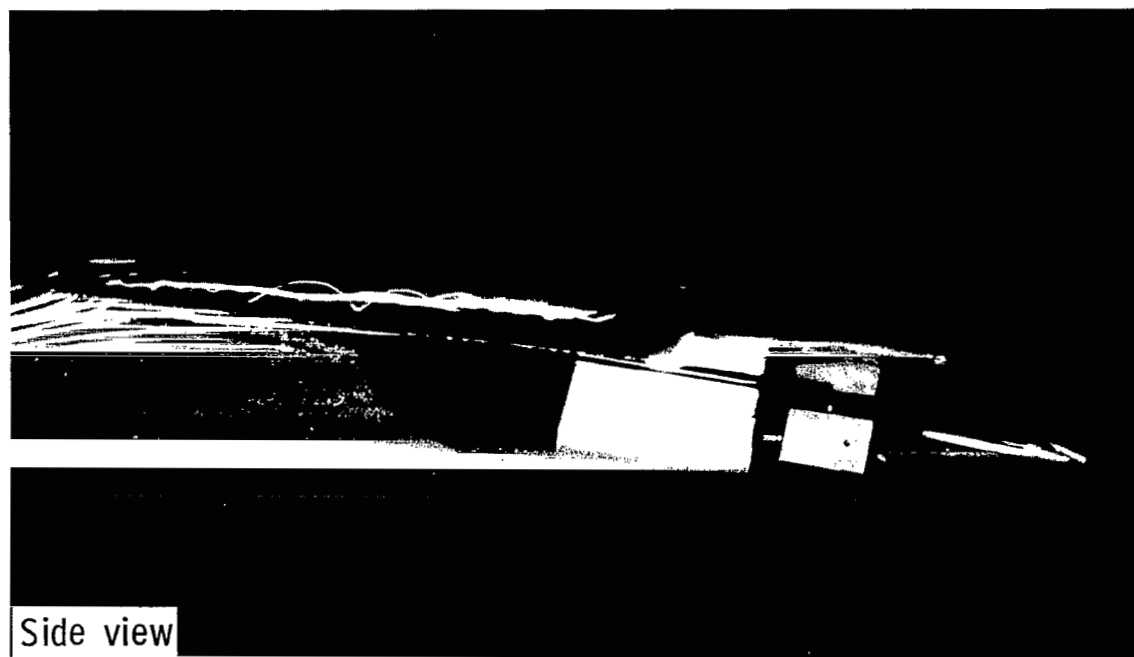
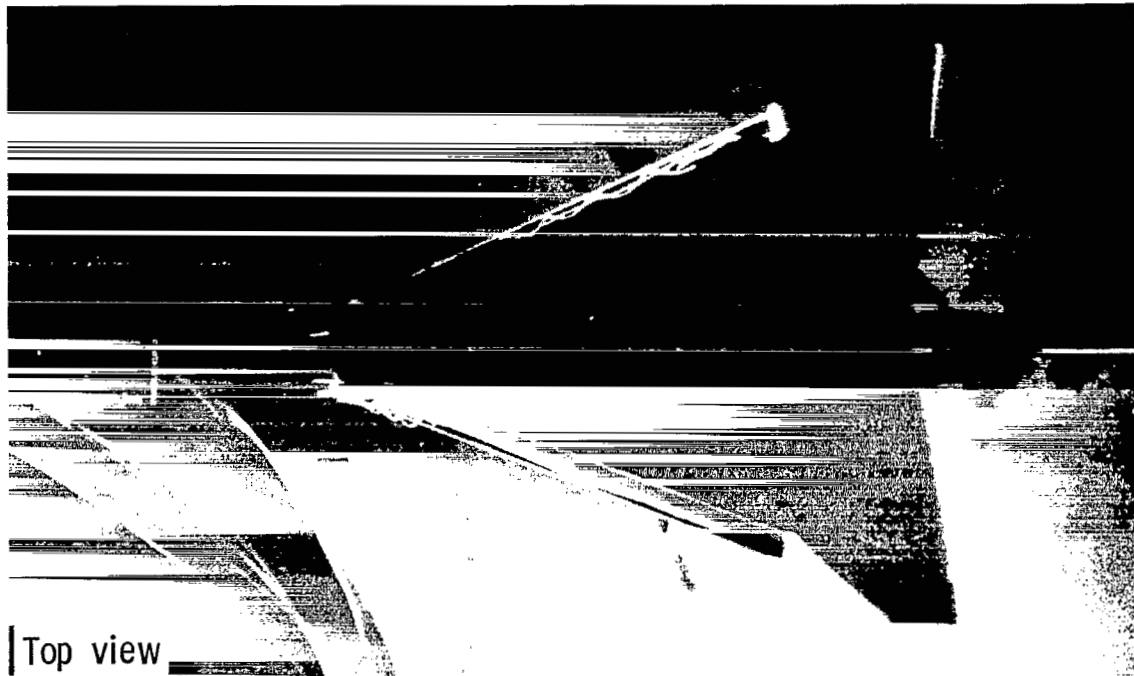
(c) $\alpha = 30^\circ$.



(d) $\alpha = 35^\circ$.

L-81-216

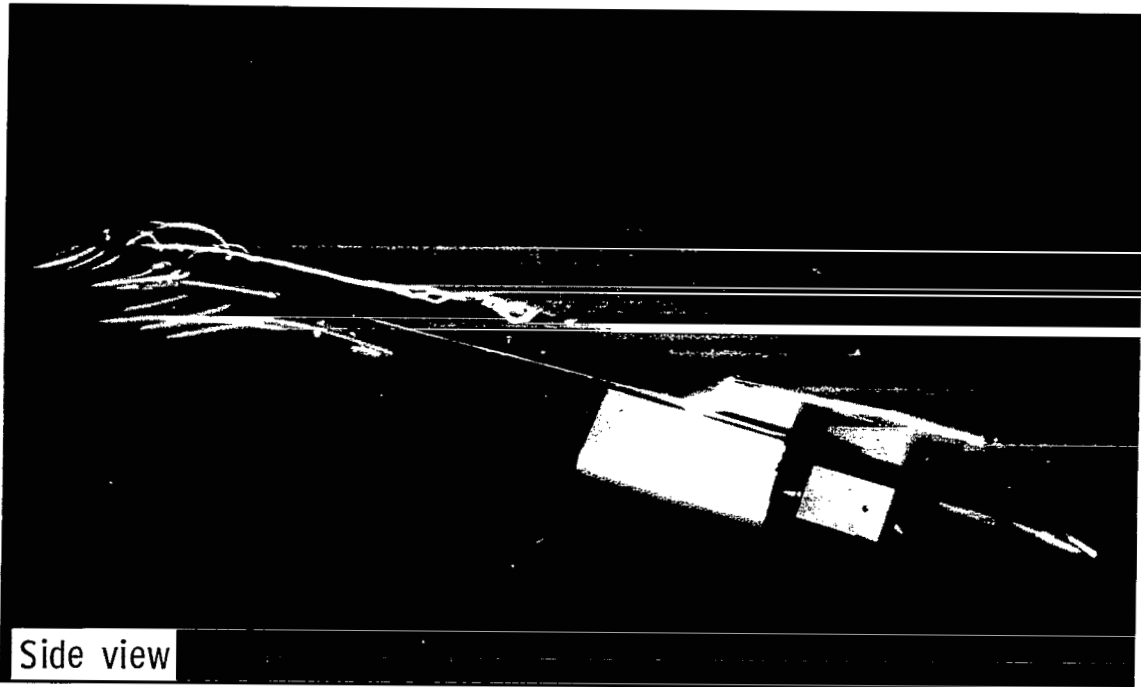
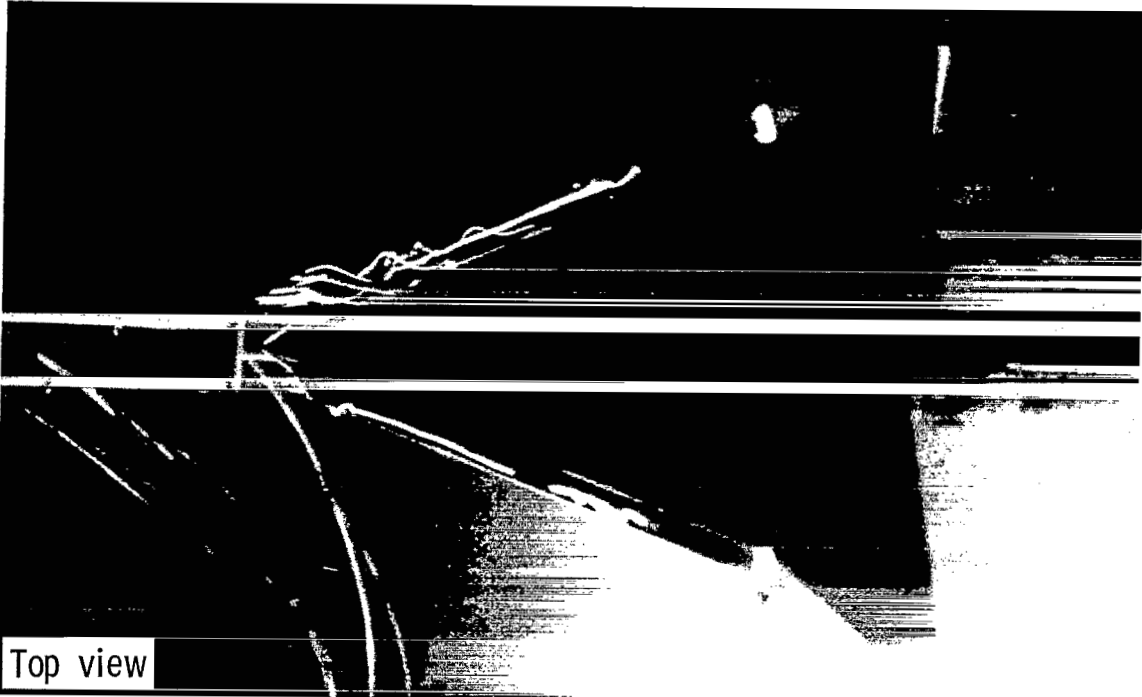
Figure 6.- Concluded.



L-81-217

(a) $\alpha = 15^\circ$.

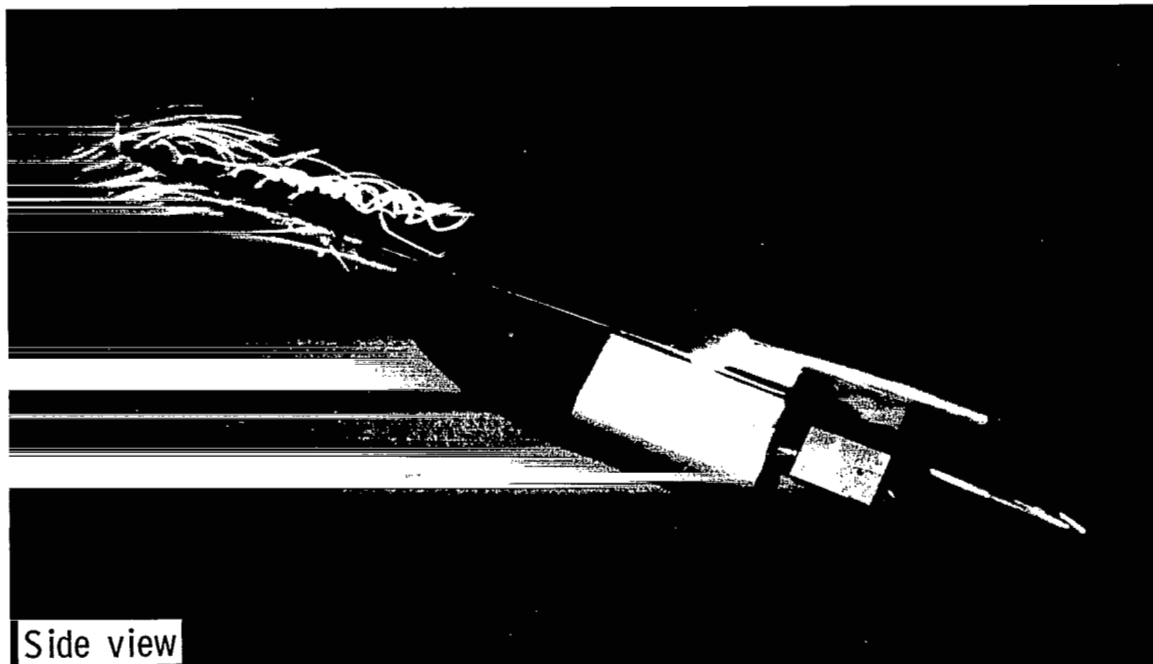
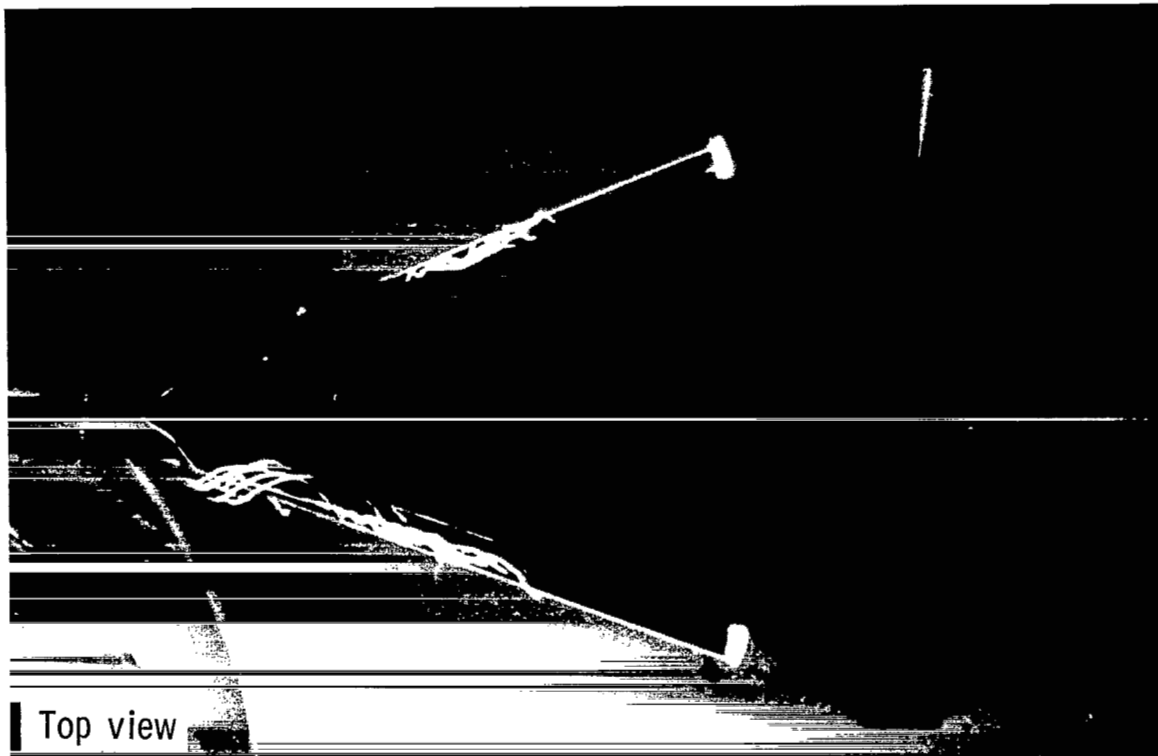
Figure 7.- Helium-bubble flow visualization. Effect of angle of attack on tabbed-vortex-flap configuration. $\beta = 0^\circ$.



L-81-218

(b) $\alpha = 20^\circ$.

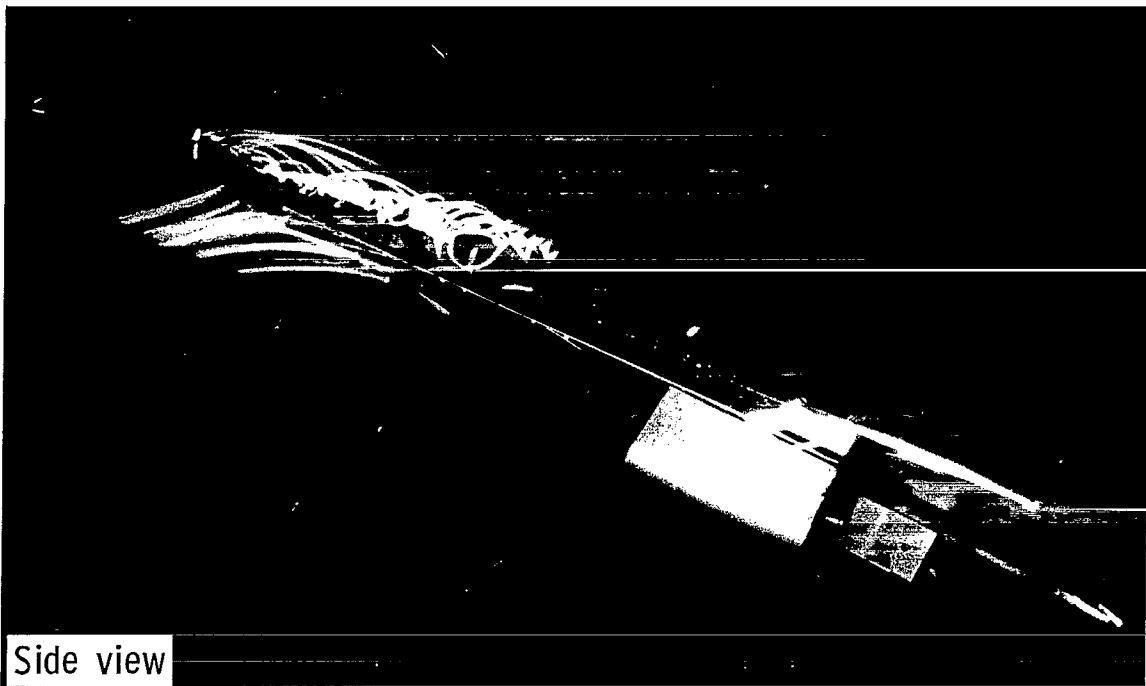
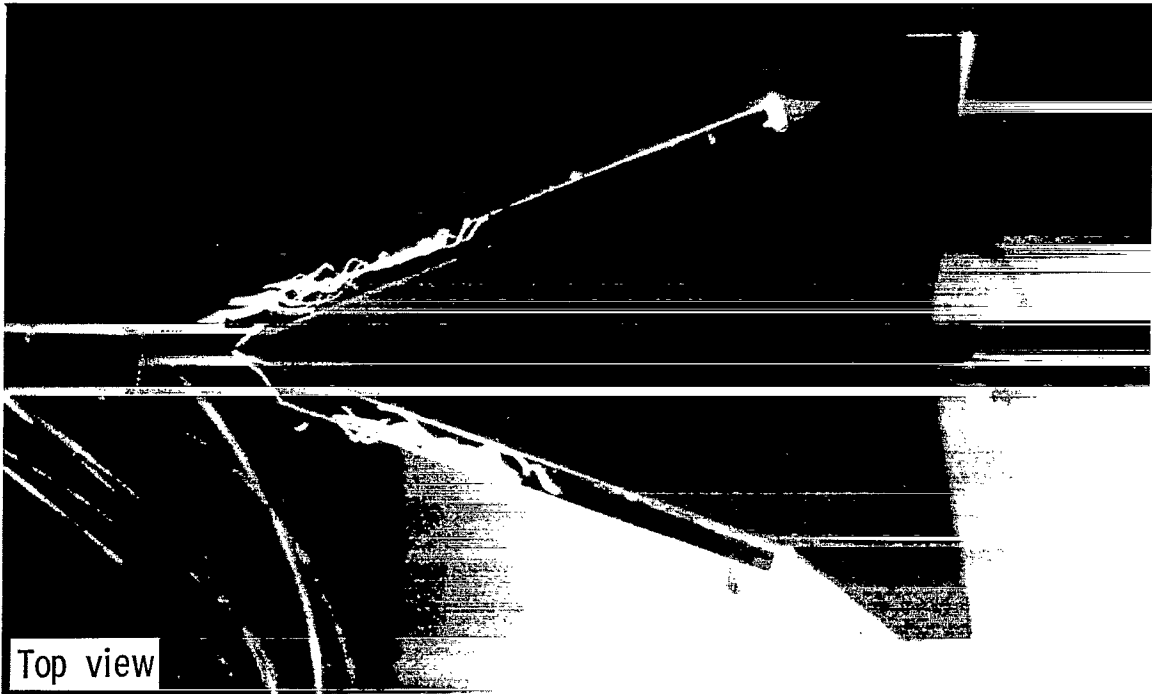
Figure 7.- Continued.



L-81-219

(c) $\alpha = 25^\circ$.

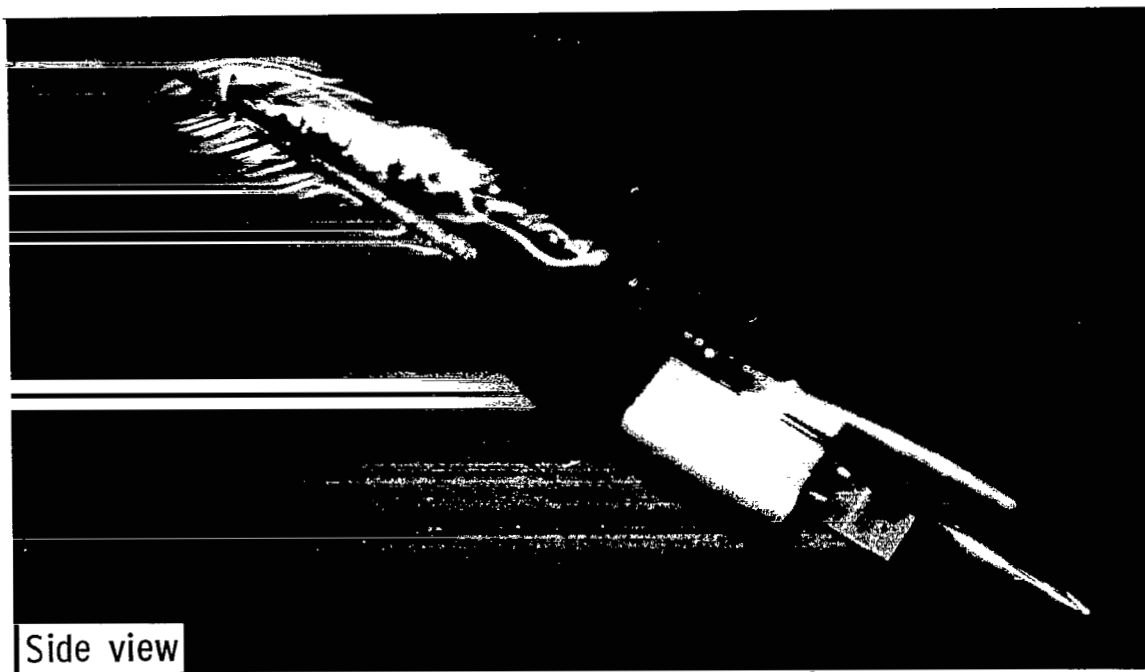
Figure 7.- Continued.



L-81-220

(d) $\alpha = 30^\circ$.

Figure 7.- Continued.



L-81-221

(e) $\alpha = 35^\circ$.

Figure 7.- Concluded.



$\beta = -4^\circ$

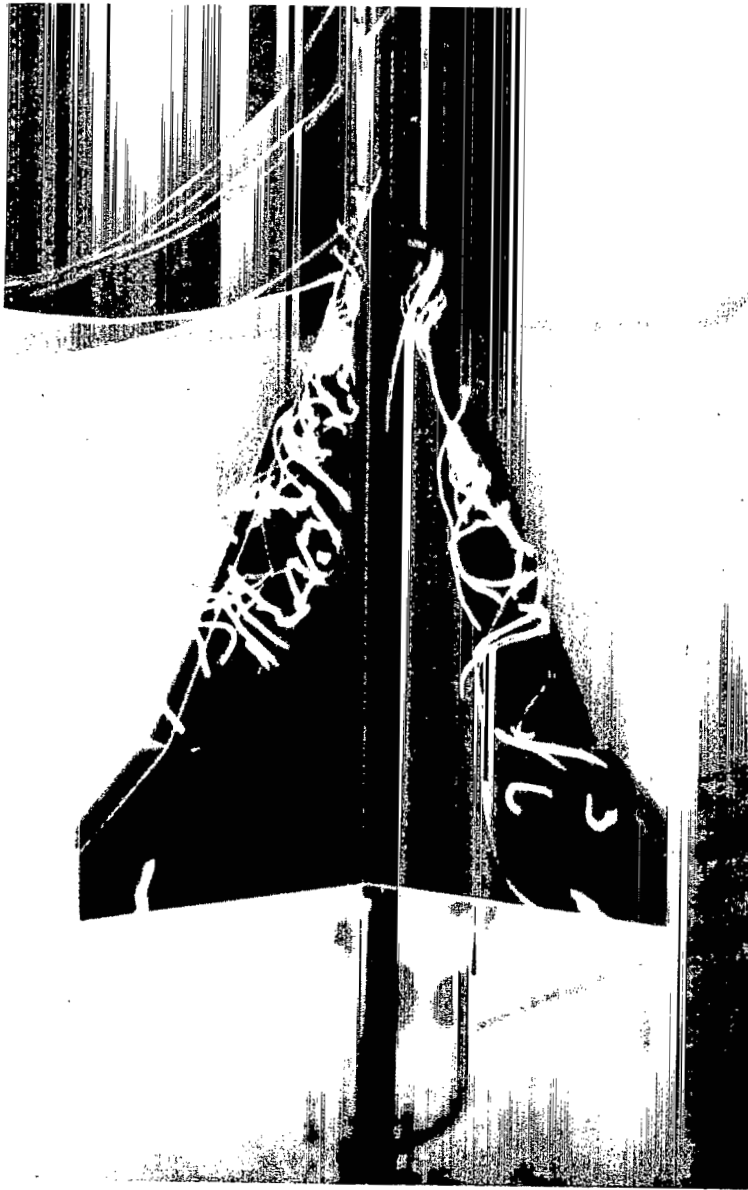


$\beta = -8^\circ$

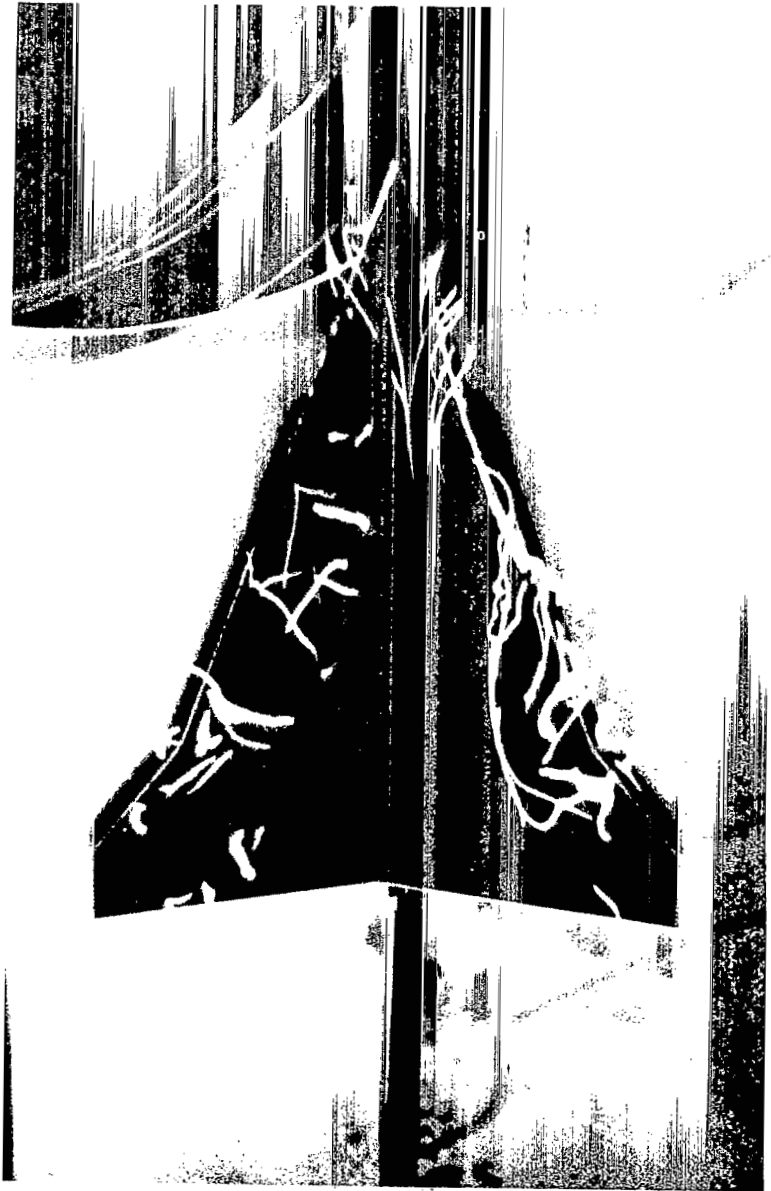
(a) Basic wing.

L-81-222

Figure 8.- Helium-bubble flow visualization. Effect of sideslip at $\alpha = 35^\circ$.



$\beta = -40^\circ$



$\beta = -80^\circ$

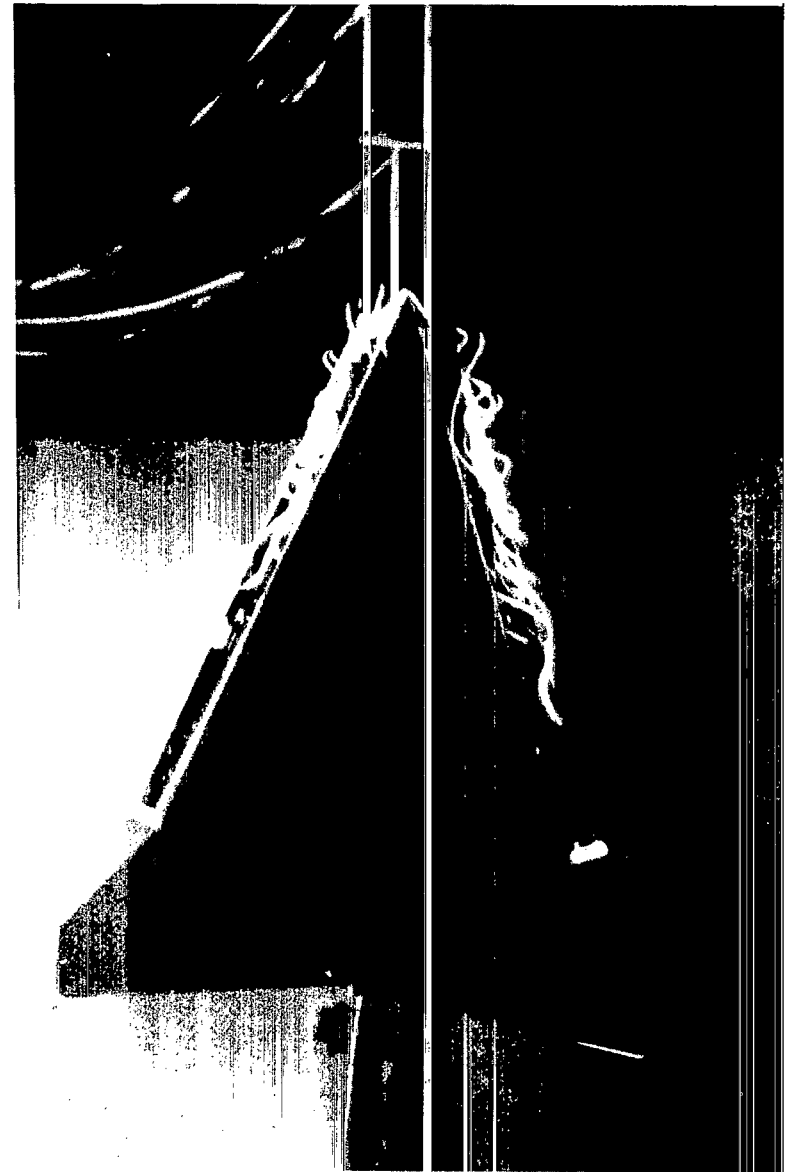
(b) Plain vortex flap.

L-81-223

Figure 8.- Continued.



$\beta = -40^\circ$



$\beta = -80^\circ$

(c) Tabbed vortex flap.

Figure 8.- Concluded.

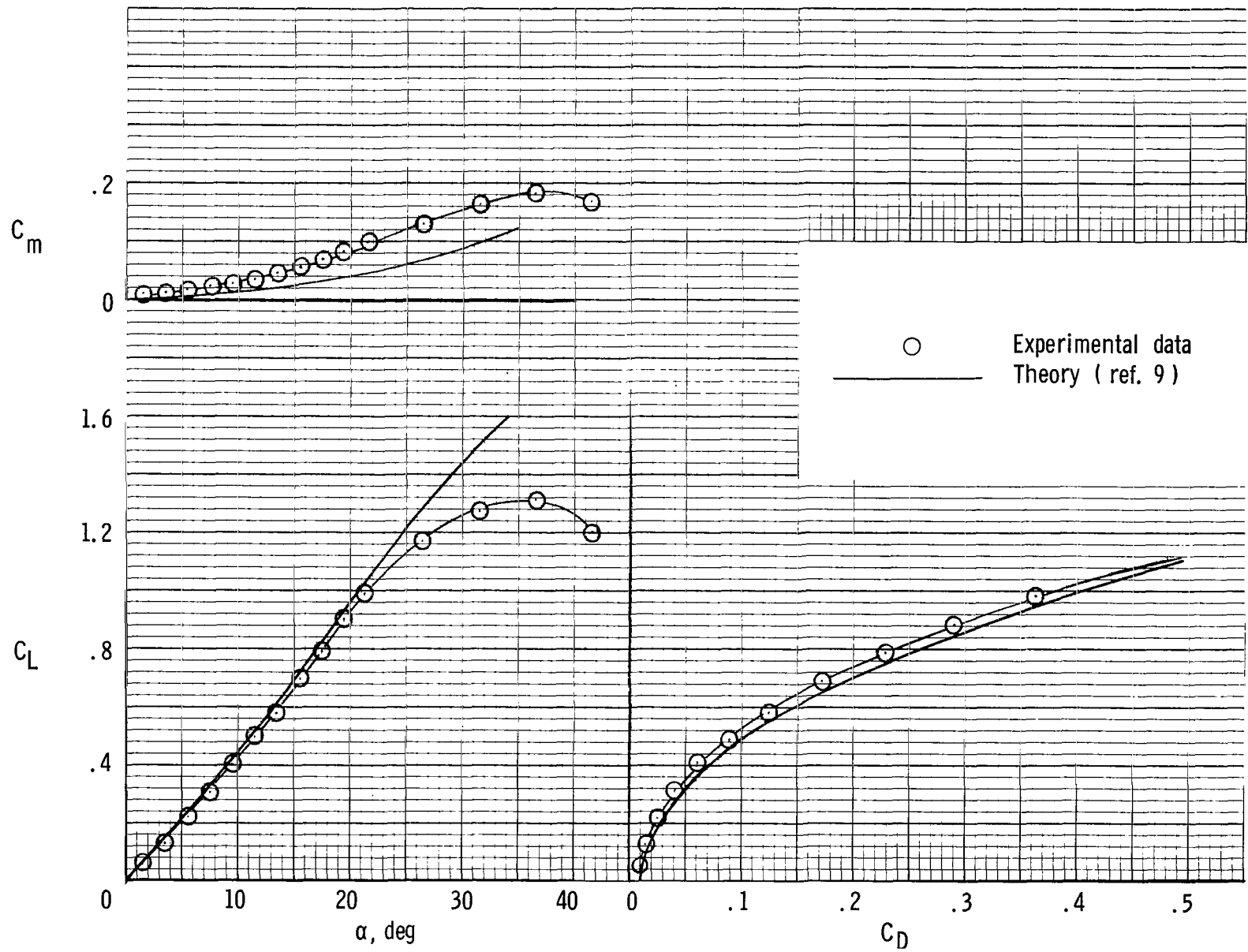
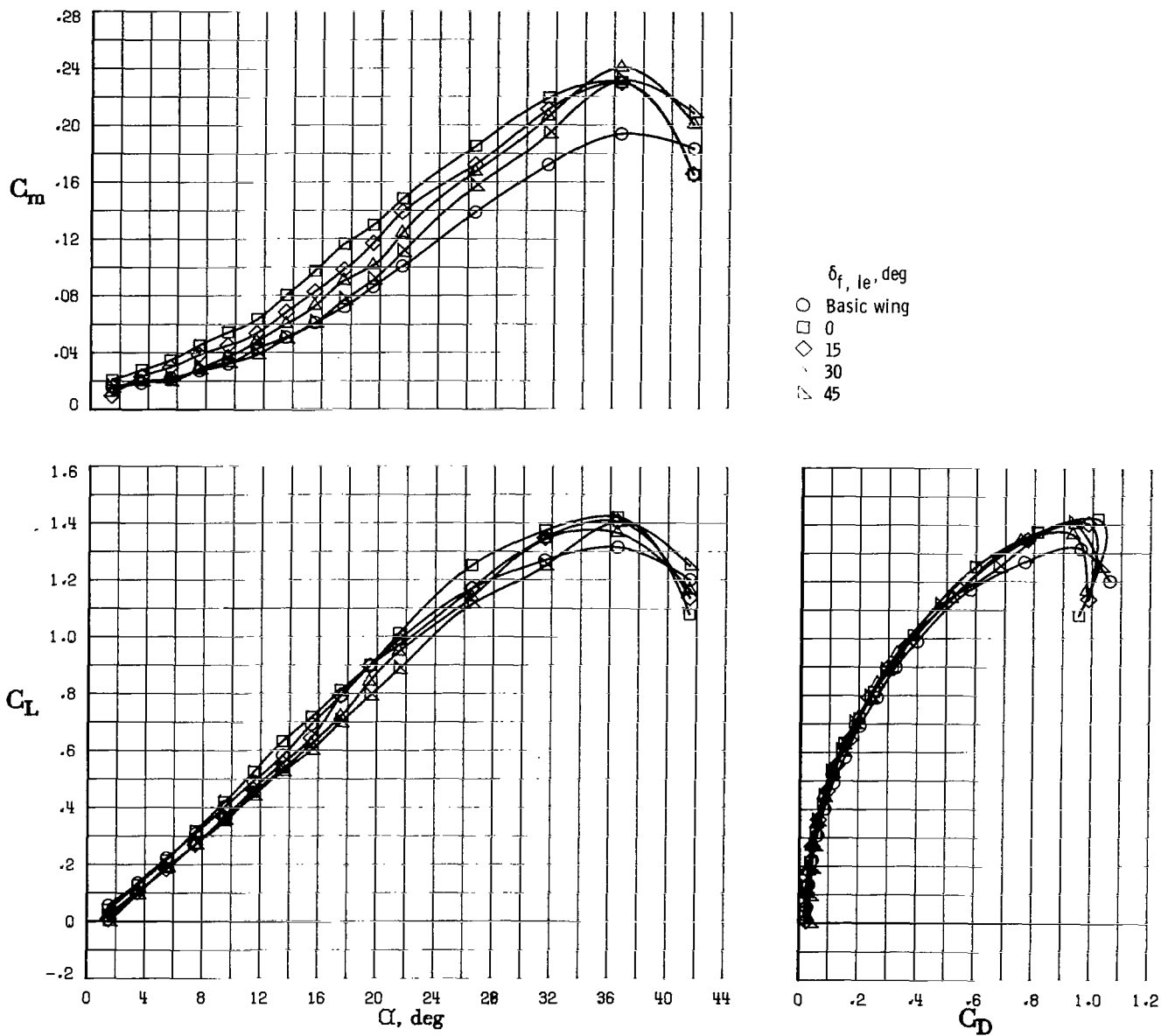
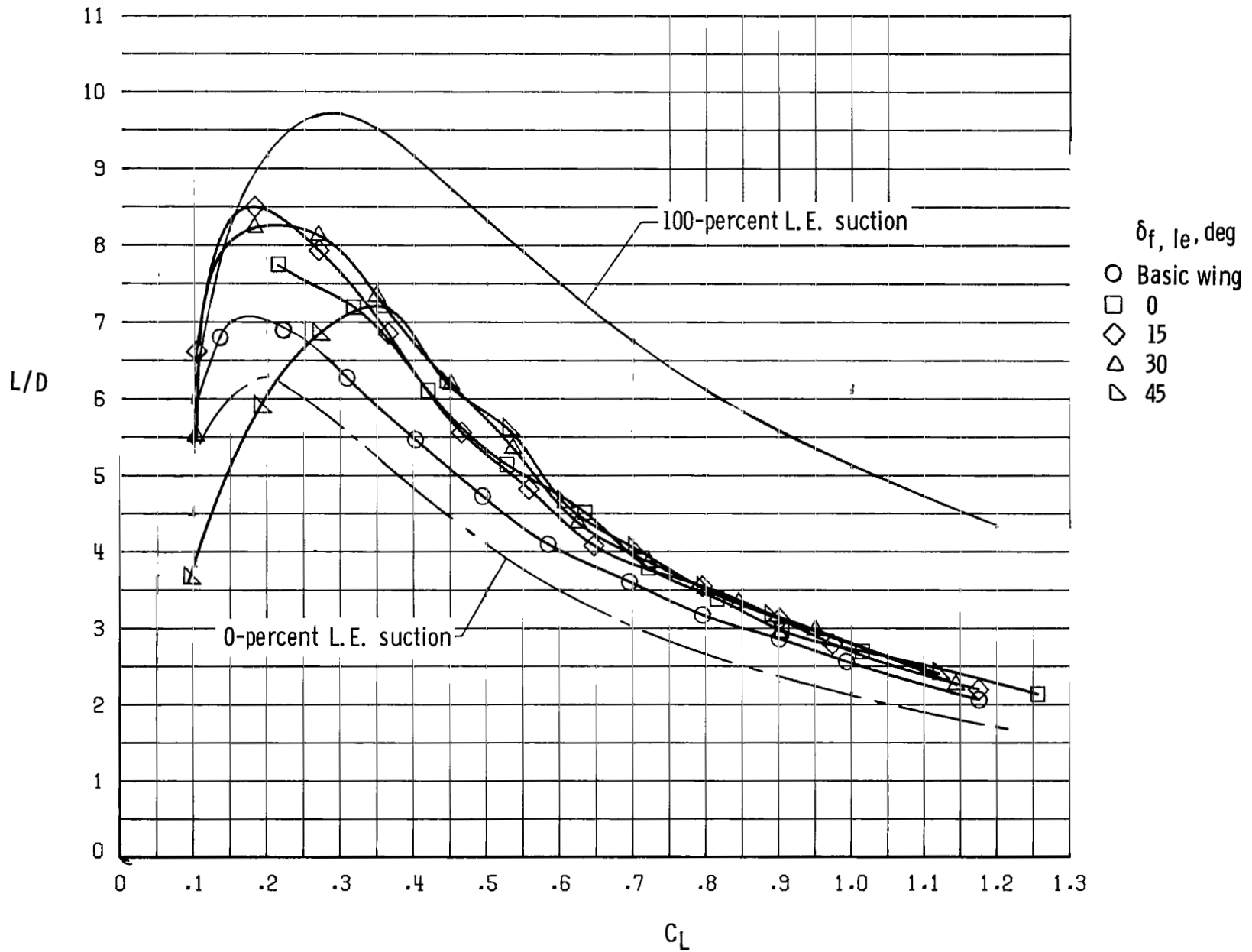


Figure 9.- Comparison of experimental data with theory.



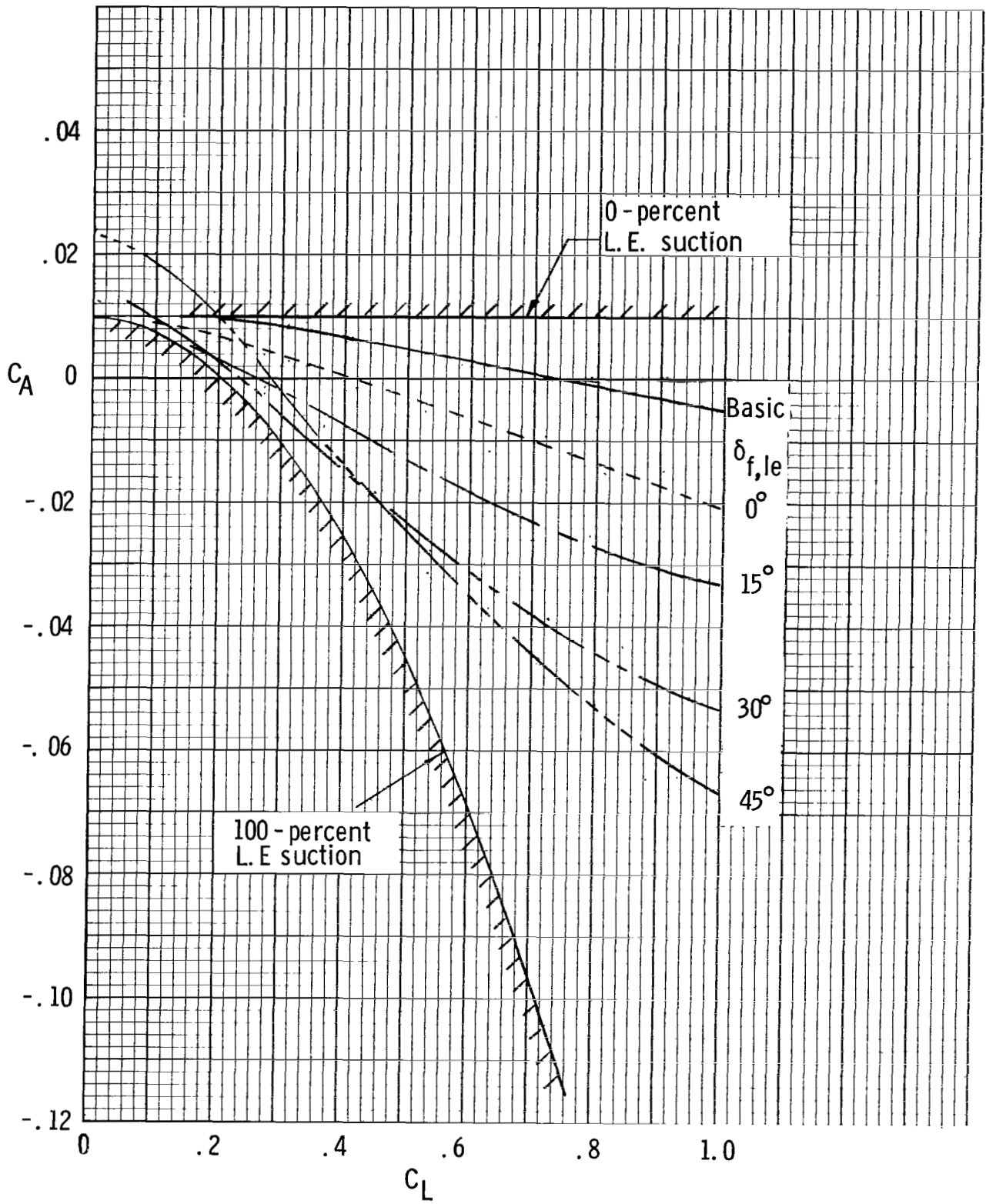
(a) Longitudinal characteristics.

Figure 10.- Effect of leading-edge-flap deflection. Basic wing with plain vortex flaps.



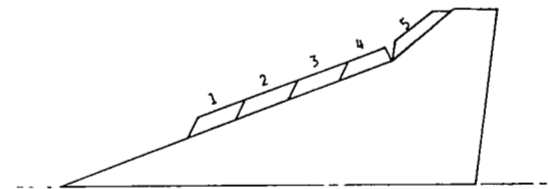
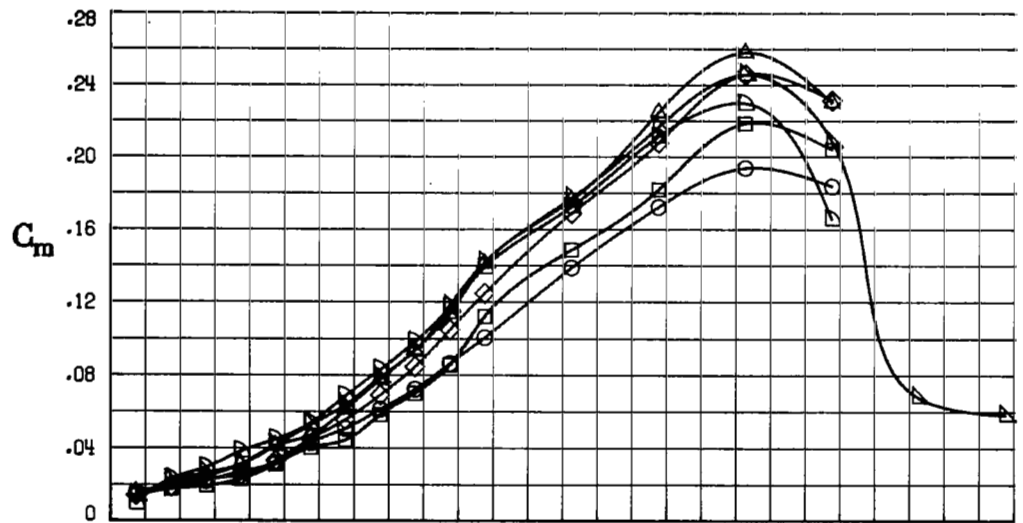
(b) L/D characteristics.

Figure 10.- Continued.

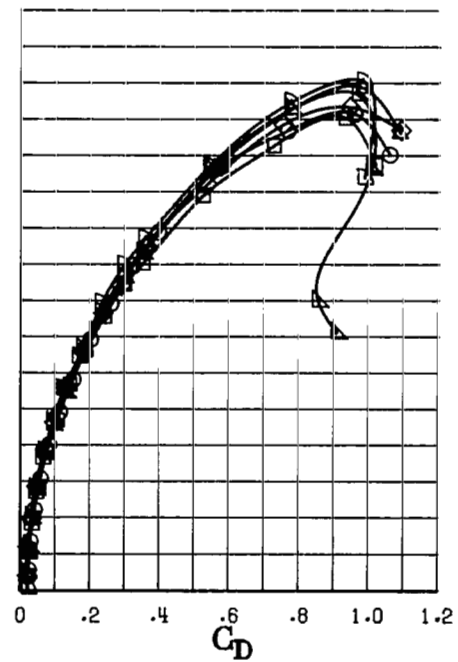
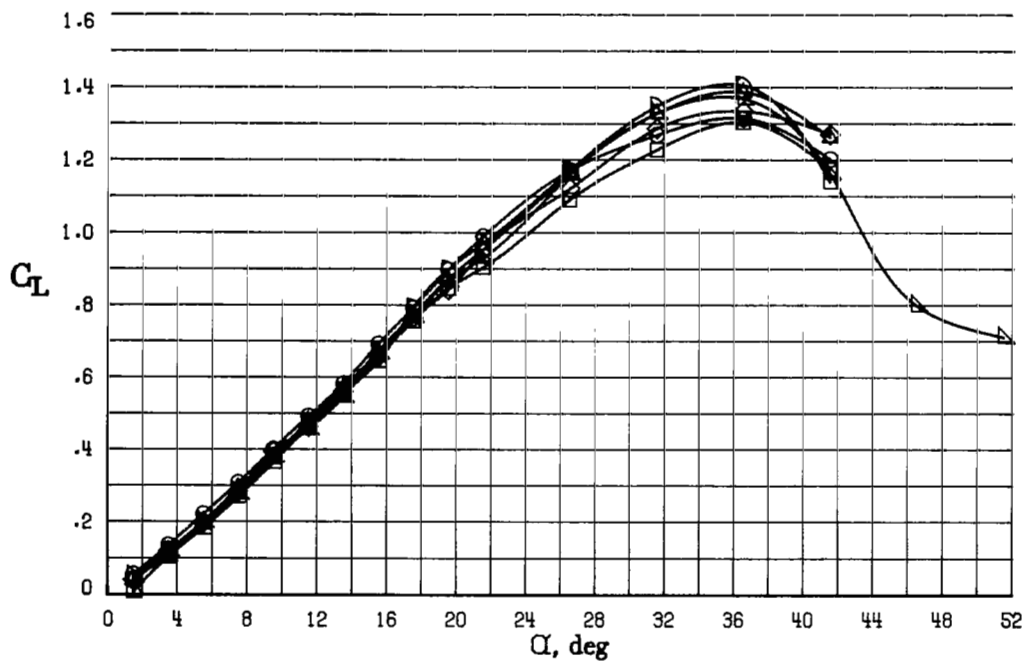


(c) Axial-force characteristics.

Figure 10.- Concluded.

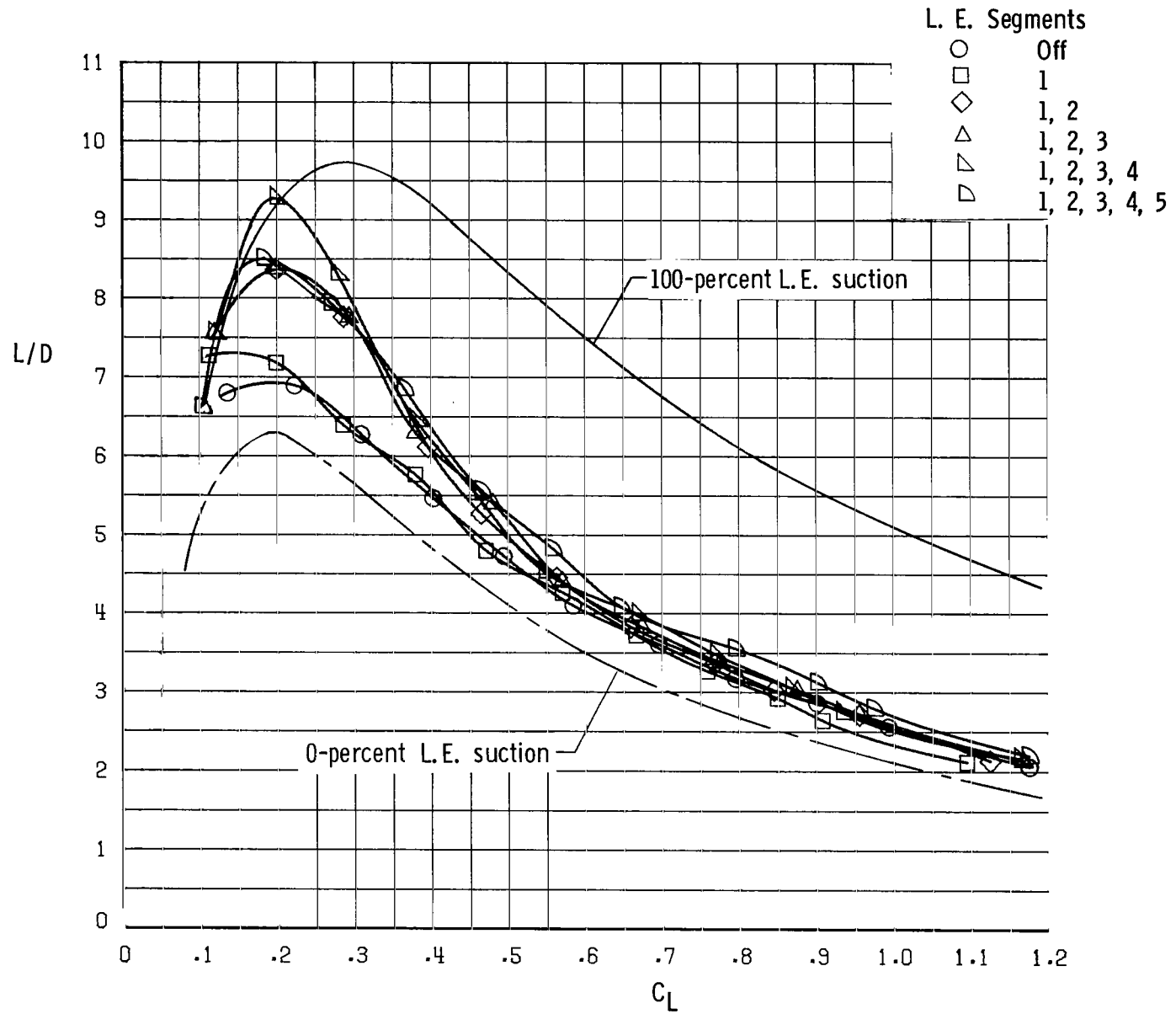


- L. E. Segments
- Off
 - 1
 - ◇ 1, 2
 - △ 1, 2, 3
 - ▽ 1, 2, 3, 4
 - ◻ 1, 2, 3, 4, 5



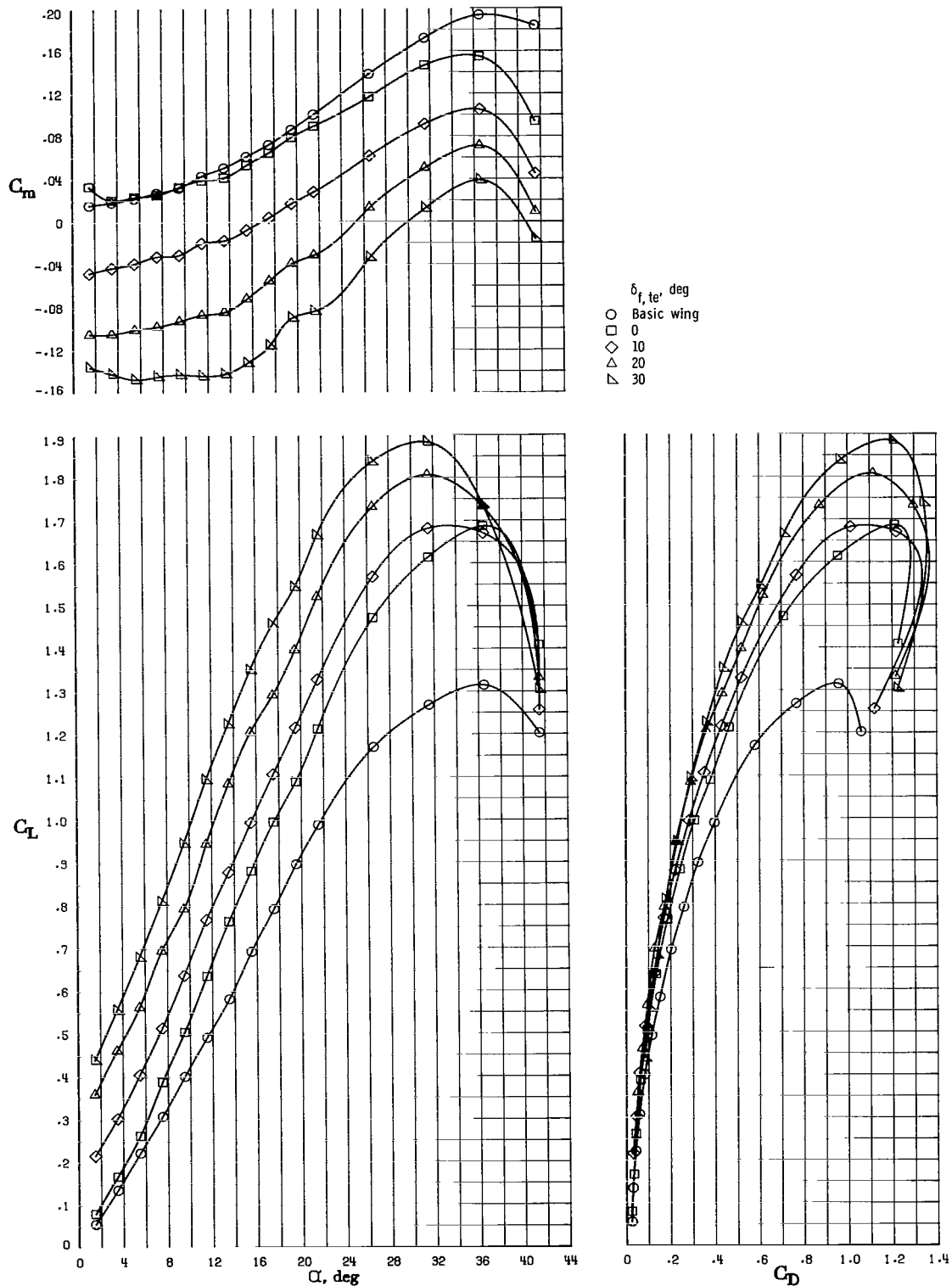
(a) Longitudinal characteristics.

Figure 11.- Buildup of leading-edge segments. Plain vortex flap. $\delta_{f,le} = 15^\circ$.



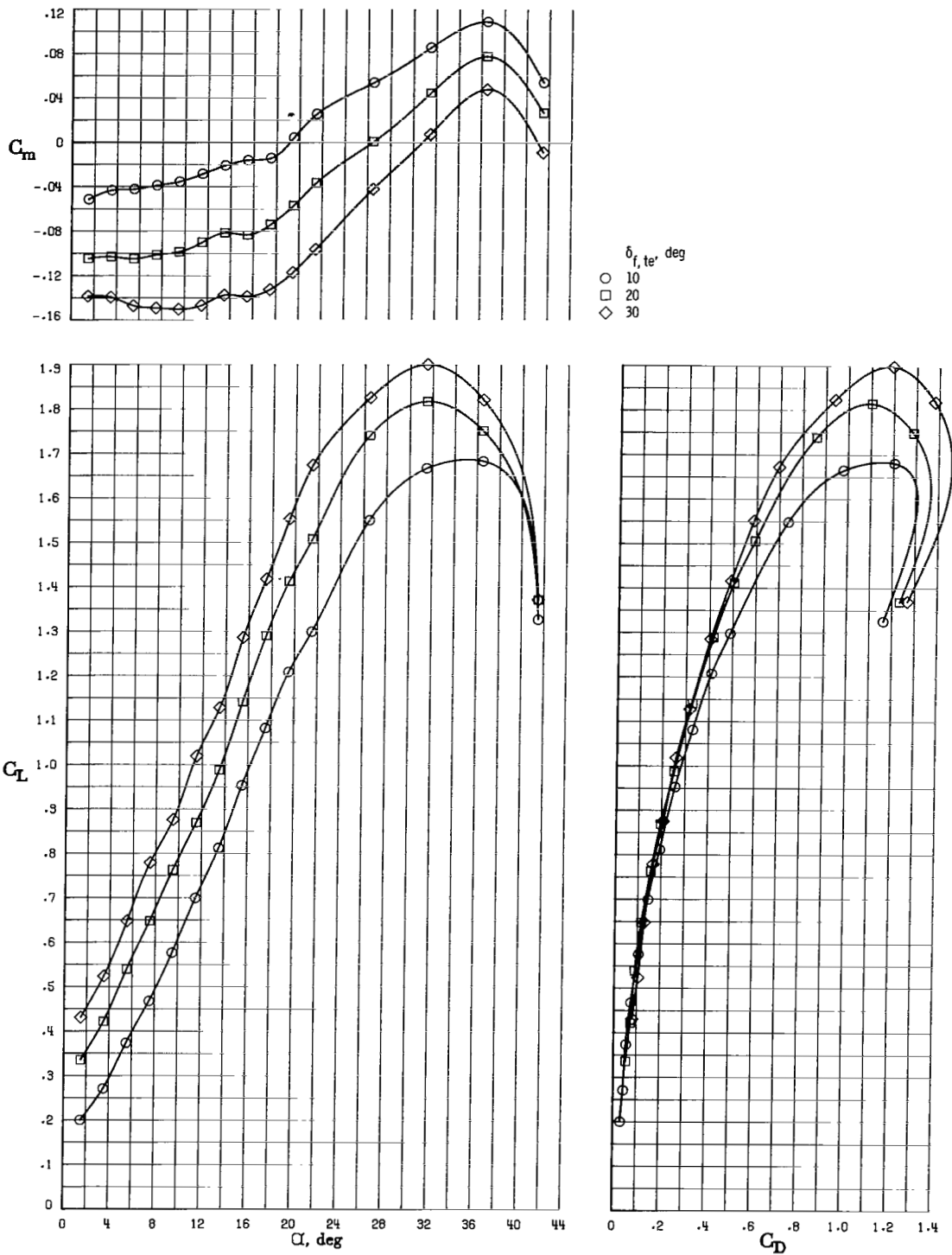
(b) L/D characteristics.

Figure 11.- Concluded.



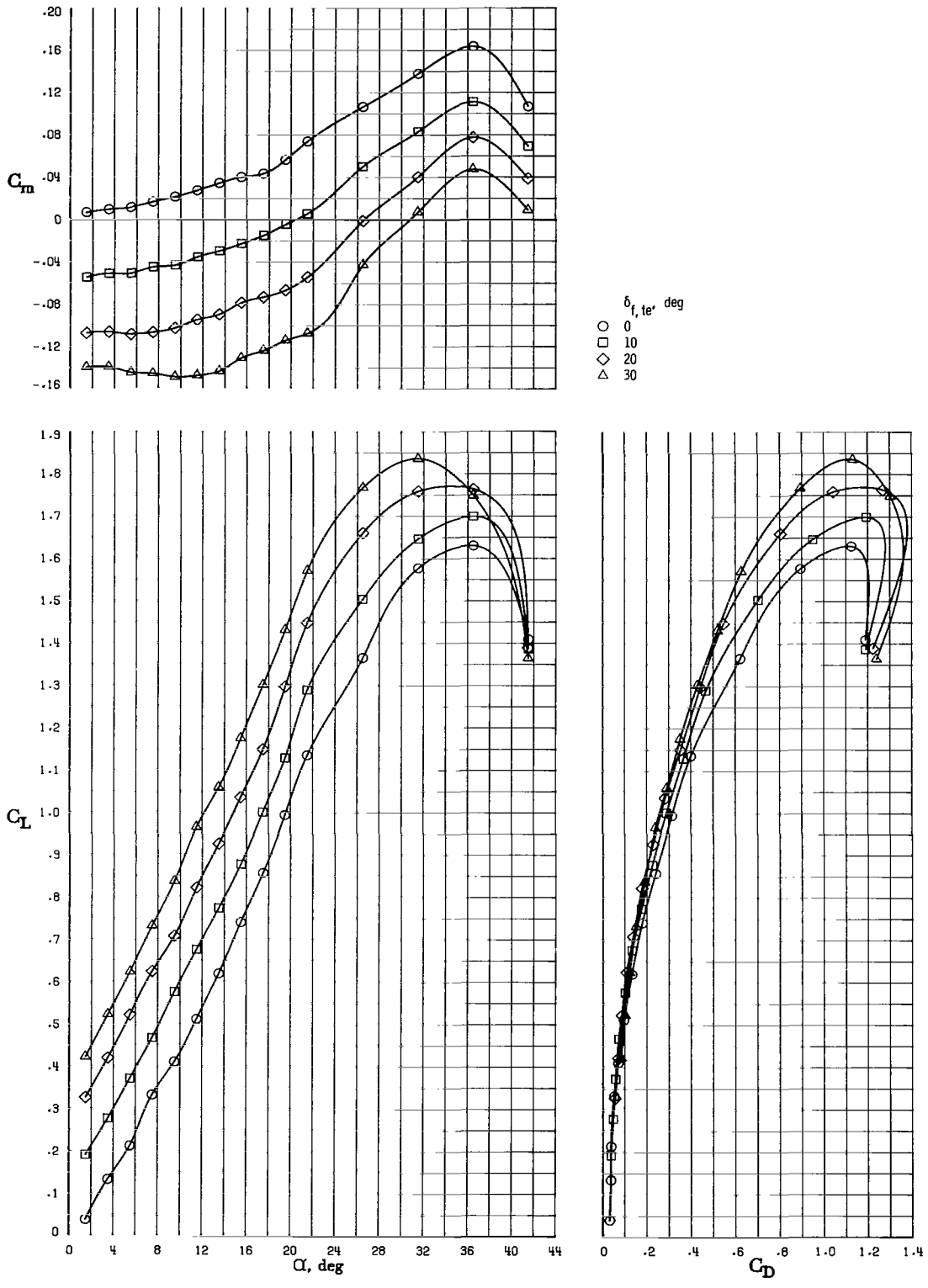
(a) $\delta_{f,le} = 0^\circ$.

Figure 12.- Effect of trailing-edge-flap deflection on plain-vortex-flap configuration.



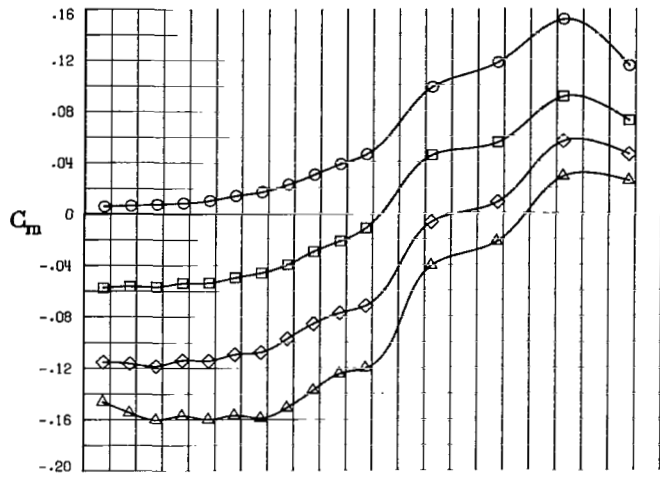
(b) $\delta_{f,le} = 15^\circ$.

Figure 12.- Continued.

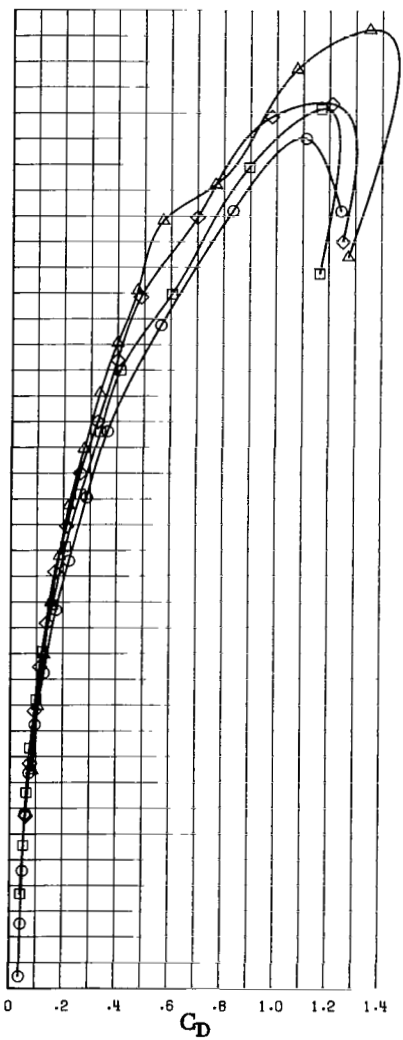
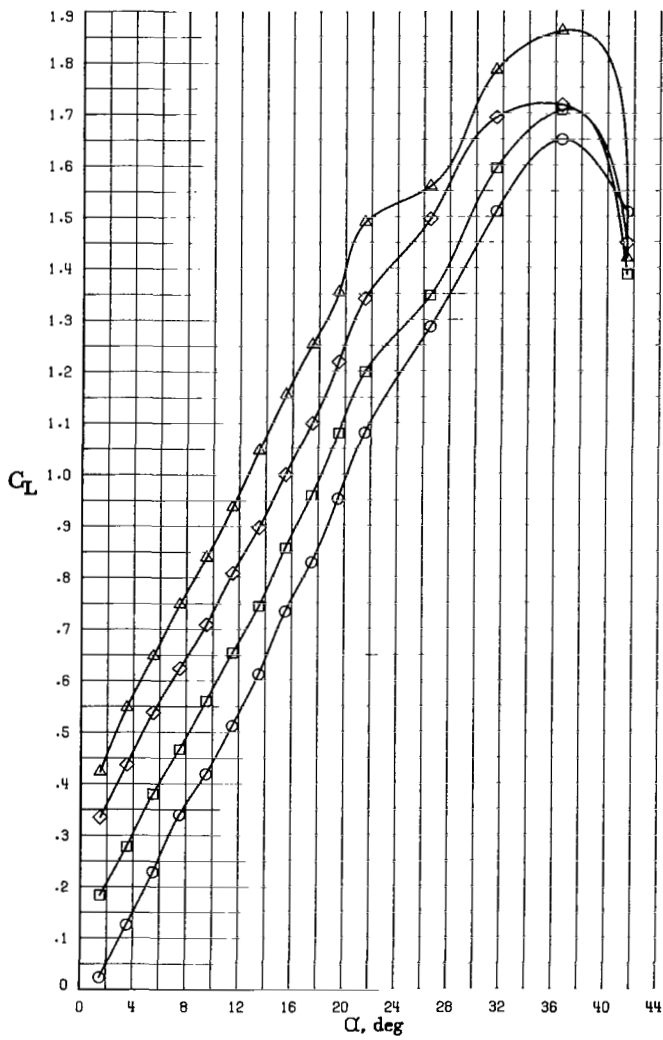


(c) $\delta_{f,le} = 30^\circ$.

Figure 12.- Continued.

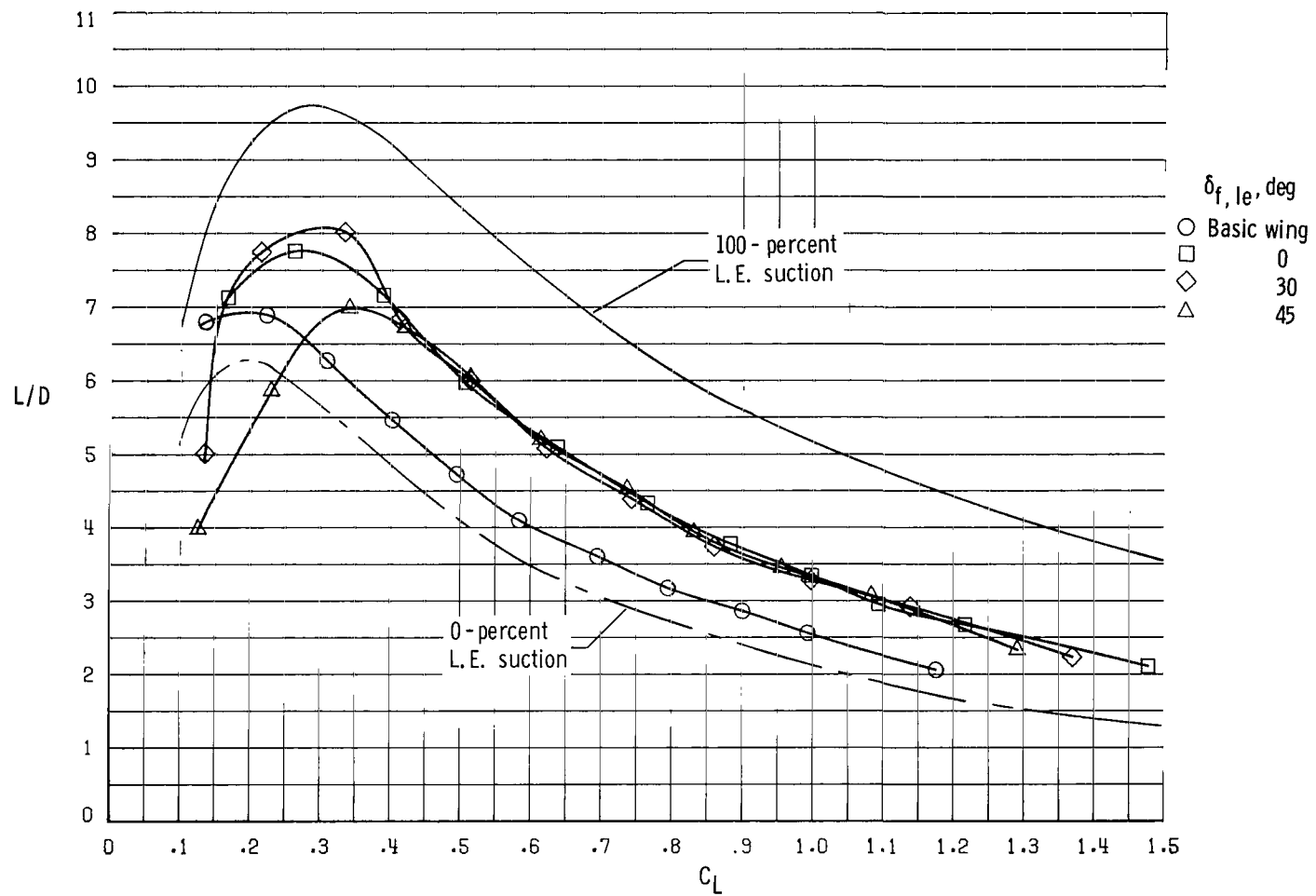


$\delta_{f,te}$ deg
 ○ 0
 □ 10
 ◇ 20
 △ 30



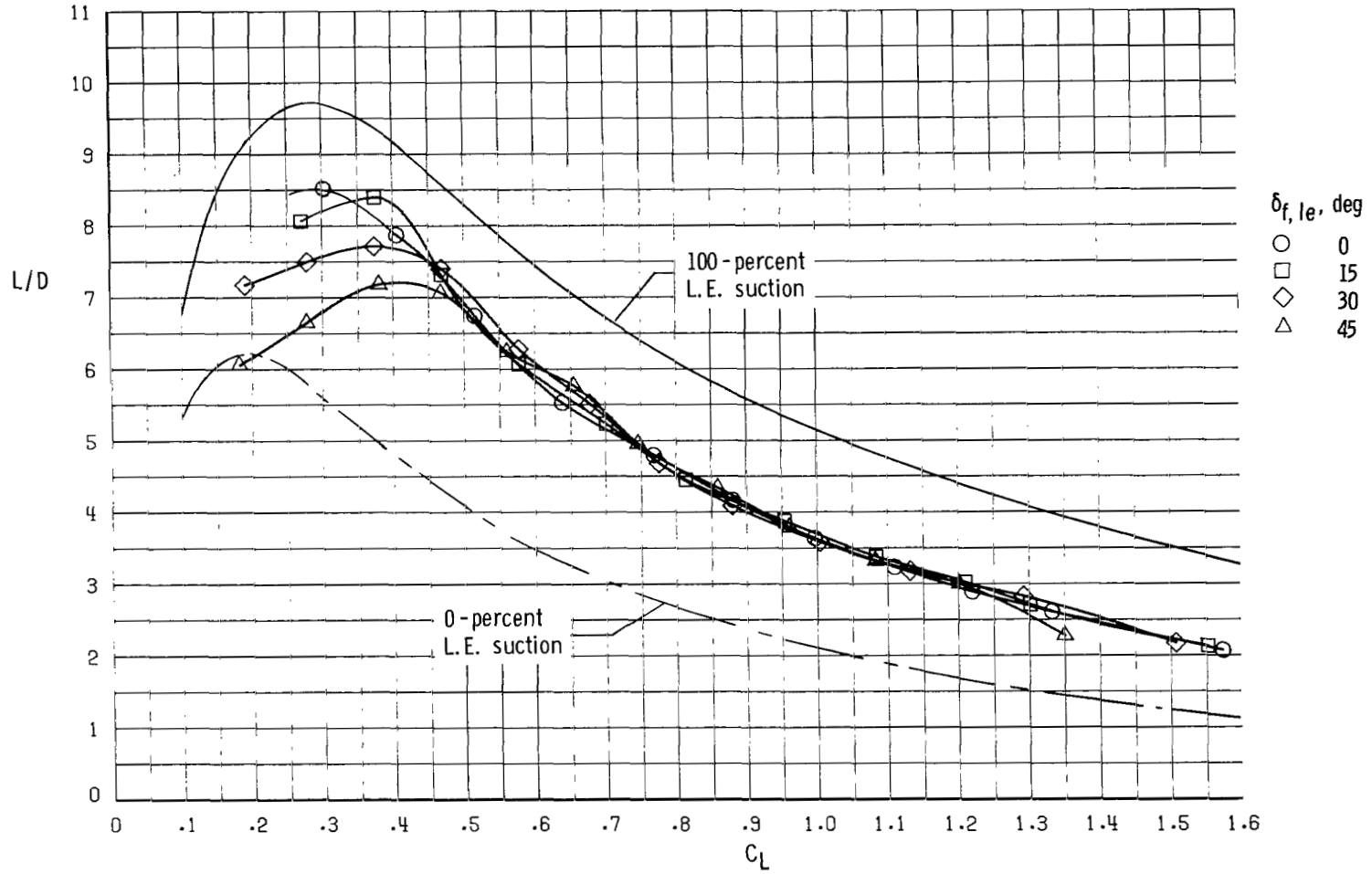
(d) $\delta_{f,le} = 45^\circ$.

Figure 12.- Concluded.



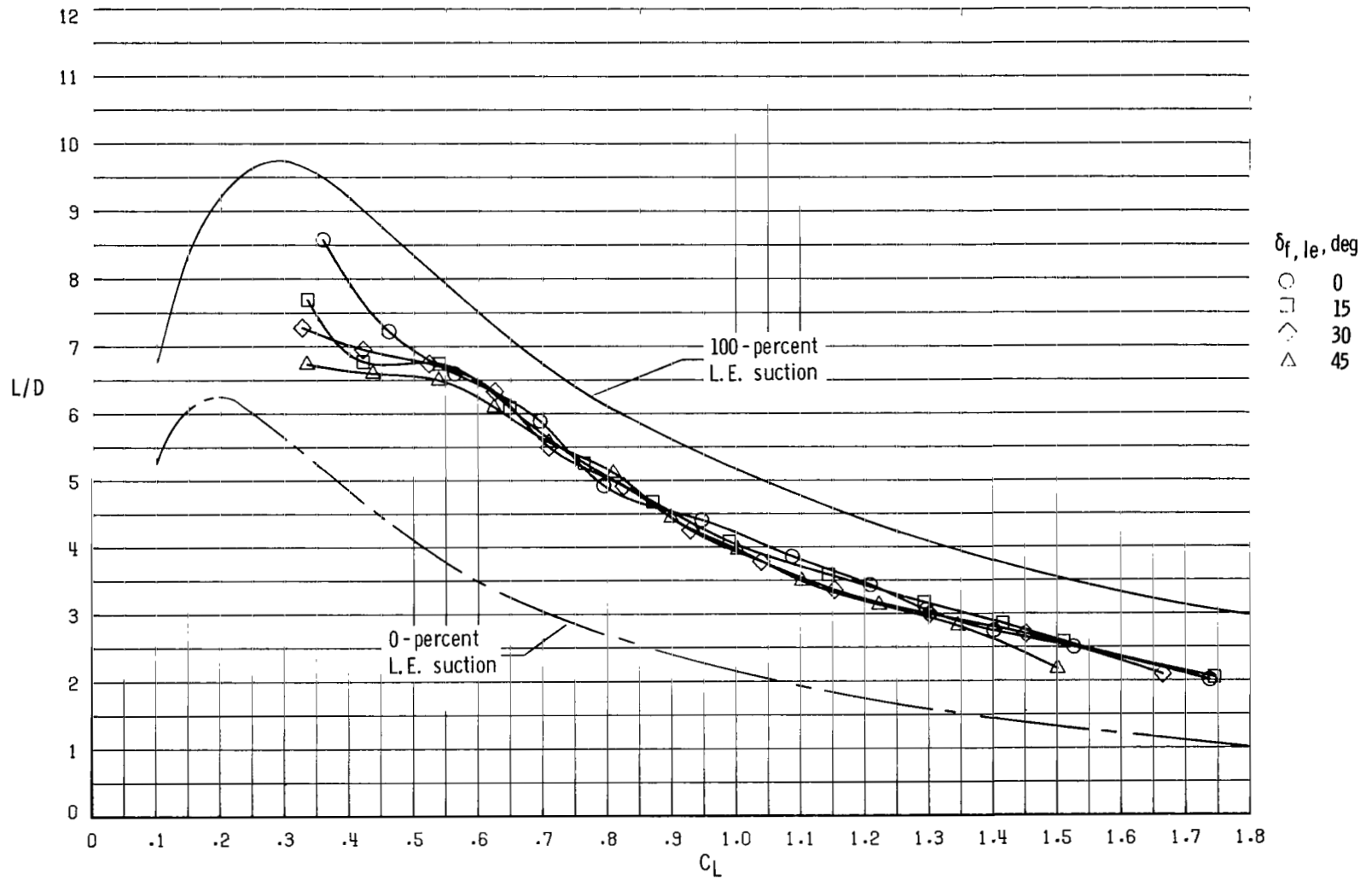
(a) $\delta_{f,te} = 0^\circ$.

Figure 13.- Untrimmed L/D characteristics for various leading- and trailing-edge combinations.



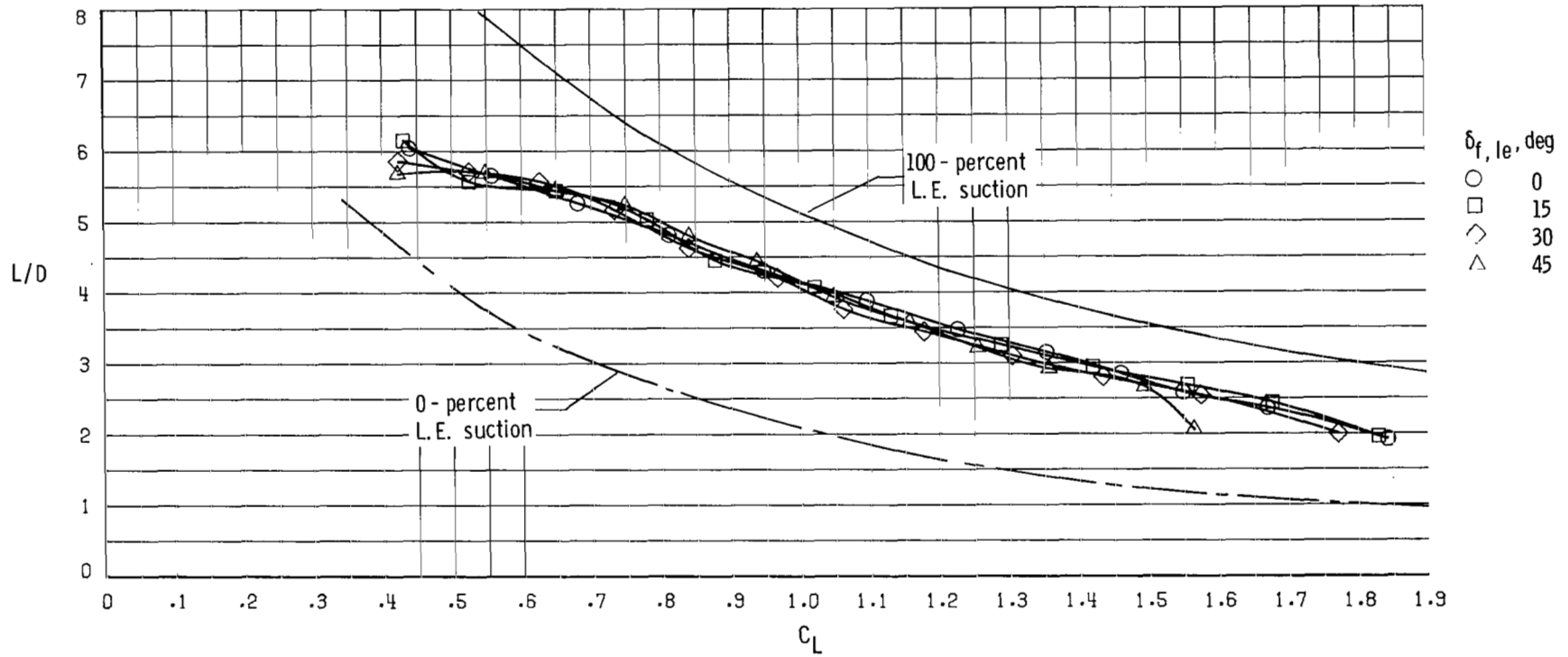
(b) $\delta_{f,te} = 10^\circ$.

Figure 13.- Continued.



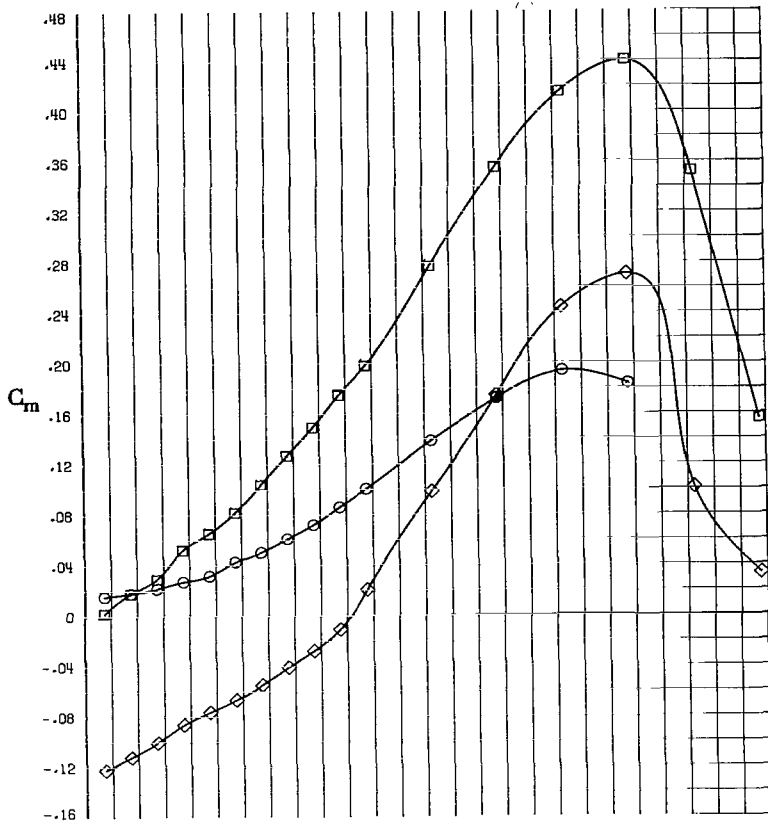
(c) $\delta_{f,te} = 20^\circ$.

Figure 13.- Continued.

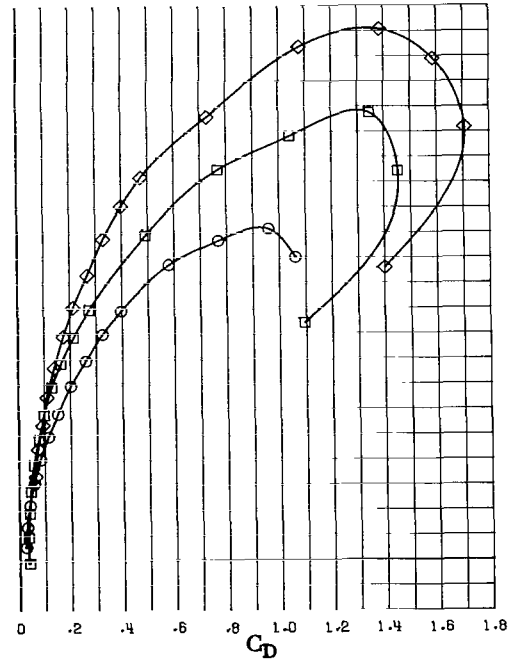
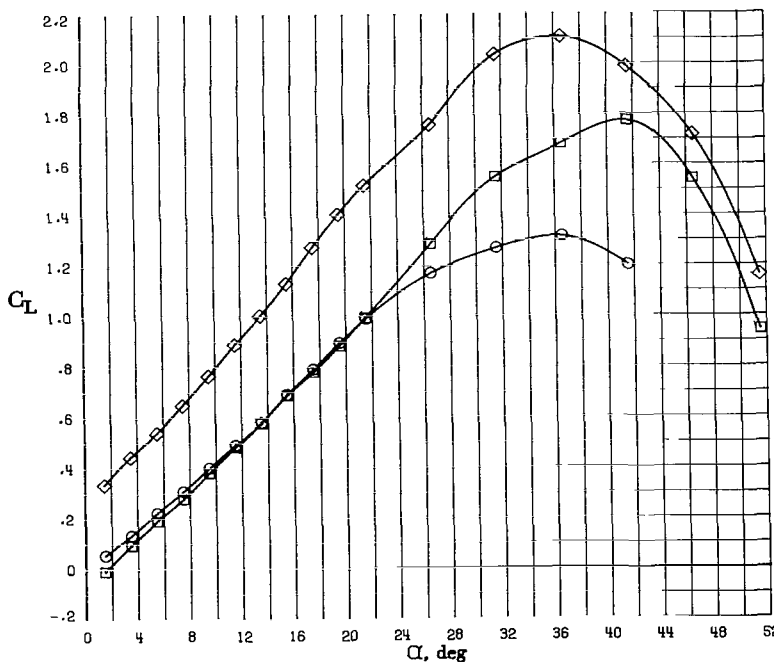


(d) $\delta_{f,te} = 30^\circ$.

Figure 13.- Concluded.

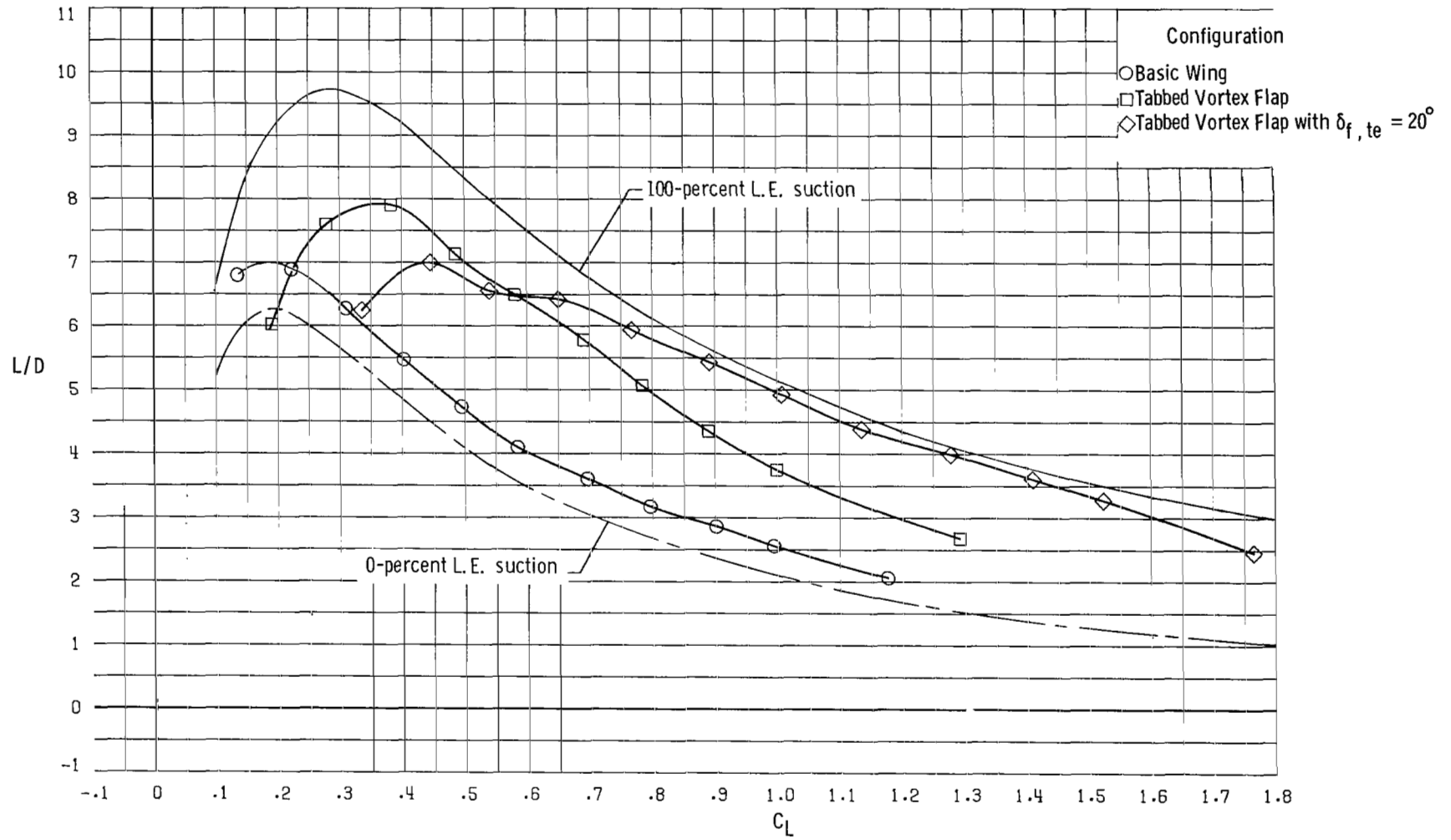


Configuration
 ○ Basic wing
 □ Tabbed vortex flap
 ◇ Tabbed vortex flap with $\delta_{f,te} = 20^\circ$



(a) Longitudinal characteristics.

Figure 14.- Effect of tabbed vortex flap on longitudinal aerodynamic characteristics.



(b) L/D characteristics.

Figure 14.- Concluded.

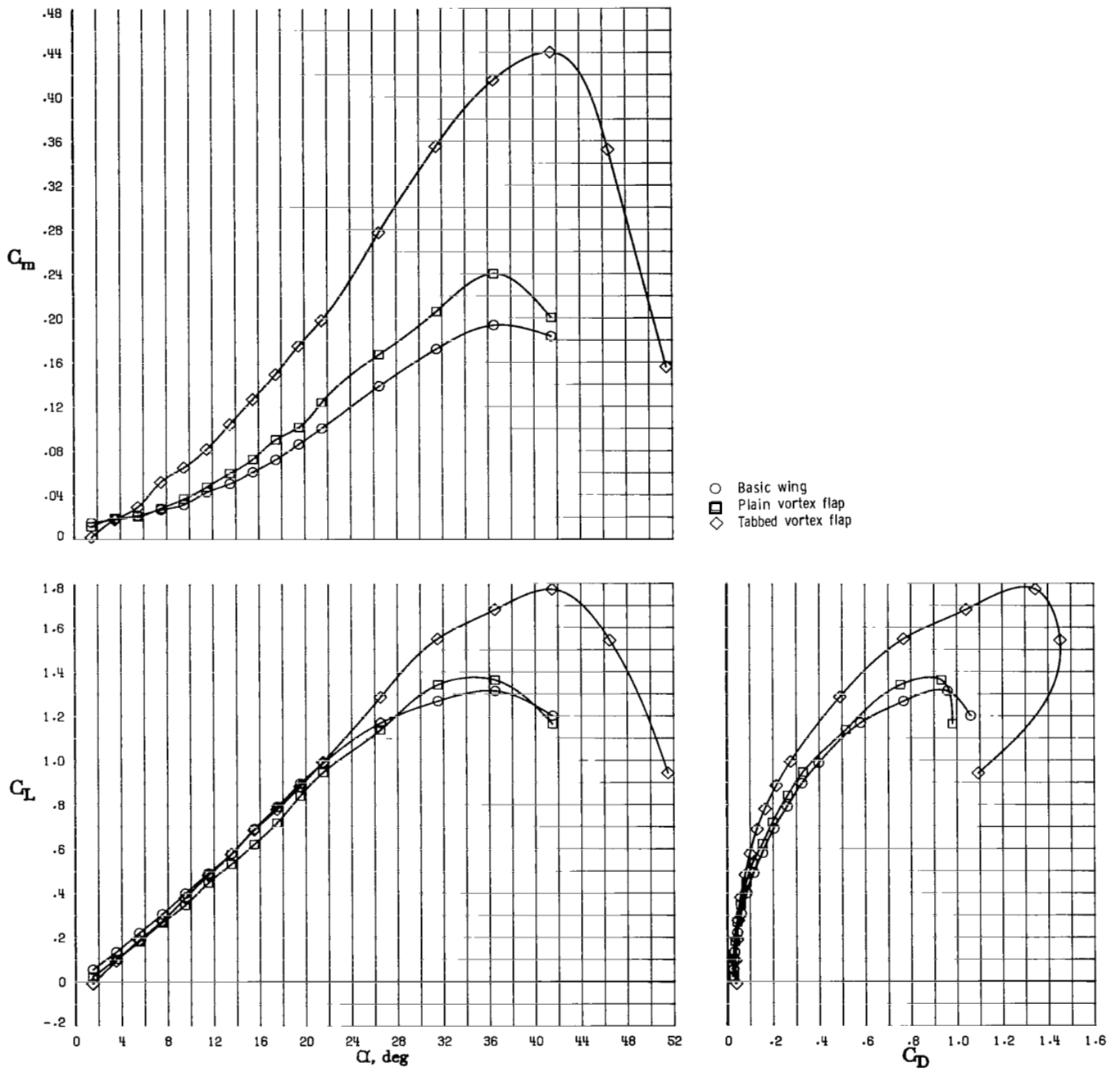
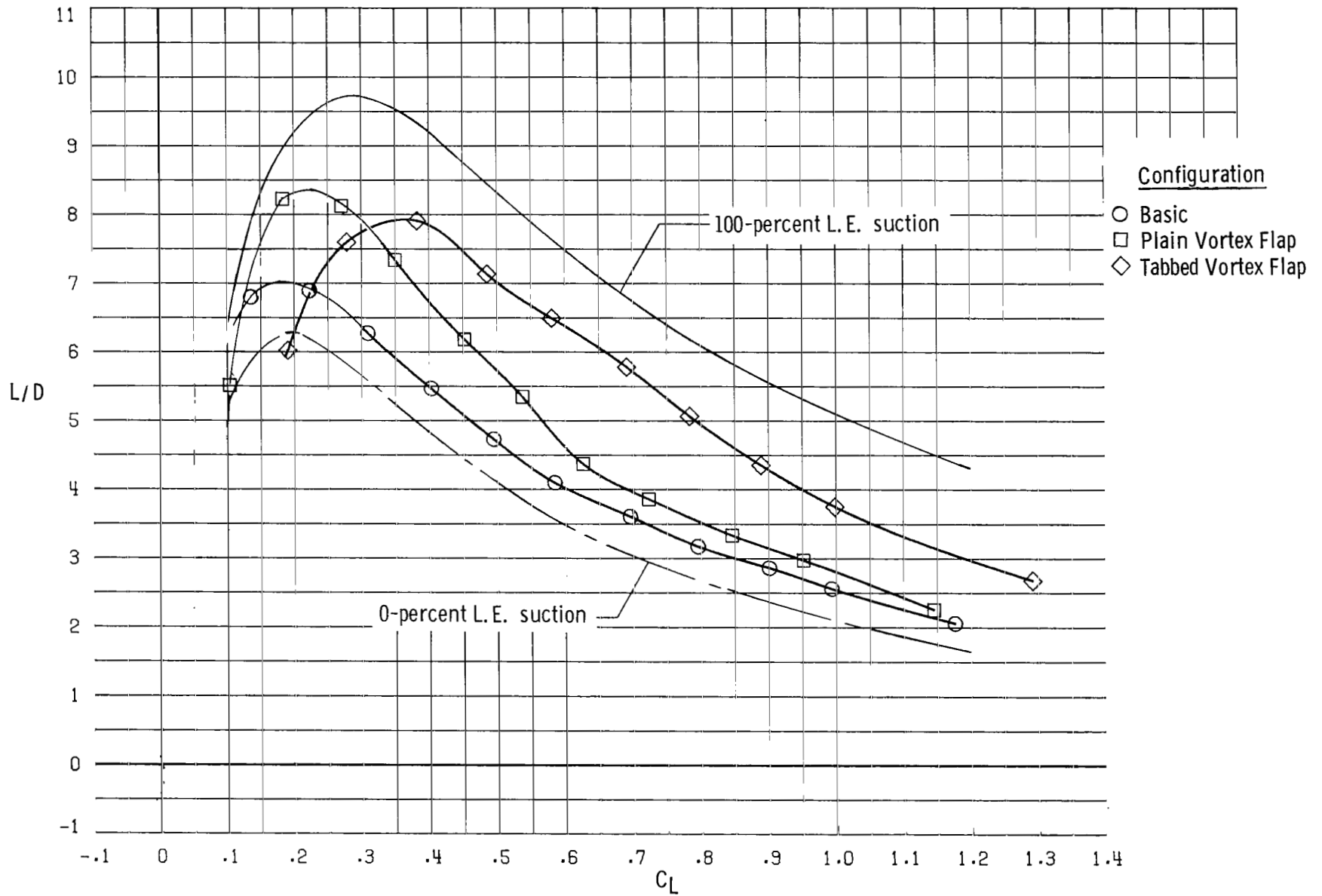
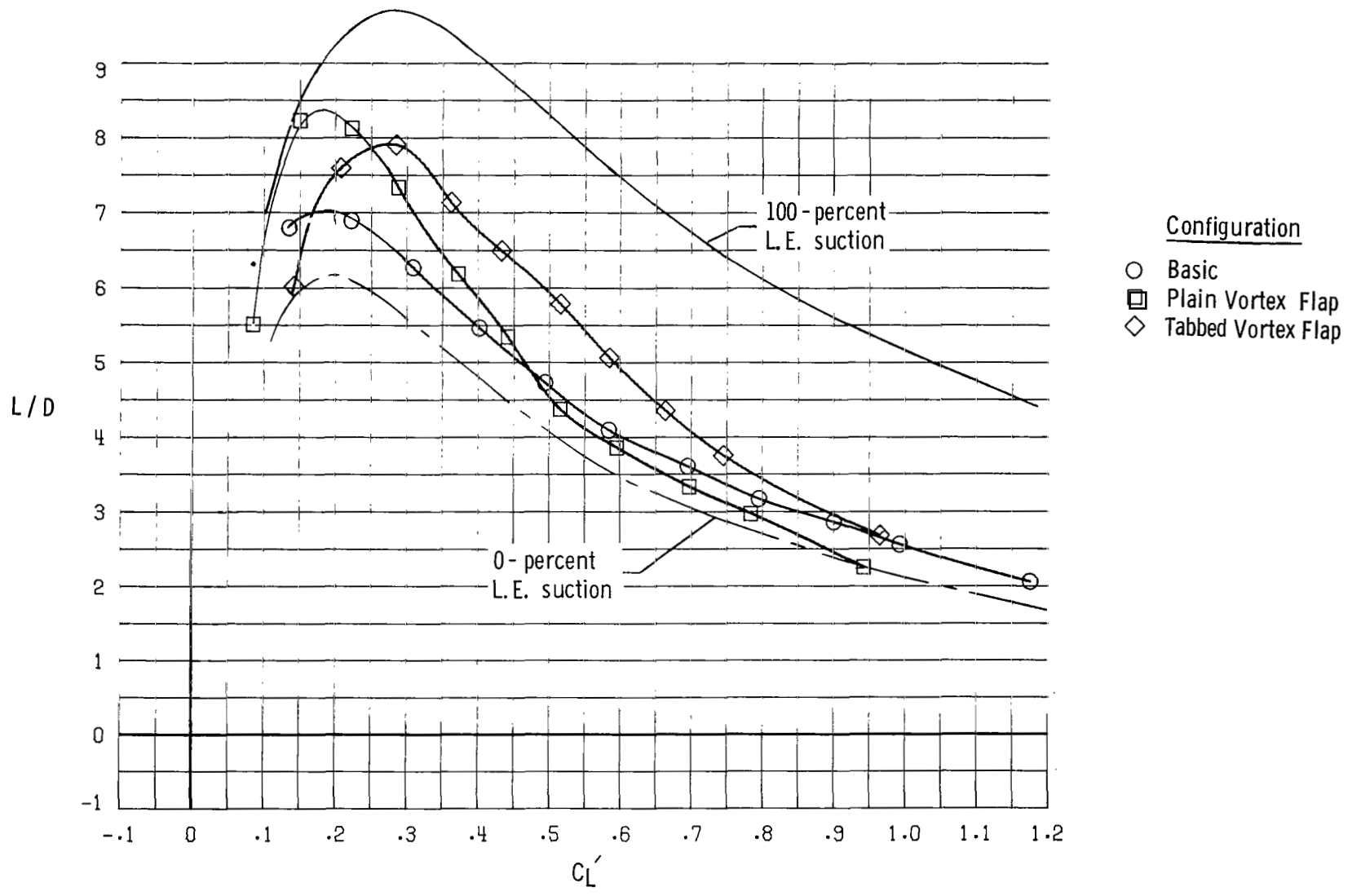


Figure 15.- Comparison of vortex flaps. Trailing-edge flaps off.



(a) Uncorrected for projected area.

Figure 16.- Comparison of L/D characteristics of vortex flaps.



(b) Corrected for projected area.

Figure 16.- Concluded.

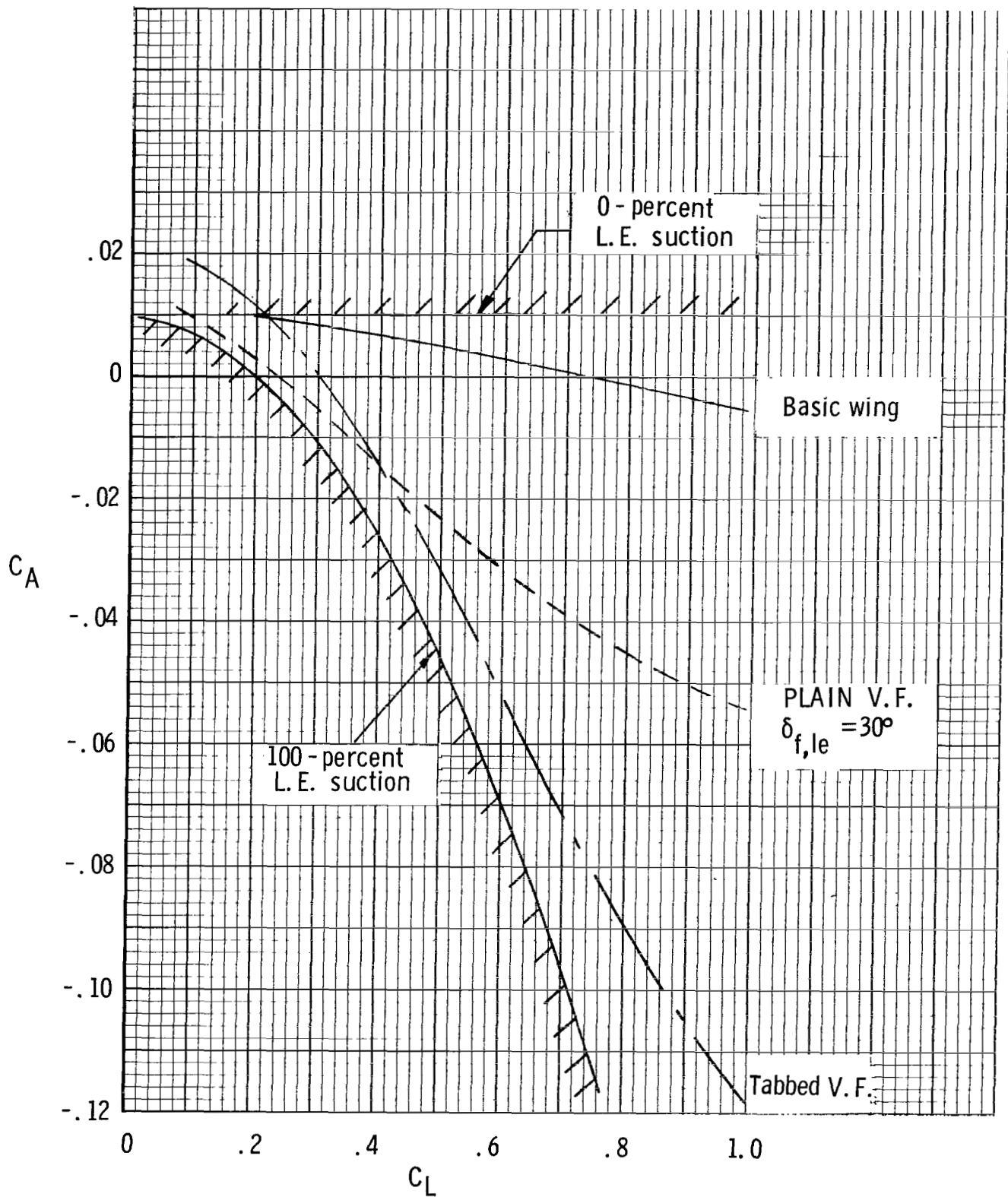


Figure 17.- Comparison of axial-force characteristics on the vortex-flap configurations.

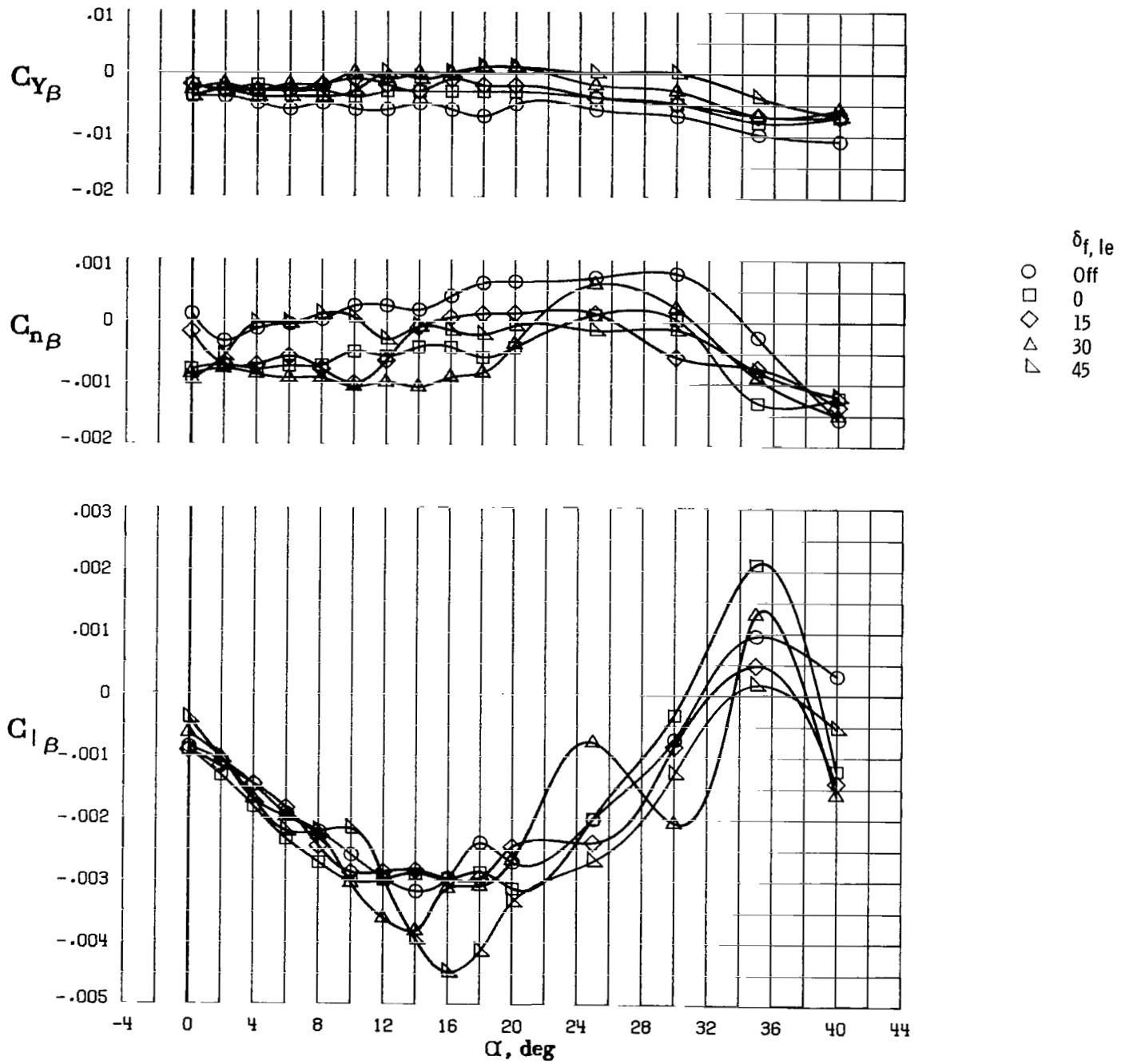


Figure 18.- Effect of leading-edge-flap deflection on the lateral-directional stability characteristics of a plain-vortex-flap configuration.

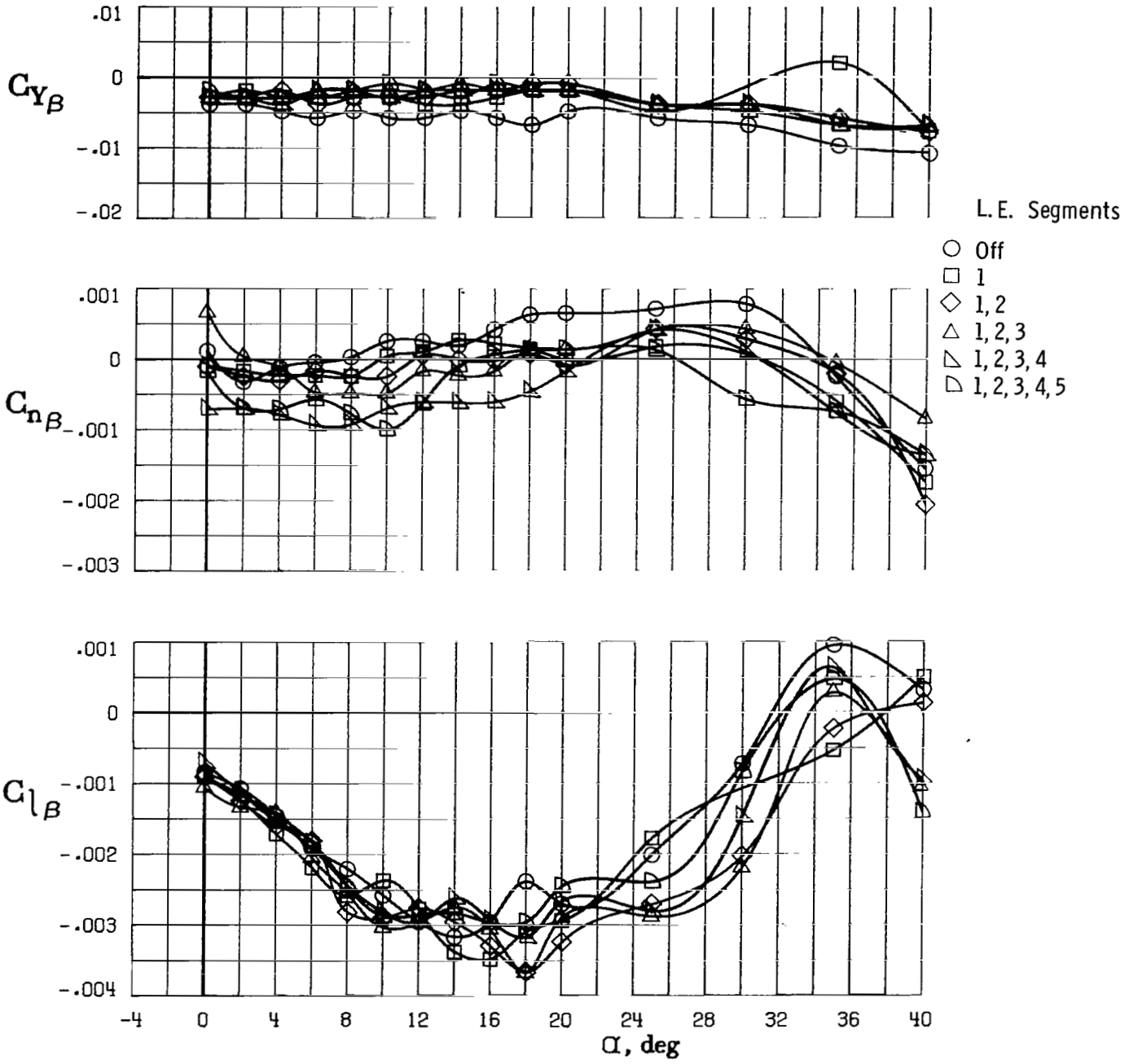
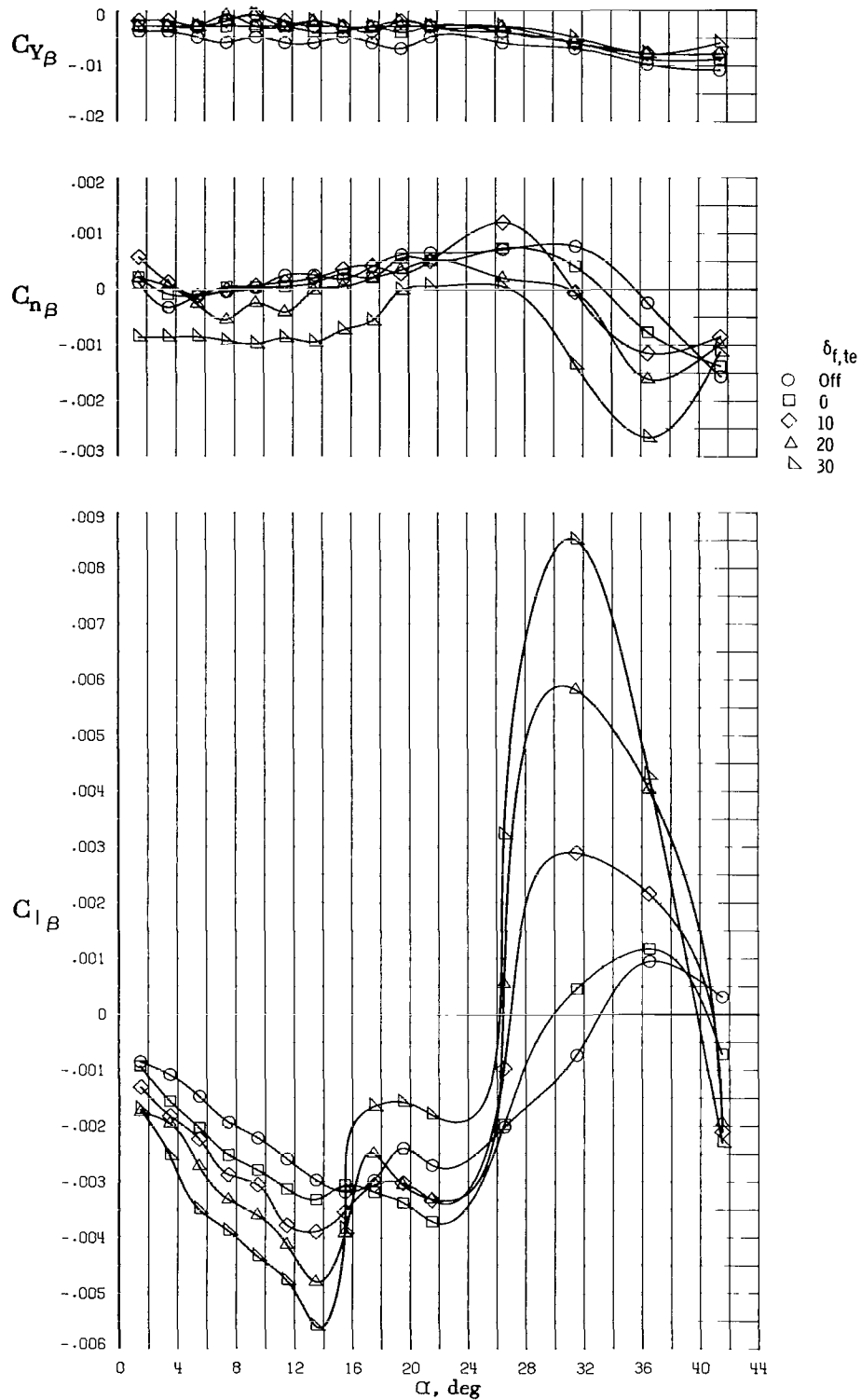
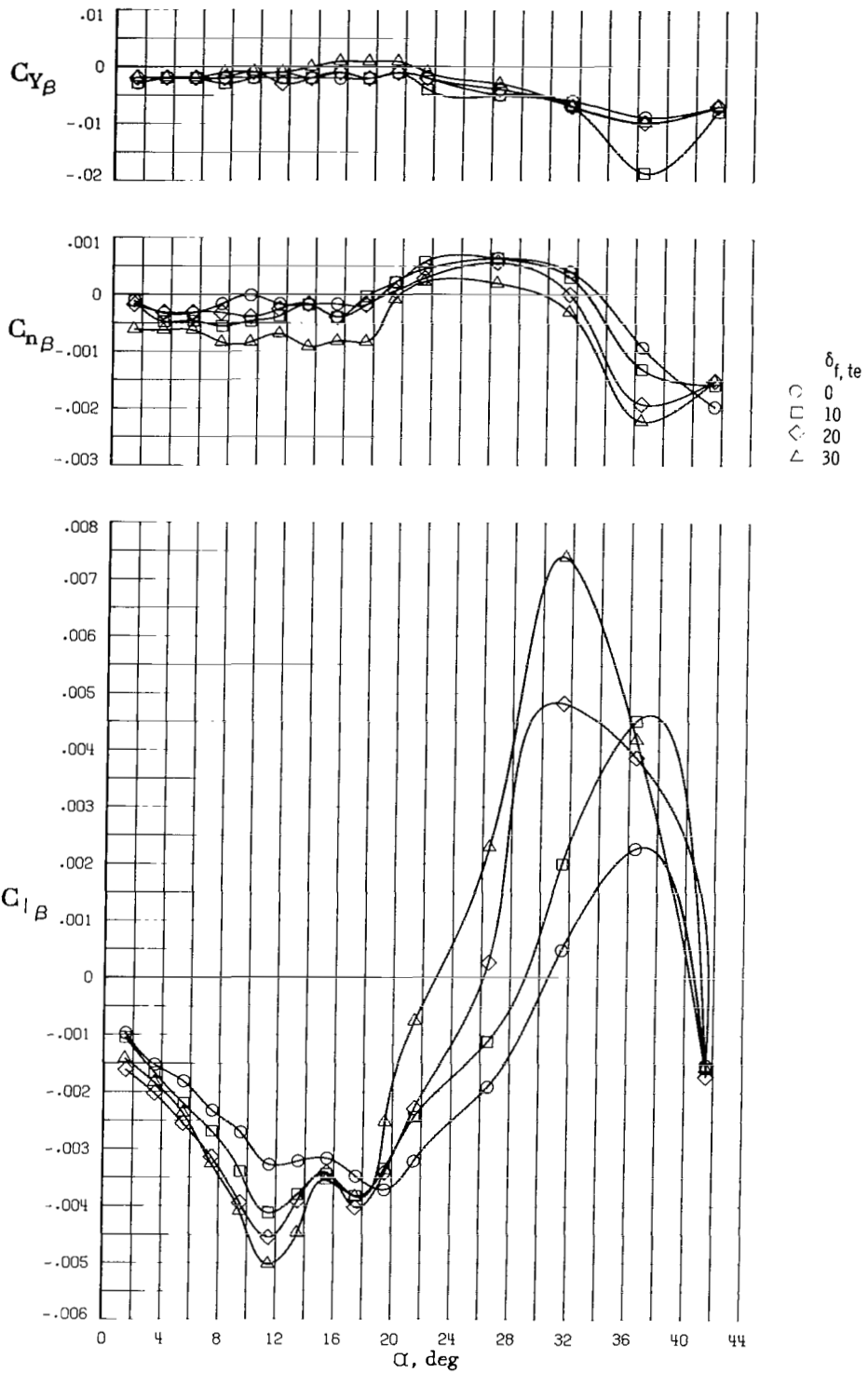


Figure 19.- Effect of leading-edge buildup in segments. $\delta_{f,1e} = 15^\circ$.



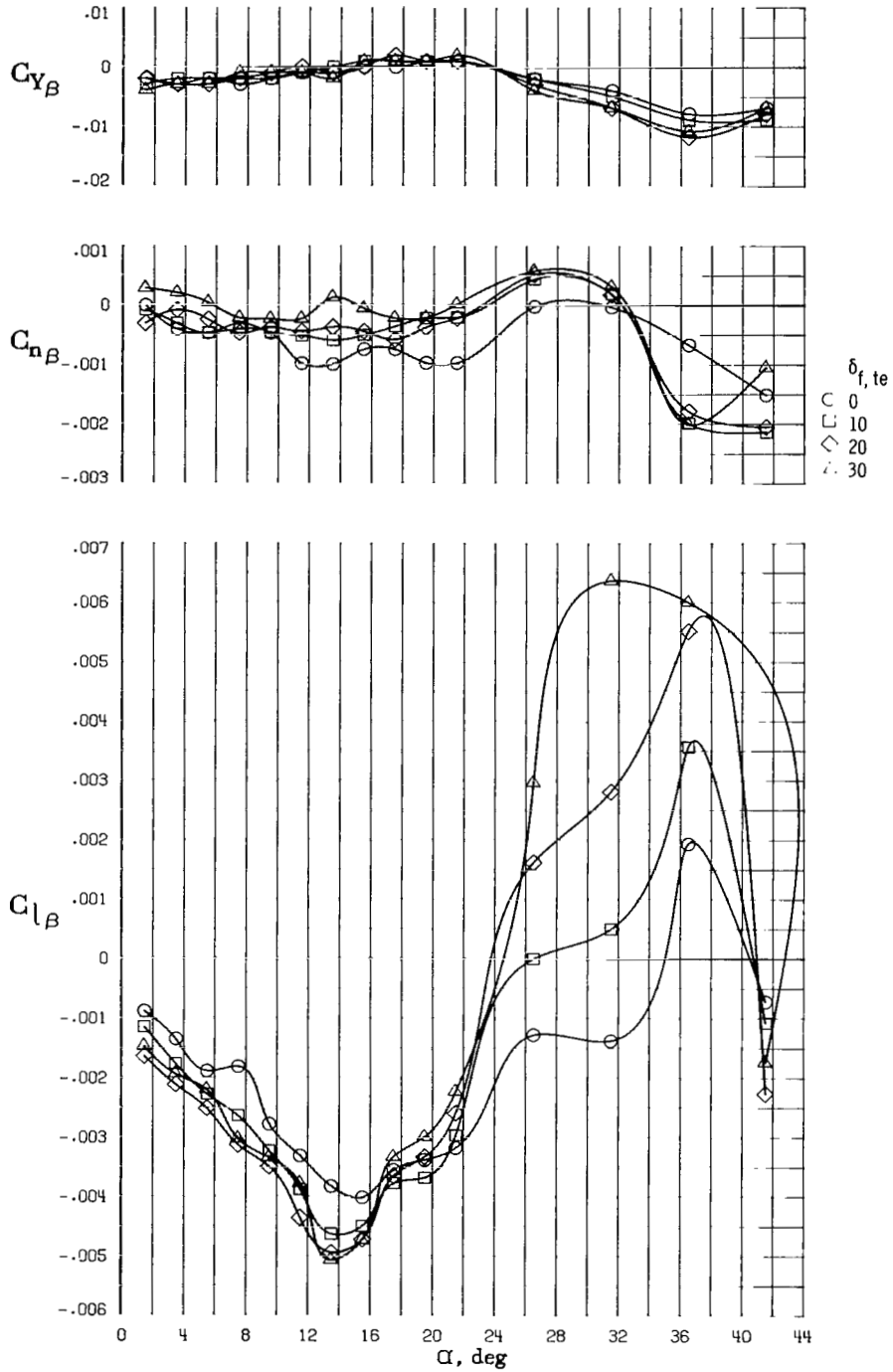
(a) $\delta_{f,le} = 0$.

Figure 20.- Effect of trailing-edge-flap deflection.
Plain-vortex-flap configuration.



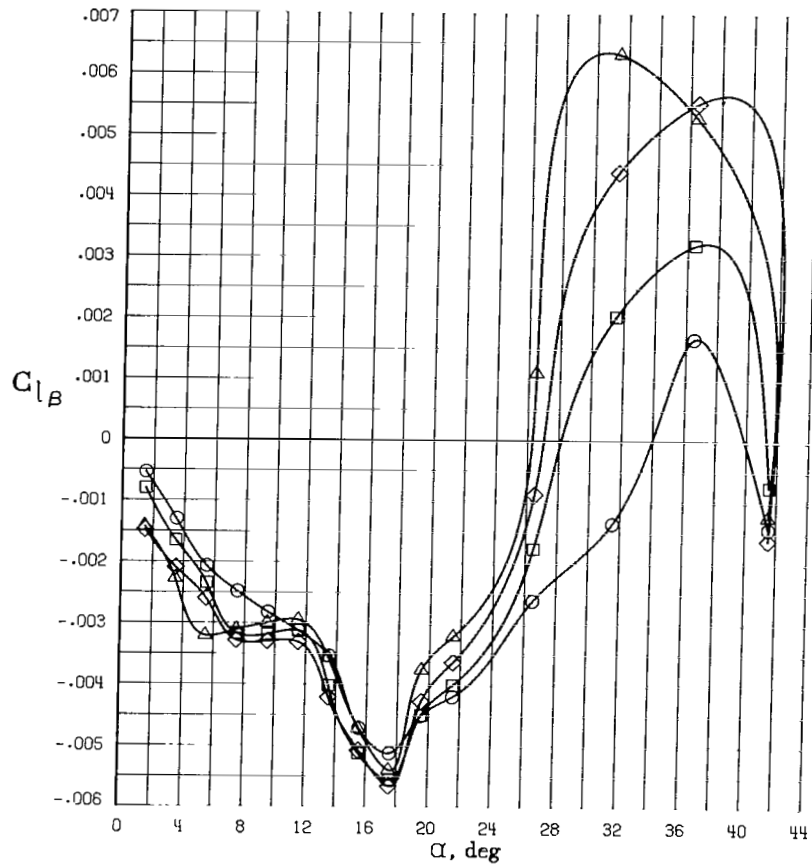
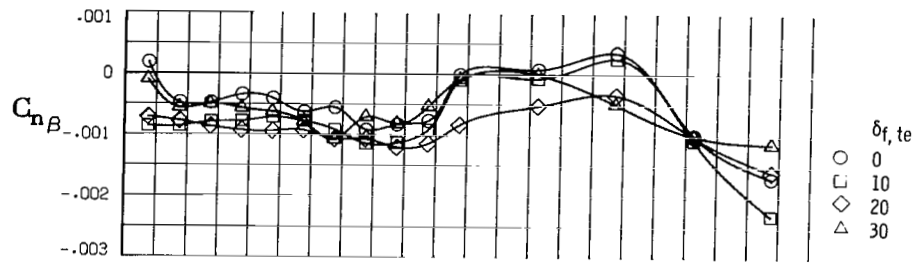
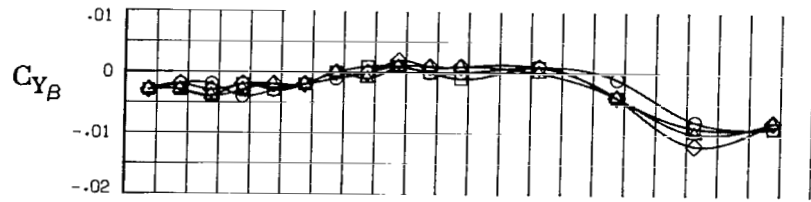
(b) $\delta_{f,le} = 15^\circ$.

Figure 20.- Continued.



(c) $\delta_{f,le} = 30^\circ$.

Figure 20.- Continued.



(d) $\delta_{f,le} = 45^\circ$.

Figure 20.- Concluded.

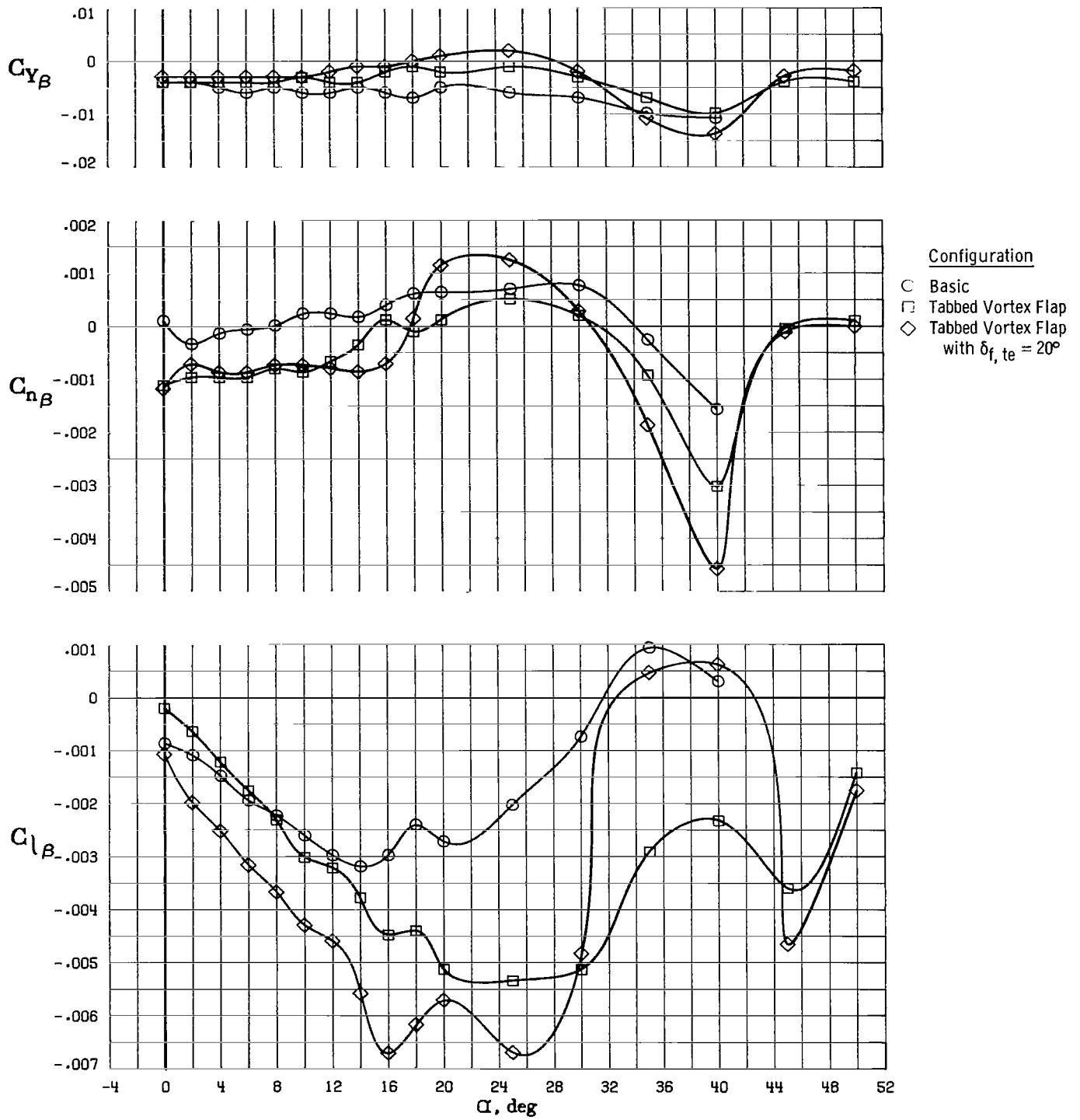
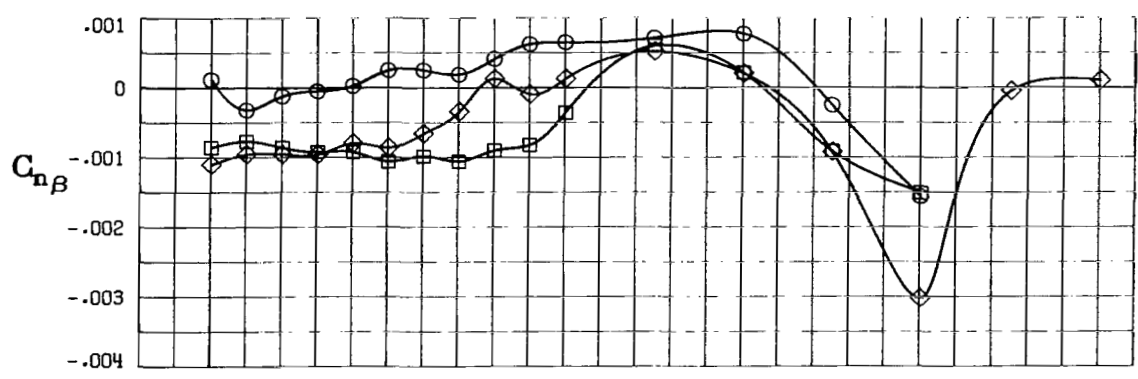
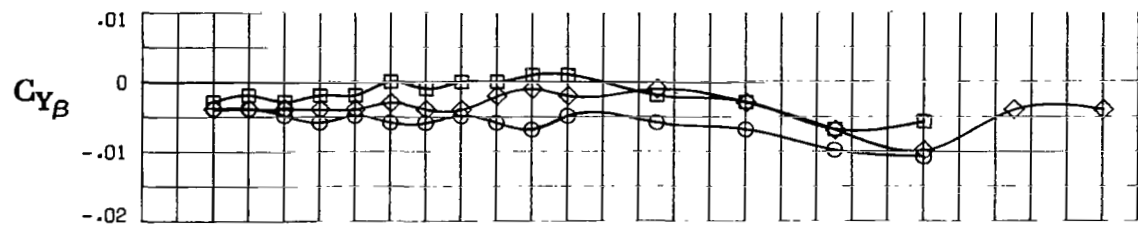


Figure 21.- Effect of tabbed-vortex-flap configuration on lateral-directional stability characteristics.



Configuration
 ○ Basic
 □ Plain Vortex Flap
 ◇ Tabbed Vortex Flap

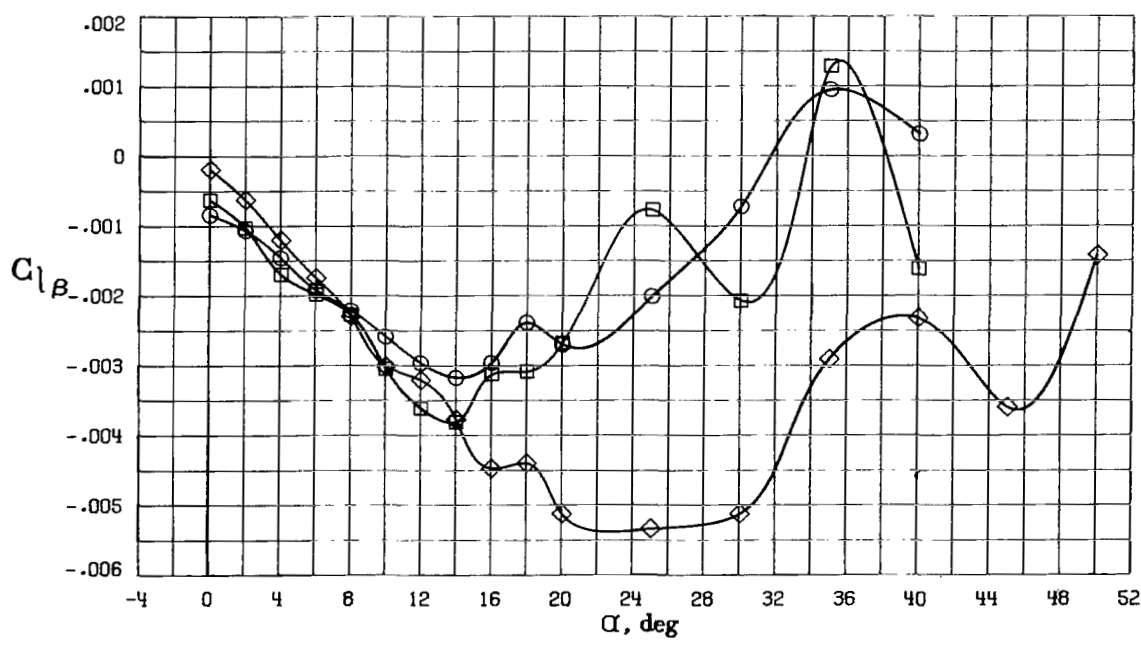





Figure 22.- Effect of configurations on lateral-directional stability characteristics.

- BASIC WING 
- - - PLAIN VORTEX FLAP 
- · - · - TABBED VORTEX FLAP 

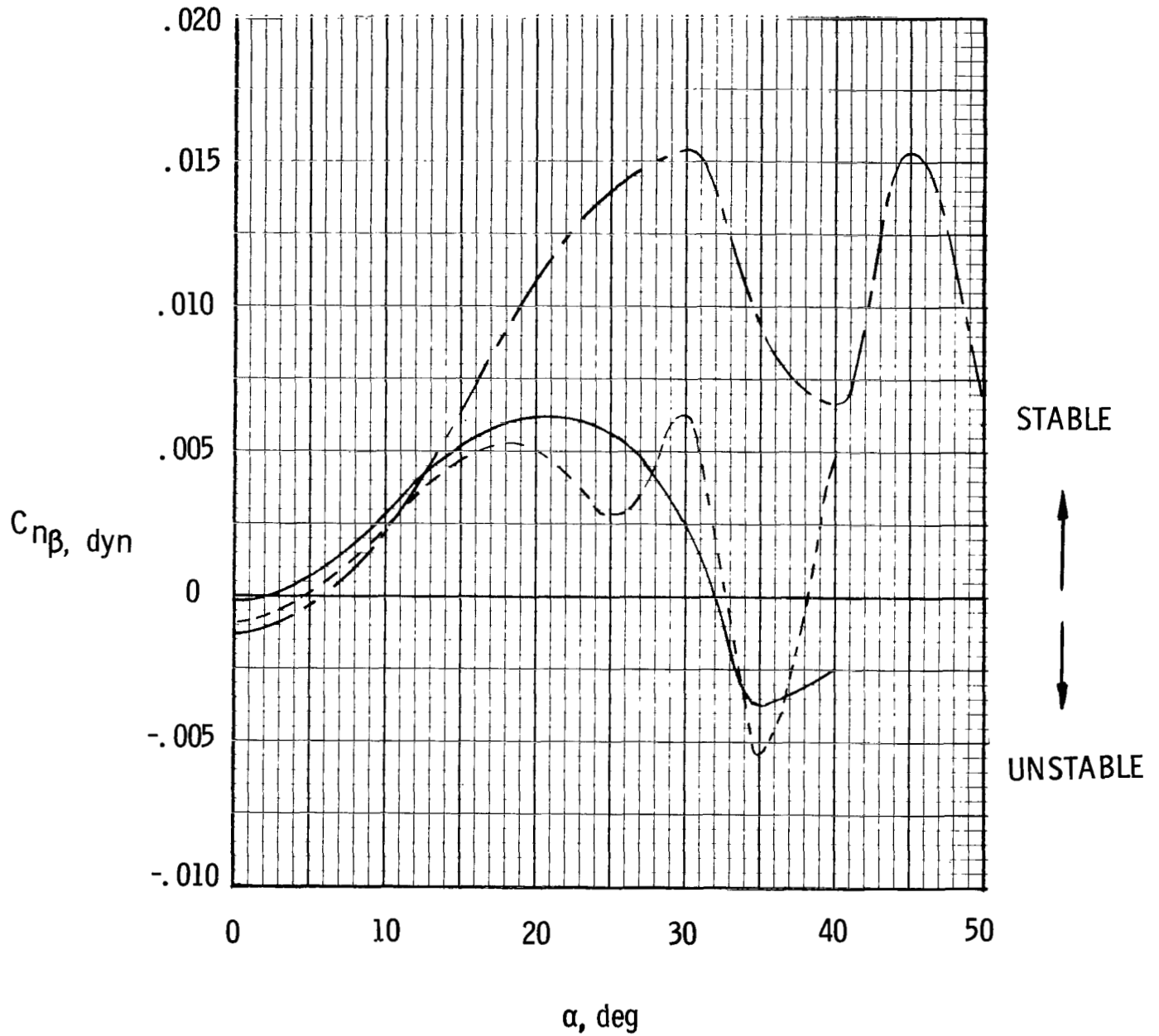


Figure 23.- Effect of vortex flaps on the lateral-directional stability parameter.

1. Report No. NASA TP-1914		2. Government Accession No.		3. Recipient's Catalog No.	
4. Title and Subtitle EFFECTS OF VORTEX FLAPS ON THE LOW-SPEED AERODYNAMIC CHARACTERISTICS OF AN ARROW WING				5. Report Date November 1981	
7. Author(s) Long P. Yip and Daniel G. Murri				6. Performing Organization Code 505-43-13-01	
9. Performing Organization Name and Address NASA Langley Research Center Hampton, VA 23665				8. Performing Organization Report No. L-14575	
12. Sponsoring Agency Name and Address National Aeronautics and Space Administration Washington, DC 20546				10. Work Unit No.	
15. Supplementary Notes				11. Contract or Grant No.	
16. Abstract A low-speed wind-tunnel investigation was made to determine the longitudinal and lateral-directional aerodynamic effects of plain and tabbed vortex flaps on a flat-plate, highly swept arrow-wing model. Flow-visualization studies were made using a helium-bubble technique. Static forces and moments were measured over an angle-of-attack range from 0° to 50° for sideslip angles of 0° and ±4°.				13. Type of Report and Period Covered Technical Paper	
17. Key Words (Suggested by Author(s)) Vortex flaps Arrow wing Flow visualization Vortex bursting				14. Sponsoring Agency Code	
18. Distribution Statement Unclassified - Unlimited Subject Category 01					
19. Security Classif. (of this report) Unclassified	20. Security Classif. (of this page) Unclassified	21. No. of Pages 62	22. Price A04		

National Aeronautics and
Space Administration

Washington, D.C.
20546

Official Business
Penalty for Private Use, \$300

THIRD-CLASS BULK RATE

Postage and Fees Paid
National Aeronautics and
Space Administration
NASA-451



3 1 10, A, 102781 S00903DS
DEPT OF THE AIR FORCE
AF WEAPONS LABORATORY
ATTN: TECHNICAL LIBRARY (SUL)
KIRTLAND AFB NM 87117

NASA

POSTMASTER: If Undeliverable (Section 158
Postal Manual) Do Not Return
